

Aim and Scope

The objective of the *Journal of Residuals Science & Technology* (JRS&T) is to provide a forum for technical research on the management and disposal of residuals from pollution control activities. The Journal publishes papers that examine the characteristics, effects, and management principles of various residuals from such sources as wastewater treatment, water treatment, air pollution control, hazardous waste treatment, solid waste, industrial waste treatment, and other pollution control activities. Papers on health and the environmental effects of residuals production, management, and disposal are also welcome.

Editor-in-Chief

P. Brent Duncan
Department of Biology
University of North Texas
Denton, TX, USA
pduncan@unt.edu

Assistant Editor

James Lee
james.lee3918@gmail.com

Editorial Advisory Board

Muhammad Abu-Orf
AECOM, USA
mohammad.abu-orf@aecom.com

Nafissa M. Bizo
City of Philadelphia Water Department
nafissa.bizo@phila.gov

Richard Dick
Cornell University, USA
rid1@cornell.edu

Eliot Epstein
Epstein Environmental Consultants
epsteinee@comcast.net

Guor-Cheng Fang, Ph.D.
Hungkuang University, Taiwan
gcfang@sunrise.hk.edu.tw

Robert Hale
Virginia Institute of Marine Science, USA
hale@vims.edu

Paul F. Hudak
University of North Texas, USA
hudak@unt.edu

Blanca Jimenez Cisneros
Inst. de Ingenieria, UNAM, Mexico
bjc@mumas.iingen.unam.mx

Julia Kopp
Technische Universitat Braunschweig,
Germany
j.kopp@tu-bs.de

Uta Krogmann
RutgersUniversity, USA
krogmann@aesop.rutgers.edu

D. J. Lee
National Taiwan University, Taiwan
djlee@ntu.edu.tw

Giuseppe Mininni
Via Reno 1, Italy
mininni@irsa.rm.cnr.it

Lynne H. Moss
CDM Smith
mosslh@cdmsmith.com

John Novak
Virginia Tech, USA
jtnov@vt.edu

Nagaharu Okuno
The University of Shiga Prefecture,
Japan
okuno@ses.usp.ac.jp

Jan Oleszkiewicz
University of Manitoba, Canada
oleszkie@ms.umanitoba.ca

Banu Örmeci
Carleton University, Canada
banu_ormeci@carleton.ca

Ian L. Pepper
University of Arizona, USA
ipepper@ag.arizona.edu

Ioana G. Petrisor
Co-Editor-in-Chief
Environmental Forensics Journal, USA
Environmental.Forensics@gmail.com

Bob Reimers
Tulane University, USA
rreimers@tulane.edu

Dilek Sanin
Middle East Technical University,
Turkey
dsanin@metu.edu.tr

Heidi Snyman
Golder Associates Africa (Pty) Ltd.,
South Africa
hsnyman@golder.co.za

Ludovico Spinosa
Consultant at Commissariat
for Env. Energ. in Region,
Puglia, Italy
ludovico.spinosa@fastwebnet.it

P. Aarne Vesilind
Bucknell University, USA
aarne.vesilind@gmail.com


Doug Williams
California Polytechnic State
University, USA
wmsenr@thegrid.net

JOURNAL OF RESIDUALS SCIENCE & TECHNOLOGY—Published quarterly—January, April, July and October by DEStech Publications, Inc., 439 North Duke Street, Lancaster, PA 17602.

Indexed by Chemical Abstracts Service. Indexed/abstracted in Science Citation Index Expanded. Abstracted in Current Contents/Engineering, Computing & Technology. Listed in ISI Master Journal.

Subscriptions: Annual \$219 per year. Single copy price \$60. Foreign subscriptions add \$45 per year for postage.

(ISSN 1544-8053)

 DEStech Publications, Inc.

439 North Duke Street, Lancaster, PA 17602-4967, U.S.A.

©Copyright by DEStech Publications, Inc. 2016—All Rights Reserved

C O N T E N T S

Research

- Mix Ratio Optimization of Cemented Coal Gangue Backfill (CGB) Based on Response Surface Method** 175
GUORUI FENG, ZHEN LIA, YUXIA GUO, DIAN LI, TINGYE QI, GUOYAN LIU, KAIGE SONG and LIXUN KANG
- Systematic Approach to Identifying Economically Feasible and Environmentally Benign Methods of Recycling Ash on a Regional Scale** 185
IVAN DEVIATKIN, JOUNI HAVUKAINEN and MIKA HORTTANAINEN
- Effective Removal of Copper (II) and Cadmium (II) by Adsorbent Prepared from Chitosan-modified Magnetic Biochar** 197
QIXUAN SONG, BAOSHAN YANG, HUI WANG, SHIPENG XU and YANAN CAO
- Modifications of Concentrations of Plant Macronutrient Ions in Digestate from Anaerobic Digestion during Nitrification Processes** 207
KENJI TAKEMURA, RYOSUKE ENDO, TOSHIO SHIBUYA and YOSHIAKI KITAYA
- Effect of Sludge Conditioning Temperature on the Thickening and Dewatering Performance of Polymers** 215
ZE YAN, BANU ÖRMECI and JINLI ZHANG
- Copper (II) Removed from Aqueous Solutions by Aminated Bagasse Pith** 225
XINLIANG LIU, CONG GAO, CHEN LIANG, SHUANGXI NIE and SHUANGFEI WANG
- Modified Electro-spun Polyvinyl Alcohol Nanofibers Used as Super Adsorbing Material for Lead Ions in Aqueous Solution** 233
NTAOTE DAVID SHOOTO, DONBEBE WANKASI, LUCKY MASHUDU SIKHWIVHILU and EZEKIEL DIXON DIKIO

Mix Ratio Optimization of Cemented Coal Gangue Backfill (CGB) Based on Response Surface Method

GUORUI FENG^{1,2,*}, ZHEN LI^{1,2}, YUXIA GUO^{1,2}, JIACHEN WANG³, DIAN LI^{1,2}, TINGYE QI^{1,2}, GUOYAN LIU^{1,2},
KAIGE SONG^{1,2} and LIXUN KANG^{1,2}

¹College of Mining Engineering, Taiyuan University of Technology, Taiyuan 030024, Shanxi, China

²Green mining engineering technology research center of Shanxi Province, Taiyuan 030024, Shanxi, China

³College of Resource and Safety Engineering, China University of Mining and Technology, Beijing 100083, China

ABSTRACT: Central composite design (CCD) experiments were performed to investigate the effect of cement content, fine gangue rate and water reducer content on the rheological properties of fresh cemented coal gangue backfill (CGB) and the compressive strength of hardened slurry. The parameter of mixture proportion was optimized by Multi-criteria optimization analysis. The results show that the fresh CGB rheological property conforms to Bingham model, the yield stress of fresh slurry is influenced by the interaction of the three factors, and the plastic viscosity increases with cement content, fine gangue rate and water reducer content. The value of 28 days uniaxial compressive strength (UCS_{28}) is proportional to cement content and water reducer content, while it is inversely proportional to fine gangue rate. The overall satisfaction of slurry rises significantly with the increase of water reducer content. However, it increases firstly and then decreases with the increase of cement content and fine gangue rate, and reaches a maximum at cement content of 210 kg/m³ and fine gangue rate of 40%. The developed design method can provide scientific reference to reduce the accumulation of waste residues.

1. INTRODUCTION

COAL, as an important fossil energy in the world, accounts for 30% of global primary energy consumption. However, coal mining has resulted in many problems, such as surface subsidence, solid waste accumulation, water contamination and gas leakage [1,2]. Coal gangue backfill (CGB) not only solves the problems of ground gangue accumulation and fly ash pollution, but also effectively obviates surface subsidence and the induced gas leakage. In recent years, paste filling mining technology has been greatly popularized and broadly applied as a new green coal mining technology [3,4].

Previous studies on CGB have gained substantial achievements. According to Miao, Yang and Qi each component (i.e. cement, milled gangues, fly ash and water reducer) of CGB plays a significant role in its rheological and mechanical performance (i.e., transportation, placement, strength and stability) [5,6,7]. In the work of Chang *et al.*, the ratio of paste filling mate-

rial was regarded as the core problem of paste filling technology, and artificial neural network method was adopted to predict and evaluate the ratio of filling material [8]. The pozzolanic effect of fly ash was found to probably improve the performance in CGB strength to certain extent by Feng [9]. Furthermore, it was concluded that the flow ability of fresh filling material is greatly enhanced by increasing the content of milled fly ash [10]. Zheng *et al.* stated that high content of fine gangue may enhance the slump and pumpability of the paste [11]. Qi studied the influences of fine gangue content on the strength, resistivity and microscopic properties of CGB for coal mining [12]. Wu studied the transportability and pressure drop of backfill slurry composed of freshly cemented coal gangue-fly ash in pipe loop [13].

However, the influences of raw material contents on coal mine CGB rheological and compressive strength properties, as well as the quantitative relationship between them, are still not well understood currently. Actually the optimization of coal mine CGB mixture ratio today is still based primarily on traditional experimental methods. This approach requires a large number of trial experiments to determine the desired

*Author to whom correspondence should be addressed.
E-mail: fguorui@163.com; Tel: +86 0351 6010177

concentrations of the CGB components. Meanwhile the mainly researches [12,14,15,16] performed on the optimization of CGB properties were only experimental and rarely taking all factors into consideration. Therefore a scientific mix proportioning method which can minimize the number of trial mixes and provides the quantitative relationship between CGB properties and raw materials are needed urgently. In the present study, the influences on CGB working properties are investigated by taking the cement content, fine gangue rate and water reducer content into consideration by using central composite experiment method (CCD). Meanwhile, a responsive surface (RS) regression model of yield stress, plastic viscosity and CGB strength is established to predict the CGB performance under various conditions. Lastly, multi-criteria optimization of CGB based on satisfaction function method are performed to provide useful reference for the prediction of CGB materials in coal mine.

2. MATERIALS AND METHODS

2.1. Materials

The raw materials used in the present study included coal gangue, fly ash, cement, water and water reducer.

2.1.1. Coal Gangue

The coal gangue samples were collected from Xinyang coal mine, which is located in Shanxi Province of China. Without dehydration and drying process, the samples were crushed mechanically and then categorized into two groups according to particle size, fine aggregate (0~5 mm) and coarse aggregate (10~15 mm). In present study both the fine and coarse gangue are selected as gangue materials. Meanwhile fine gangue rate means the percentage content of fine gangue in all gangue materials. The fineness modulus μ of the fine gangue (0~5 mm) was 3.02. Relative physical properties of the gangue samples are lists in Table 1. The chemical composition of the gangue samples was determined by A Thermo Fisher Scientific Thermo iCAP 6300 inductively coupled plasma optical emission spectrometer (ICP-OES) (Table 1).

It should be noted that in the measurement of SiO₂ percentage, samples were first burned at 800°C to remove organic matter and then measured in NaOH solution at 650°C. All the other oxides were measured from samples subject to sealed digestion in HF + HNO₃ at 185°C.

2.1.2. Fly Ash

The fly ash samples obtained from power plant of Xinyang coal mine falls in the category of Class II fly ash. An ICP-OES was used to analyze the chemical composition (Table 1). The physical properties listed in Table 1 were determined according to the Technical Specification for Fly Ash Used in Concrete and Mortar (JGJ28-86).

2.1.3. Cement and Water

Ordinary portland cement (Grade 42.5) with flexural strength of 6.5 MPa and compressive strength of 48.0 MPa was used in the present study. Its physical properties and chemical composition are listed in Table 1 (provided by the manufacturer). Tap water was used as the water source.

2.1.4. Water Reducer

Highly effective poly carboxylic acid water reducer was used in the present study. The consumption of water reducer is determined by the percentage content of cemented materials [17]. In this study the fly ash were regarded as cemented materials as well as cement due to the cementation effect of fly ash caused by pozzolanic reactions [9,16].

2.2. Sample Preparation and Test method

2.2.1. Sample Preparation

Introduced by Box and Wilson [18], the response surface method (RSM) provides a scientific method to discover the relationship (polynomial equations) be-

Table 1. Chemical Components and Physical Properties of the CGB Materials.

Major Element	Gangue (%)	Fly Ash (%)	Cement (%)
SiO ₂	35.46	52.42	22.27
Al ₂ O ₃	16.11	32.48	5.59
Fe ₂ O ₃	3.86	3.62	3.47
CaO	7.15	3.05	65.90
MgO	3.50	1.01	0.81
TiO ₂	0.80	1.26	–
Specific gravity (g/cm ³)	2.0	2.2	3.1
Specific surface (m ² /kg)	499	415	349
Fineness (> 45 μm), %	53.78	42.54	5
Moisture content, %	8.0	0.56	–
Lose on ignition, %	–	3.8	2

Table 2. Factors and Their Levels in Respond Surface Analysis.

Values	Cement, Kg/m ³	Fine Gangue, %	Water Reducer, %
-1.682	156.36	13.18	0.23
-1	170	20	0.3
0	190	30	0.4
1	210	40	0.5
1.682	223.64	46.82	0.57

tween an output variable and the levels of a number of input variables. Base on response surface method (RSM) principles, the concrete three factors and their five levels of response surface analysis are listed in Table 2. In the present work all the test groups have a constant fly ash content of 380 kg/m³, and the control

group (0 # group) contains no water reducer. All the solid content of the paste mixtures was 81% by weight. The content of cement ranges from 156.36 Kg/m³ to 223.64 Kg/m³; the fine gangue rate is between 13.18% and 46.82%; and the content of poly carboxylic acid water reducer is in the range of 0.23–0.57%.

During each test the raw materials were mixed according to RS design and then mechanically stirred [Figure 1(a)]. Once well blended, the raw materials were tested for rheological properties [Figure 1(b)]. Then, the slurry was stirred again and poured into 10 × 10 × 10 cm³ testing moulds. As suggested by Ren [16], the specimens were cured in a curing room (temperature: 20 ± 2°C, humidity: 80%) for 28 days. Figure 1(c) shows the cured CGB samples. After that, the compressive tests were performed as shown in Figure 1(d).



(a)



(b)



(c)



(d)

Figure 1. Preparation and testing of CGB samples: (a) mixing; (b) rheological test apparatus; (c) cured CGB samples; and (d) UCS tests.

2.2.2. Rheological and Compressive Strength Test

The rheological properties of the fresh CGB samples, including yield stress and plastic viscosity, were tested by using a torque rheometer (ICAR RHM-3000) [19]. The rheometer allows for a maximum test sample size of 40 mm, which is much greater than the size of the samples prepared in the present study. The tests of CGB sample compressive strength after 28 days of curing (UCS₂₈) were performed by using a computer controlled mechanical press with a load capacity of 1000 kN and a force change speed of 6.75 kN/min according to GB/T50080-2002.

3. RESULTS AND DISCUSSION

3.1. Experimental Results and Model Validation

Based on RSM design (Table 2), the experimental results are summarized in Table 3. Multivariate regression analysis [as shown in Equations (1)–(3)] on yield stress (Y_1), plastic viscosity (Y_2) and UCS₂₈ (Y_3) is performed based on the data from Table 3, where X_1 is cement content, X_2 represents fine gangue rate and X_3 denotes water reducer content. The main results of variance analysis of above regression model are summarized in Tables 4. In variance analysis the interaction item P value is used to determine whether there is a significance effect of variables. If $p \leq 0.05$ there is a significant effect on y ; $P \leq 0.01$, there is a quite significant effect on y ; $P > 0.05$, it means there is no significant effect on y .

Yield stress:

$$\left\{ \begin{array}{l} Y_1 = 1938.57321 - 15.93198X_1 - 17.32805X_2 + \\ 1234.42384X_3 + 0.090250X_1X_2 - 3.48750X_1X_3 \\ - 0.875X_2X_3 + 0.039593X_1^2 + 0.025789X_2^2 \\ + 1129.80599X_3^2 \end{array} \right\} \quad (1)$$

Plastic viscosity:

$$\left\{ \begin{array}{l} Y_2 = 0.13548X_1 + 0.18426X_2 + \\ 39.88511X_3 - 37.01671 \end{array} \right\} \quad (2)$$

UCS₂₈:

$$\left\{ \begin{array}{l} Y_3 = 0.050619X_1 - 0.016908X_2 + \\ 6.22826X_3 - 3.19611 \end{array} \right\} \quad (3)$$

As illustrated in Equation (1) and Table 4, The yield stress (Y_1) regression model conforms to the a second-order response surface. The factors that significantly influence the yield stress of the CGB are water reducer and fine gangue rate. The interactions between cement content and fine gangue rate also play a quite significant role on the yield stress of fresh CGB ($P < 0.01$). The quadratic terms X_1^2 and X_3^2 are also statistically significant ($P < 0.05$).

The plastic viscosity (Y_2) and the UCS₂₈ (Y_3) are calculated by first-order equations, as expressed in Equations (2) and (3). The cement, fine gangue rate and water reducer are both have quite significantly influence on plastic viscosity ($P < 0.01$). Table 4 also listed the results of variance analysis on UCS₂₈ by regression model. All the P values of X_1 , X_2 and X_3 are smaller than 0.01, indicating that all the factors have quite significantly influence on UCS₂₈. The interactions between each factor are not significant ($P > 0.05$).

In present study the P values of each model were less than 0.0001, indicating that the regression model results are rather significant. Meanwhile the P values of “lack of fit” items are greater than 0.05, which indicates that every regression model is correct [20,21,22].

To verify the validity of the developed models, the model predictions results were compared with experimental tests data. Figure 2 listed the experimental verification of the accuracy of the models. As is shown there is a good agreement between model predictions and experimental values. The distribution of the scattered points approximately follows the straight line of $y = x$, which indicates that the model fits very well.

3.2. Influence of Response Surface Parameters on Transport Characteristics

Figure 3 shows the relationship between torque and speed, the values of which are obtained by rheometer (ICAR RHM-3000). The figure indicates there is a linearly increasing relationship between shear force and the shear rate of fresh CGB. The slurry flow behavior index has a value of $n = 1$. As is shown in Figure 3, the intercept of Y -axis gives the slurry yield stress and the slope of the line indicates the plastic viscosity. It is evident that the slurry flow falls in a non-Newtonian fluid Bingham model [16,21]. When water reducer is increased by 0.4% from 0 # to 2 #, the yield stress decreases by 25% and the plastic viscosity increases by about 100%. The reasons can be explained as follows. On the one hand, the water reducer molecules are adsorbed on the surface of cement particles, which is

Table 3. Results of RS Experiment.

No	Cement (X_1) Kg/m ³	Fine Gangue (X_2), %	Water Reducer (X_3), %	Yield Stress (Y_1), Pa	Plastic Viscosity (Y_2), Pa·s	UCS ₂₈ (Y_3), MPa
0	190	30	0	540.7	5.4	6.32
1	210	20	0.3	413.4	4.9	9.1
2	190	30	0.4	400	10.8	8.44
3	170	20	0.5	381.2	8.7	8.42
4	210	40	0.5	387.5	18.4	9.8
5	190	30	0.4	408.9	10.4	8.11
6	190	30	0.23	427.8	3.32	7.2
7	156.4	30	0.4	407.8	4.8	6.8
8	190	30	0.4	358.9	9.5	8.48
9	190	30	0.4	384.4	8.9	8.49
10	190	46.82	0.4	420	10.9	7.9
11	190	30	0.57	303.1	19	9.57
12	210	20	0.5	333.2	15.5	10.2
13	170	40	0.5	367.1	13.6	7.6
14	223.6	30	0.4	476.6	13.9	10.05
15	190	30	0.4	360.7	11.3	8.62
16	170	20	0.3	437.3	4	6.69
17	190	30	0.3	408.9	10.3	8.43
18	210	40	0.3	475	14.2	8.84
19	190	13.18	0.4	389.4	6.7	8.5
20	170	40	0.3	422.9	5	6.87

Table 4. Results of Variance Analysis on Yield Stress, Plastic Viscosity, UCS₂₈ by Regression Model.

Variance Analysis	Variation Source	Sum of Squares	Freedom	Mean-square	F Value	P Value	
Yield Stress	Model	29031.00	9	3255.67	15.28	< 0.0001	Significant
	X1	990.52	1	990.52	1.82	0.0555	
	X2	1411.96	1	1411.96	2.59	0.0271	
	X3	17532.12	1	17532.12	18.55	< 0.0001	
	X1 X2	2606.42	1	2606.42	4.78	0.0056	
	X2 X3	6.13	1	6.13	0.011	0.8681	↓
	X1 X3	389.20	1	389.20	0.71	0.2044	
	X12	3614.58	1	3614.58	12.24	0.0020	
	X22	95.85	1	95.85	1.80	0.5157	
	X32	1839.55	1	1839.55	8.56	0.0145	
	Residual	2111.11	10	211.11			
	Lack of fit	1428.04	5	285.61	2.09	0.2188	Not Significant
Plastic Viscosity	Model	363.89	3	121.30	49.78	< 0.0001	Significant
	X1	100.27	1	100.27	41.15	< 0.0001	
	X2	46.37	1	46.37	19.03	0.0005	↓
	X3	217.26	1	217.26	89.16	< 0.0001	
	Residual	38.99	16	2.44			
	Lack of fit	35.19	11	3.20	4.24	0.0624	Not Significant
UCS ₂₈	Model	19.68	3	6.56	173.73	< 0.0001	Significant
	X1	14.00	1	14.00	53.38	< 0.0001	
	X2	0.39	1	0.39	1.27	0.0054	↓
	X3	5.30	1	5.30	18.85	0.0001	
	Residual	0.6	16	0.038			
	Lack of fit	0.46	11	0.042	1.44	0.3602	Not Significant

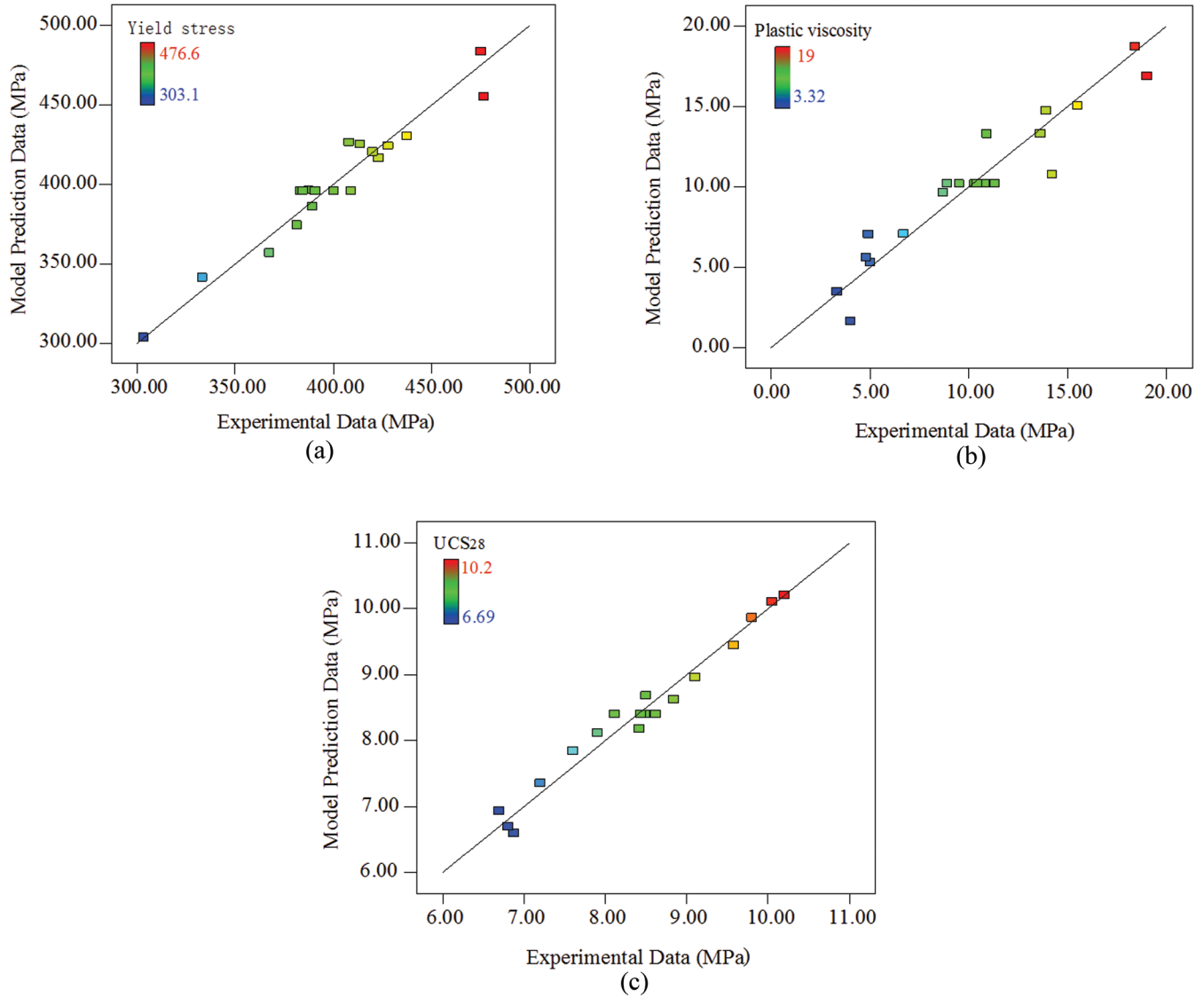


Figure 2. Comparison between predicted and the tested values: (a) Yield stress; (b) Plastic viscosity; and (c) UCS₂₈.

adverse to aggregation of cement particles and results in disintegration of flocculated cement structure. The free water released from the flow of cement effectively increases the liquidity of the slurry. On the other hand, water reducer reduces the liquid-gas interfacial tension and creates a certain air entraining effect. In addition to the bubble ball and floating effect, there is stronger tendency of relative sliding between the cement particles and the aggregates.

Figure 4 shows the effects of cement content and fine gangue content on fresh CGB yield stress when the content of water reducer takes up 0.4%. With the increase of cement content, the yield stress decreases firstly and then increases. The slurry has the lowest yield stress when cement content is 190 kg/m³. With the increase of the fine gangue rates, the yield stress

shows an upward trend. As is shown in Table 4 and Equation (2), cement content, fine gangue rate and water reducer have significant influences on slurry plastic viscosity. The impact of these factors on plastic viscosity follows the order: water reducer > cement content > fine gangue rate.

3.3. Influence of Response Surface Parameters on UCS₂₈

UCS₂₈ increases by about 50% when cement content rises from 156.4 kg/m³ (7#) to 223.6 kg/m³ (14#) under the same experimental conditions. This is mainly due to gelling properties of the cement. The more cement, the greater the strength is. However, more cement means greater cost too. When fine gangue rate is

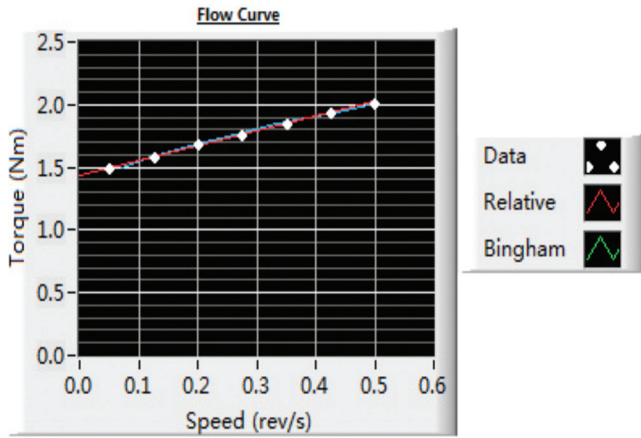


Figure 3. Relational graphs of rheological parameters.

increased from 20% in 1 # to 40% in 18 #, the UCS_{28} drops from 9.1 MPa to 8.84 MPa, which is a slight decline of 2.8%. The water reducer rate increases from 0% in 0 # to 0.4% in 2 #, and UCS_{28} climbs from 6.32 MPa to 8.44 MPa, which is a 33% increase. The reasons are as follows: the water reducer disperses the cement particles and promotes the release of free water trapped in cement flocules. Larger amount of water effectively promotes hydration and pozzolanic reactions, and brings an increase of CGB strength. The corresponding SEM images of cube specimens failure section are shown in Figure 5 [Figure 5(a) is for 0# and Figure 5(b) is for 2#]. By contrast the reasons can be drawn as follows: the molecular structure of the long side chain of poly carboxylic acid water reducer tightens the connection between the particles and aggregates.

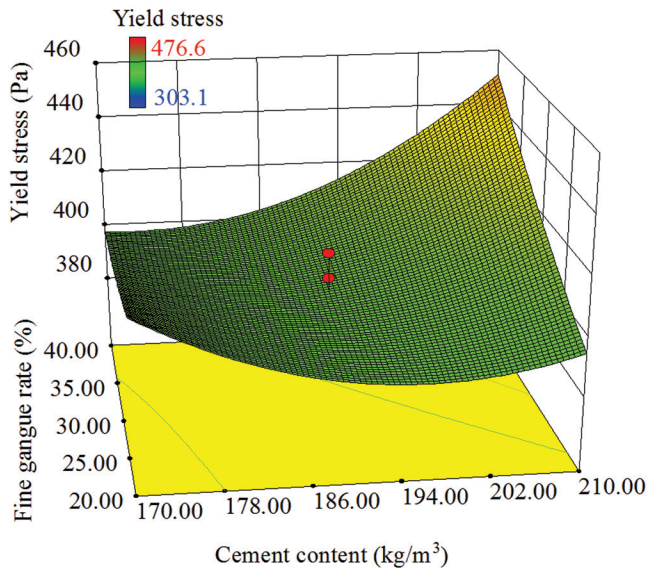
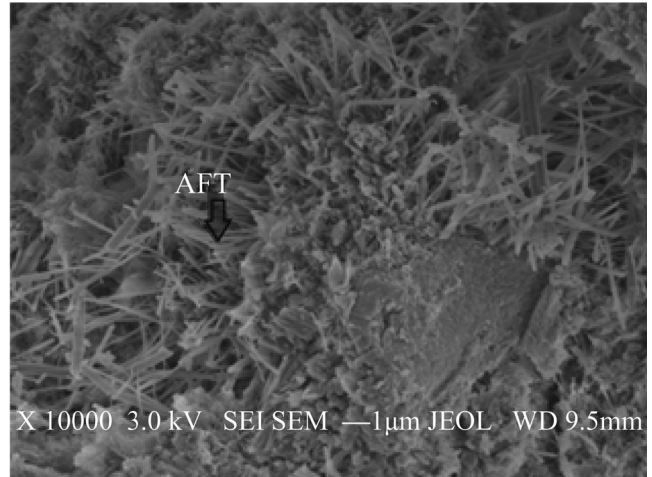
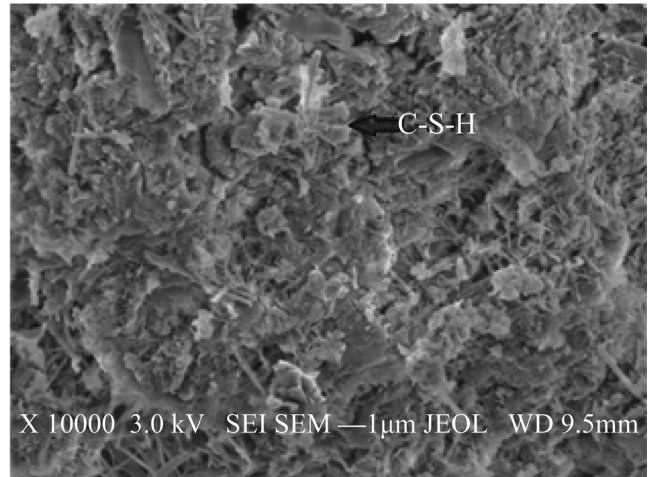


Figure 4. Interaction effects of cement and fine gangue rate on fresh CGB with water reducer content of 0.4%.



(a)



(b)

Figure 5. The microscopic scanning image of specimen failure section: (a) 0% water reducer and (b) 0.4% water reducer.

This promotes the formation of dense and compact grid structure of C-S-H (hydrated calcium silicate), which can be seen in in Figure 5(b) easily. The dense spatial structure greatly improves the CGB body strength.

4. NONLINEAR MULTI-CRITERIA OPTIMIZATION OF CGB

4.1. Optimization Method

The aim of the optimization is to find optimal CGB mixes. Based on the former experimental results, the optimization principles must simultaneously satisfy the following criteria:

1. Suitable values of yield stress and plastic viscosity to guarantee slurry transport;
2. Sufficient UCS_{28} to ensure sufficient roof support.

Table 5. Optimization Range of Response Objectives.

Response Objectives	Yield Stress, Pa	Plastic Viscosity, Pa·s	UCS ₂₈ , MPa
Range	350 < Y ₁ < 470	6 < Y ₂ < 14	7 < Y ₃ < 10.5

Since the experiment involves optimization of multiple factors response, the Multi-criteria optimization of CGB mixture ratio was applied. This optimization is based on Multi-criteria decision-making principles according to Derringer and Suich [23]. This method is based on construction of a satisfaction function for each individual model response, as expressed in Equation (4) and Equation (5) [22,24]. According to Equation (4), larger values of UCS₂₈ and the plastic viscosity are desirable; while according to Equation (5), smaller value of yield stress is expected in optimization. Taking the actual mining conditions of Xinyang coal mine into account, the determined range of response optimization targets are illustrated in Table 5.

Hence, the satisfaction function of each regression model [$d_i(Y_i(X))$] are established firstly. Then the multi-objective optimization function based on mean weighted geometry of each single satisfaction, namely overall satisfaction function, was established [Equation (6)].

$$d_i(Y_i(X)) = \begin{cases} 0 & Y_i(X) \leq L_i \\ \frac{Y_i(X) - L_i}{Y_{i,\max}(X) - L_i} & L_i \leq Y_i(X) \leq Y_{i,\max}(X) \\ 1 & Y_i(X) \leq Y_{i,\max}(X) \end{cases} \quad (4)$$

$$d_i(Y_i(X)) = \begin{cases} 0 & Y_i(X) \geq Y_{i,\max}(X) \\ \frac{Y_i(X) - Y_{i,\max}(X)}{L_i - Y_{i,\max}(X)} & L_i \leq Y_i(X) \leq Y_{i,\max}(X) \\ 1 & Y_i(X) \leq L_i \end{cases} \quad (5)$$

where d_i is the satisfaction degree function of the i th response, $Y_i(X)$ is the i th response value, L_i is the i th lower limit of response values, $Y_{i,\max}(X)$ is the i th upper limit of response values.

$$D = (\prod_{i=1}^q d_i^{r_i})^{1/\sum r_i} \quad (6)$$

where r_i is weights, depending on the importance of the response surface in the optimal design.

4.2. Analysis of Optimization Results

In practical engineering applications, slurry transport performance is determined by yield stress and plastic viscosity, and UCS₂₈ determines its carrying capacity of the overburden. Thus in this work we set the same degree of importance for each response surface regression model, i.e., $r_1 = r_2 = r_3$. According to Equations (4) and (5), the CGB performance satisfaction distribution is calculated as shown in Figures 6(a), 6(b), and 6(c) for single factor. Meanwhile, the CGB overall performance satisfaction distribution based on multi-objective combinations is established according to Equation (6) [Figure 5(d)].

By increasing the cement content and fine gangue rate, the CGB satisfaction degree increases firstly and then goes down and reaches the maxima at cement content of 210 kg/m³ and fine gangue rate of 40%. The CGB satisfaction degree increases rapidly with the rise of water reducer content. There is no obvious inflection point in Figure 6(c), which indicates individually increase water reducer dosage to improve the overall transport performance can obtain obvious satisfaction.

As is shown in Figure 6(d), at water reducer content of 0.23% the highest satisfaction degree reaches 0.2, while at water reducer content of 0.3% the highest satisfaction degree is greater than 0.4. With the increase of water reducer content, the satisfaction degree presents an increasing trend. When water reducer dosage is greater than 0.3%, the overall performance of CGB is very sensitive to the change of cement content. More cement content corresponds to higher overall satisfaction. The group of 223.64 Kg/m³ cement content, 30% fine gangue and 0.57% water reducer leads to the highest satisfaction degree. However, the unit volume of cemented materials and admixtures directly determines the amount of CGB costs. Therefore, the results suggests an optimal CGB composition of 190 Kg/m³ cement content, 30% fine gangue and 0.5% water reducer ratio.

5. CONCLUSION

In this study, a response surface method by CCD experiment is proposed to investigate the influence of cement content, fine gangue rate and water reducer content on CGB transport and mechanical properties. The prediction model for yield stress, plastic viscosity and UCS₂₈ is developed, in which a second-order response surface model is applied to yield stress and a first-order

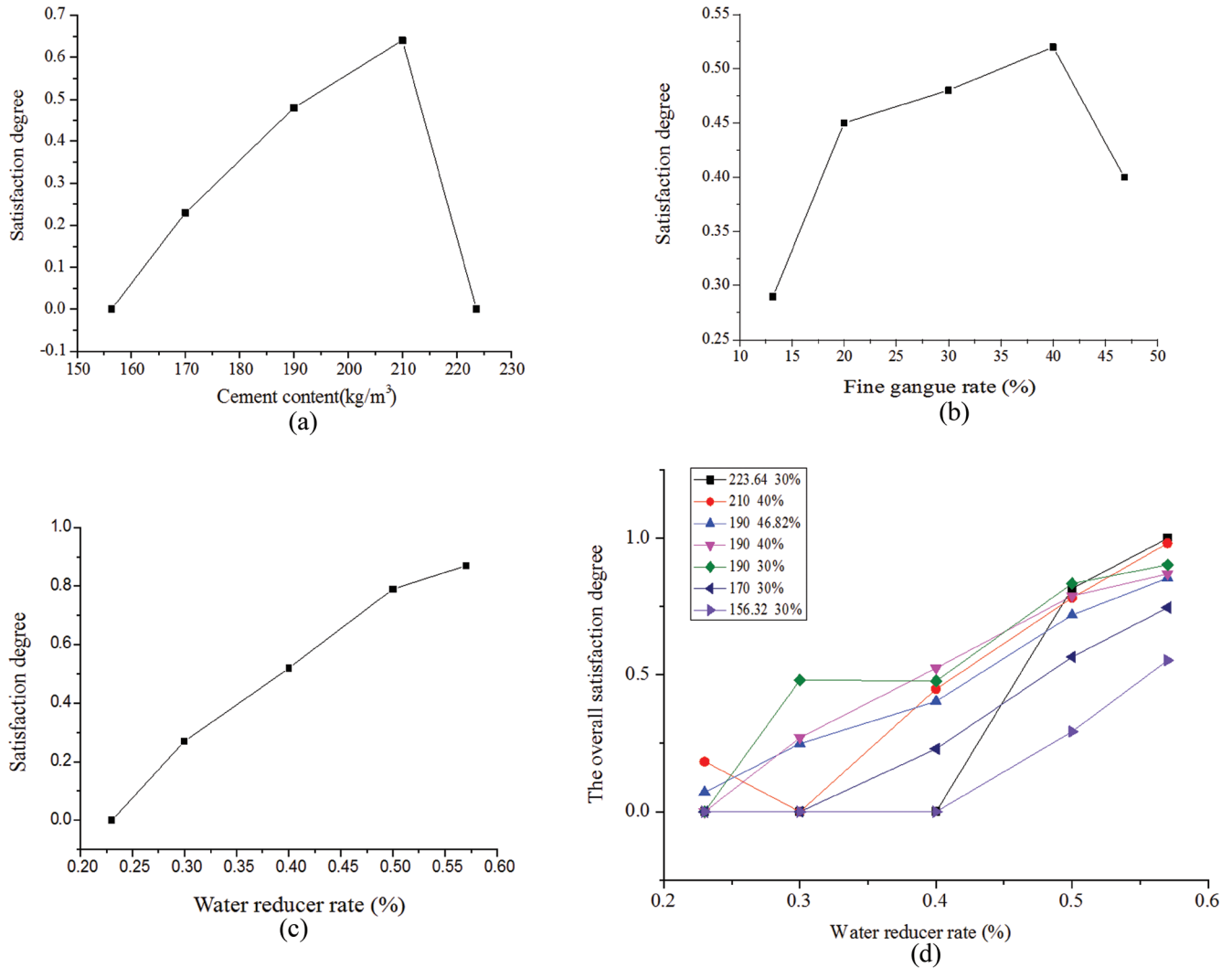


Figure 6. (a), (b), (c) CGB satisfaction degree under the single factor and (d) multi-objective combinations.

response surface function model is adopted for Plastic viscosity and UCS28. This method is able to accurately predict the test results and provides useful guides for practical design.

The fresh CGB rheological properties conform to the bingham plastic model by using type ICAR rheometer measurements to test yield stress and plastic viscosity. The relevant rheological parameter can realize the quantitative evaluation on the properties of fresh CGB transport.

Based on the response surface function, an overall satisfaction function of CBG is established to evaluate the performance of CGB. The study shows that the satisfaction degree increases quickly with the increase of water reducer content. Meanwhile the satisfaction degree first increases and then decreases with the increase of cement and fine gangue rate. It reaches the highest value at cement content of 210 kg/m³ and fine gangue

rate of 40%. Therefore, the optimal mixing proportion is suggested.

6. ACKNOWLEDGEMENTS

This research is supported by the National Science Fund for Excellent Young Scholars (No.51422404), the National Natural Science Foundation of China (No.51174142, 51574172), the Key Scientific and Technological Coal Projects of Shanxi Province (MQ2014-12), the Program for the Innovative Talents of Higher Learning Institutions of Shanxi, the Program for New Century Excellent Talents in University of China (NCET-11-1036), the Fok Ying Tung Education Foundation (No.132023), the Scientific and Technological Achievements Promotion Project of Shanxi Province (No.2013071050) and Postgraduate Innovate Project of Shanxi Province (No.800104/02100739).

7. REFERENCES

- Bell F.G., Stacey T.R., Genske D.D., Mining subsidence and its effect on the environment: some differing examples, *Environ. Geol.*, Vol. 40, No. 1, 2000, pp. 135–152. <http://dx.doi.org/10.1007/s002540000140>
- Tiwary R.K., Environmental impact of coal mining on water regime and its management, *Water Air Soil Pollution*, Vol. 132, No. 1, 2001, pp. 185–199. <http://dx.doi.org/10.1023/A:1012083519667>
- Miao X.X., Qian M.G., Research on green mining of coal resources in China: current status and future prospects, *J. mining & Safety Eng.*, Vol. 26, No. 1, 2009, pp.1–14.
- Khaldoun A., Ouadif L., Baba K., Bahi L., Valorization of mining waste and tailings through paste backfilling solution, Imiter operation, Morocco, *Int J. Min Sci Tech*, Vol. 26, No. 3, 2016, pp. 511–516. <http://dx.doi.org/10.1016/j.ijmst.2016.02.021>
- Yang B.G, Li Y.L, Dang P., Peng Y.H., Wang Y.K, Influence of fly ash on performance of high concentration cemented backfill material in coal mine, *J. Chem. Pharm. Res.*, Vol. 7, No. 2, 2015, pp. 351–3561.
- Qi T.Y, Feng G.R., Zhang Y.J., Guo J., Guo Y.X., Effects of fly ash content on properties of cement paste backfilling. *J. Residuals Sci Tech*, Vol. 12, No. 3, 2015, pp. 133–141. <http://dx.doi.org/10.12783/issn.1544-8053/12/3/3>
- Yilmaz E., Kesimal A., Ercikdi B., Strength properties in varying cement dosages for paste backfill samples. In: *Proceedings of the 10th International Conference on Tailings and Mine Waste, Balkema, Swets and Zeitlinger*, Lisse12-15 October, Colorado, USA, 2003, pp. 109–114.
- Chang Q.L., Zhou H.Q., Qin J.Y., Using Artificial Neural Network Model to Determine the Prescription of Paste Filling Materials, *J mining & Safety Eng.*, Vol.26, No.1, 2009, pp. 74–77.
- Feng G.R, Ren Y.F, Zhang X.Y. The activating experimental research of fly ash for mining filling material in Tashan Mine, *J. China Coal Society*, Vol. 36, No. 5, 2011, pp. 732–737.
- Yao Y. and Sun H.H., Characterization of a new silica alumina-based backfill material utilizing large quantities of coal combustion byproducts, *Fuel*, Vol. 97, 2012, pp. 329–336. <http://dx.doi.org/10.1016/j.fuel.2012.01.057>
- Zheng B.C, Zhou H.Q., He R.J., Experimental research on coal gangue paste filling material, *J. Mining & Safety Eng.*, Vol. 23, No. 4, 2006, pp. 460–463.
- Qi T.Y, Feng G.R, Li Y.R, Guo Y.X., Effects of Fine Gangue on Strength, Resistivity, and Microscopic Properties of Cemented Coal Gangue Backfill for Coal Mining, *Shock and Vibration*, Vol. 2015, Article ID 752678, 11 pages.
- Wu D., Yang B.G., Liu Y.C., Transportability and pressure drop of fresh cemented coal gangue-fly ash backfill (CGFB) slurry in pipe loop. *Powder Technol.*, Vol. 284, 2015, pp. 218–224. <http://dx.doi.org/10.1016/j.powtec.2015.06.072>
- Kesimal A., Ercikdi B., Yilmaz E., The effect of desliming by sedimentation on paste backfill performance, *Miner. Eng.*, Vol. 16, No. 10, 2003, pp. 1009–1011. [http://dx.doi.org/10.1016/S0892-6875\(03\)00267-X](http://dx.doi.org/10.1016/S0892-6875(03)00267-X)
- Fall M., Benzaazoua M., Ouellet S., Effect of tailings properties on paste backfill performance. In: *Proceedings of the 8th International Symposia on Mining with Backfill, Beijing, China, 2004*, pp. 193–202.
- Ren A., Feng G.R., Guo Y.X., Influence on performance of coal mine filling paste with fly ash, *J. China Coal Society*, Vol. 39, No. 12, 2014, pp. 2374–2380.
- Zhou Y. Experimental study on the effect caused by water reducer on concrete, *Concrete*, Vol.11, 2012, pp. 86–88.
- Box G.E.P., Wilson K.B., On the experimental attainment of optimum conditions, *J. Royal Stat. Soc.*, Vol. 13, No. 1, 1951, pp. 45–65.
- Xie H.B., Liu F., Fan Y.R., Workability and proportion design of pumping concrete based on rheological parameters. *Constr and Build Mater.*, Vol. 44, 2013, pp. 267–275. <http://dx.doi.org/10.1016/j.conbuildmat.2013.02.051>
- Fall M., Benzaazoua M., Modeling the effect of sulphate on strength development of paste backfill and binder mixture optimization, *Cement Concrete Res.*, Vol. 35, No. 2, 2005, pp. 301–314. <http://dx.doi.org/10.1016/j.cemconres.2004.05.020>
- Zhang X.G. 2013. *The study of key techniques of coal paste filling*, Beijing, China: Coal Industry Publishing Press.
- Khanchi A.R., Sedighi H., Ansar S., Fasihi J., Preconcentration of rare earth elements from Iranian monazite ore by spiral separator using multi-response optimization method, *Int J. Min Sci Tech*, Vol. 24, No. 1, 2014, pp. 117–121. <http://dx.doi.org/10.1016/j.ijmst.2013.12.020>
- Derringer, G., Suich, R., Simultaneous optimization of several responses variables, *J. Qual Technol.*, Vol. 12, No. 4, 1980, pp. 214–219.
- Fall M., Benzaazoua M., Mix proportioning of underground cemented tailings backfill. *Tunn Undergr Sp Tech.*, Vol. 23, No. 1, 2008, pp. 80–90. <http://dx.doi.org/10.1016/j.tust.2006.08.005>

Systematic Approach to Identifying Economically Feasible and Environmentally Benign Methods of Recycling Ash on a Regional Scale

IVAN DEVIATKIN*, JOUNI HAVUKAINEN and MIKA HORTTANAINEN

Department of Sustainability Science, School of Energy Systems, Lappeenranta University of Technology,
Skinnarilankatu 34, 53850, Lappeenranta, Finland

ABSTRACT: This study systematically assessed and compared four ash recycling possibilities, namely forest fertilization, landfill construction, road construction, and road stabilization through the use of cost-benefit analysis and life cycle assessment methods. The results indicated that forest fertilization with ash was the most economically attractive method with a 60% increase in the net present value compared to ash landfilling, while reducing the environmental impact by 0.3%. On the contrary, road construction with ash resulted in a 13% reduction in the environmental impact and an increase in net present value of 25%. Landfill construction with ash was overall the least attractive proposition.

INTRODUCTION

ASH, which results from the combustion of solid fuels, is generated in large amounts throughout the world. The mass of fly ash generated during coal combustion is estimated to be 750×10^6 t globally [1,2]. Taking into account the fact that the percentage of fly ash in the total amount of ash generated is 85% [1,3], the total amount of ash generated via coal combustion is around 880×10^6 t. Vassilev *et al.* [4] estimated that approximately 476×10^6 t of biomass ash is generated via the combustion of biomass. In total, the amount of ash generated globally is around 1.4×10^9 t, which is nearly equal to the mass of municipal solid waste generated globally at 1.3×10^9 t [5].

According to Iyer and Scott [6] and Wang [7], less than 25% of the coal fly ash that is generated throughout the world on an annual basis is recycled. However, more recent statistics and recent reviews indicate that the recycling rates of fly ash are significantly higher: 46% in the USA [8], 60% in India [1], and 67% in China [1]. Primary ash recycling methods include cement and concrete production and mine backfilling [1–3]. There are several methods of recycling biomass avail-

able [9–11]. However, no aggregated data about the recycling rates is currently available.

Approximately 1.6×10^6 t of ash was generated in Finland in 2006. In terms of composition, 60% of this ash came from coal combustion, 30% from peat and wood co-combustion, and the remaining from the mono-incineration of either peat or wood [12]. Recycling rates vary significantly from plant to plant within the range of 5–100% for coal ash, 25–100% for peat and biomass ash, and 0–100% for residues from waste incineration [13]. Peat and woody biomass are mainly combusted by the Finnish pulp and paper industry. From 2011 onwards, with the publication of the waste act 646/2011, the amount of ash that was recycled increased by up to 80%, with most of the ash being utilized in earth construction and forest fertilization [14].

In addition to the fact that ash has technical applications that make it suitable for certain recycling methods, further motivating factors that underpin efforts to increase the amount of ash that is recycled are the economic feasibility of such recycling efforts and the environmental benefits they bring [3,9]. However, the use of ash to replace the ordinary utilized raw materials is economically impractical in some situations. This is partly explained by the low price of conventional raw materials, as well as the probably economic risks associated with the use of ash as it generally has an unpredictable composition. It is only through the implementation of appropriate economic regulations, primarily

*Author to whom correspondence should be addressed.
Permanent address: Laboratory of Environmental Engineering, Lappeenranta University of Technology, Skinnarilankatu 34, 53850, Lappeenranta, Finland. Email: ivan.deviatkin@lut.fi; Tel: +358 40 7619673

increased landfill taxes [15], that waste recycling initiatives can be promoted to ensure that the advantages of avoiding ash landfilling cover the expenses of ash recycling and the risks embodied there.

Although recycling is known to have many positive benefits from an economics perspective, research on the specific economic impact of recycling is scarce [2,3,6,9]. This study assessed the economic feasibility of recycling the ash that is generated within a chosen case study area located in Finland through the application of a cost-benefit analysis (CBA) method. The results of a previously performed life-cycle assessment study [16] were weighted and combined with the results of the current CBA study to generate recommendations concerning the economic and environmental impacts of four ash recycling methods.

MATERIALS AND METHODS

Economic analysis was performed by applying the CBA methodology introduced by James and Predo [17], which was built upon the study by Boardman *et al.* [18]. Figure 1 illustrates the steps involved in a conventional CBA study. Steps 1–6 of a conventional CBA are identical to the goal and scope definition phase and to the life cycle inventory stage of a conventional life cycle assessment (LCA) study. Since the LCA study was previously performed by the authors [16], steps 1–6 will only be briefly described in this paper. The rest of the CBA steps, 7–10, were included in the study scope. Step 7 is described in the methodology section, while steps 8–10 are described in the results and recommendations sections. In addition, the results of the

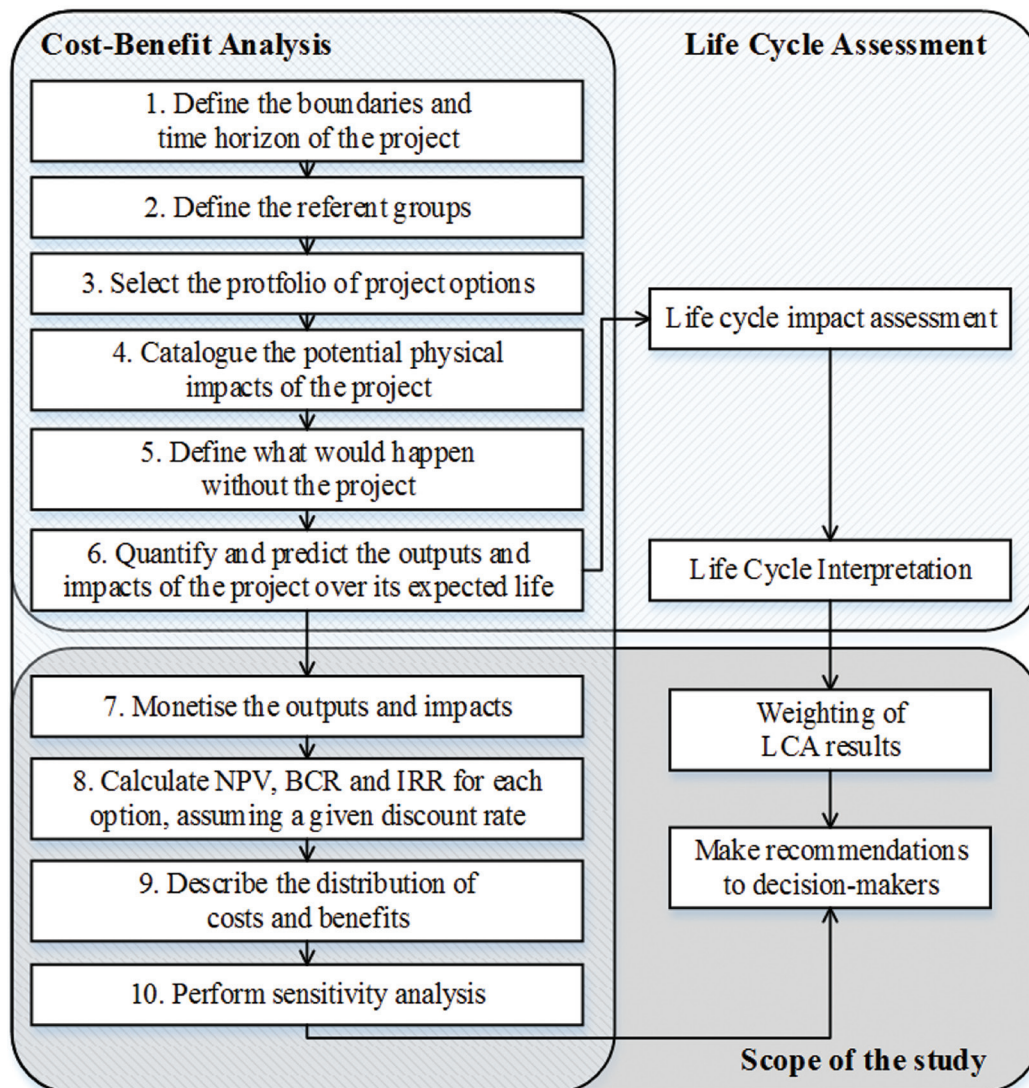


Figure 1. Scope of the present study based on the integration of a cost-benefit analysis [17] and a life cycle assessment method [16].

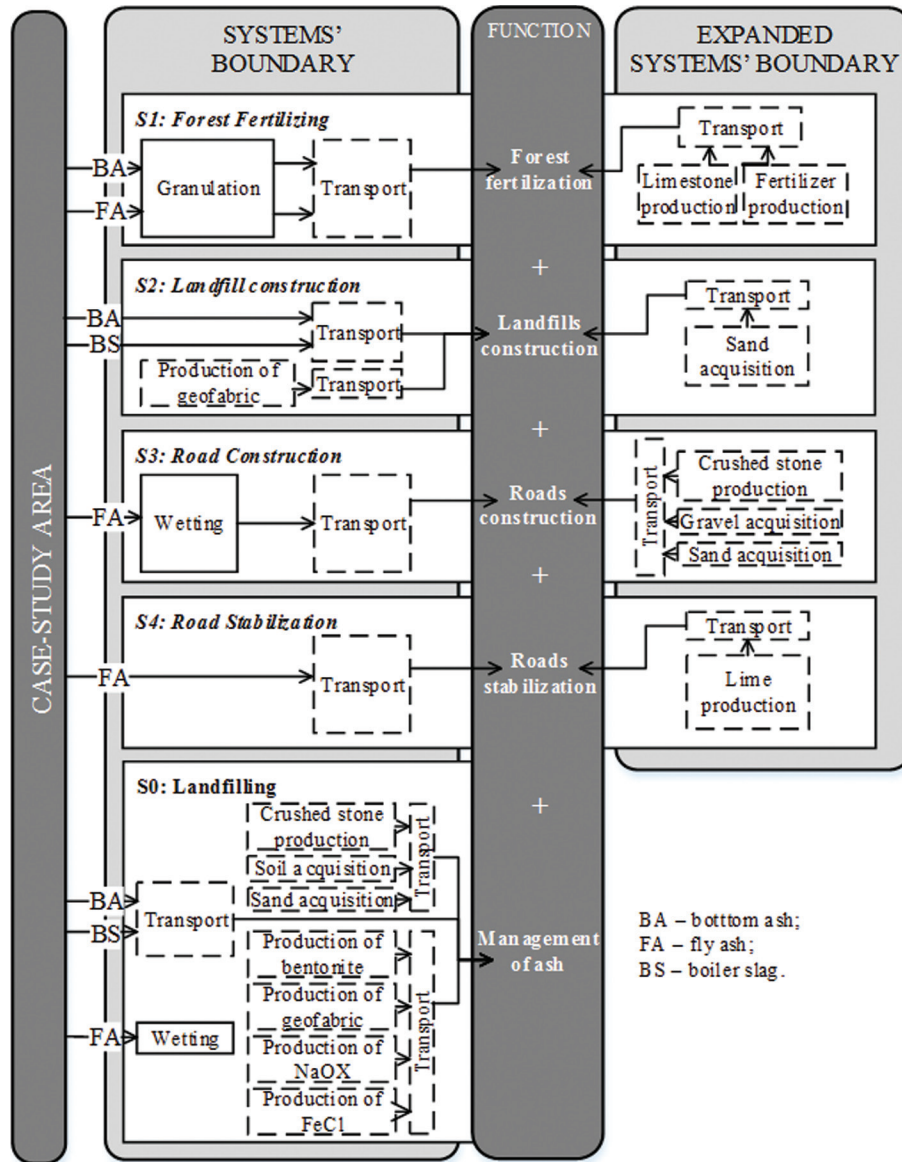


Figure 2. System boundaries of the study.

previously conducted LCA study were weighted and included in the scope of the present study to aggregate values from several categories of environmental impact into a single value to be employed to compare each of the respective recycling methods.

System Boundaries, Scenarios, and Inventory Data

The Southeast region of Finland was chosen as the case study area in this research. Eight ash generating units were identified in the region, and these produce an average annual amount of fly ash of 58,400 t, and bottom ash and boiler slag of 35,100 t. The function of the system was determined in accordance with the scenarios included in the study and formulated as man-

agement of ash generated in the case study area, fertilization and neutralization of forest soil, construction of landfills, construction of roads, and stabilization of roads. The system boundaries of the study are presented in Figure 2.

Description of Scenarios

Overall, four alternative utilization scenarios were assessed as part of this study along with a reference scenario that was ash landfilling. The selection of the alternatives was determined in accordance with the general practices in the region, whereas applicability of certain residues was determined by ash composition and legal requirements. Ash that was not suitable for

a certain utilization method was assumed to be land-filled.

The first scenario involved forest fertilization and neutralization with ash (S1-FF), where fly and bottom ashes were assumed to be granulated, transported to a utilization site, and spread over the forest area. An alternative method of fertilizing the forest would be through the use of commercial fertilizer and limestone. The second recycling scenario was the use of ash in the construction of landfills (S2-LC) where bottom ash and boiler slag were assumed to be used for landfill construction in a cover layer. Geofabric would be required when using ash. Alternatively, the layer would be constructed using sand. The third recycling scenario was road construction (S3-RC) where fly ash was assumed to be wetted, transported to a utilization site, and used as a sub-base layer of a road. An alternative to ash in this process would be gravel. However, as the other layers of a road would be affected when ash was utilized as a sub-base layer, the additional materials required to build a base course and a protection layer were included in the study. The fourth recycling scenario was road stabilization (S4-RS), where dry fly ash was assumed to be transported to a utilization site and mixed with weak soil using an excavator. An alternative method of stabilizing a road would be through the use of fine lime.

Regional Optimization Scenarios

In addition to the alternative utilization methods included in the study, regional optimization scenarios were identified due to the high degree of uncertainty related to the distances that ash would be transported from the location at which they were generated to their place of utilization. Moreover, the studied utilization possibilities imply single time utilization of residues in one particular place meaning that the transportation distance to the utilization place would vary.

Three regional optimization scenarios were identified: a local scenario (SL), which implied that ash was pretreated at a location close to its place of generation and within 20 km of the place at which it was utilized; a regional scenario (SR), which implied that ash was transported to regional centers for possible pretreatment and storage before being transported up to 50 km to a final utilization place; and a case study area scenario (SA), which implied that the ash was transported to the center of the case study area for pretreatment before being transported up to 100 km to a final utilization place.

Monetization of the Outputs and Impacts

All processes included in the present study were determined using the LCA that was previously performed by Deviatkin *et al.* [16]. As can be observed in Table 1, each process either incurred additional costs or delivered benefits to the system studied. The prices used in the study were free of value added tax (VAT).

Granulation of Ash

The cost of the granulation unit was included in the first scenario since granulation cannot be performed using conventional machinery. The cost of this granulation process included the capital cost of the granulation unit itself and the associated operating expenditures. The cost of granulation was calculated as follows:

$$C_G^{TR} = N_G \cdot CAPex + Q_G^{TR} \cdot OPex \quad (1)$$

where N_G is the number of granulation units, $CAPex$ the capital expenditure, €/unit; Q_G^{TR} the mass of ash to be granulated, t, and $OPex$ the operating expenditures in €/t. The mass of ash to be granulated was 55,700 t. The number of granulation units for the local scenario was set equal to the number of ash generating units; i.e., eight, for the regional scenario—two, and for the case study area wide scenario—one.

Operating and capital expenditures were applied from the study by Pekkala [19]. The investment costs of a single granulation unit were converted into annual payments using the capital recovery factor as follows:

$$\begin{aligned} C_{GU,a} &= I_{GU} \cdot \frac{i(1+i)^n}{(1+i)^n - 1} \\ &= 1,404,000 \cdot \frac{0.05(1+0.05)^{15}}{(1+0.05)^{15} - 1} = 136,000\text{€} \end{aligned} \quad (2)$$

where I_{GU} is the investment cost of a single granulation unit in €; i is the social discount rate, which was assumed to be 5% [20]; and n is the service life, which was assumed to be 15 years. In addition to the cost of the granulation unit, the annual cost of personnel, 45×10^3 €, maintenance cost, 2×10^3 €, insurance cost, 5×10^3 €, and sampling and quality control cost, 10×10^3 € were included. All together, the annual capital expenditures were 198×10^3 €. The operating expenditures included the costs of water, heat, and electricity, which were 1.3 €/m³, 20 €/MWh, and 37.1 €/MWh respectively.

Table 1. Categories of Costs and Benefits Included in the Study.

	Scenario 1 Forest Fertilization	Scenario 2 Landfill Construction	Scenario 3 Road Construction	Scenario 4 Road Stabilization	Scenario 0 Landfilling
Cost categories	<ul style="list-style-type: none"> Granulation of ash Transportation of ash Spreading of ash Cost of unqualified ash landfilling^a 	<ul style="list-style-type: none"> Transportation of ash Cost of geofabric^b Cost of unqualified ash landfilling 	<ul style="list-style-type: none"> Transportation of ash Cost of unqualified ash landfilling 	<ul style="list-style-type: none"> Transportation of ash Cost of unqualified ash landfilling 	<ul style="list-style-type: none"> Waste tax Cost of landfill maintenance Transportation of ash
Benefit categories	<ul style="list-style-type: none"> Cost of commercial fertilizer Cost of limestone Transportation of materials Spreading of materials 	<ul style="list-style-type: none"> Cost of sand Transportation of sand 	<ul style="list-style-type: none"> Cost of sand Cost of gravel Cost of crushed stone Transportation of materials 	<ul style="list-style-type: none"> Cost of lime Transportation of lime 	

^aThe cost was calculated as the total cost of landfilling in S0-LF for the amount of ash unqualified for a certain utilization possibility.

^bThe shipping cost of geofabric was assumed to be included in the cost of the geofabric itself.

Transportation of Materials

The cost of transporting all materials, with the exception of ash, was calculated as follows:

$$C_T^i = \frac{Q_T^i}{PL} \cdot \frac{c_{TR} \cdot (2 \cdot d_T^i)}{v_T} \quad (3)$$

where Q_T^i is the mass of material i to be transported, t ; PL is the payload of a single vehicle, t ; c_{TR} is the specific cost of renting a single vehicle, €/h; d_T^i is the one-way distance to transport material i in km; and v_T is the velocity of transportation in km/h. The material masses and transportation distances are presented in Table 2. The payload of a single vehicle was assumed to be 25 t as implemented in MELI software [21] which was used in the previously performed LCA study. The materials were assumed to be transported by dump trucks, which are widely used for the transportation of loose materials. The specific cost of renting a single dump truck in 2014 was 70 €/h [22]. The velocity of a dump truck was set to 60 km/h.

The cost of ash transportation was calculated as follows: $C_T^{tr} = C_{T,CP}^{tr} + C_{T,FP}^{tr}$, where $C_{T,CP}^{tr}$ is the cost of ash transportation to a collection point, €; and $C_{T,FP}^{tr}$ is the cost of ash transportation from a collection point to a final utilization place, €. The cost of ash transportation to a collection point was calculated as follows:

$$C_{T,CP}^{tr} = \frac{\Sigma(Q_u^{tr} \cdot d_{CP}^{tr}) \cdot c_{TR} \cdot 2}{PL \cdot v_T} \quad (4)$$

where Q_u^{tr} is the mass of ash generated in a unit u , t ; and d_{CP}^{tr} is the distance from an ash generating unit u

to a collection point, km. The cost of ash transportation from a collection point to a final utilization place was calculated as follows:

$$C_{T,FP}^{tr} = \frac{Q_{CP}^{tr}}{PL} \cdot \frac{c_{TR} \cdot (2 \cdot d_{FP}^{tr})}{v_T} \quad (5)$$

where Q_{CP}^{tr} is mass of ash to be transported from a collection point to a final utilization place, t ; and d_{FP}^{tr} is the distance from a collection point to a final utilization point, which was 20 km for SL, 50 km for SR, and 100 km for SA. The masses of ash to be transported are presented in Table 2 and the distances the ash were transported are presented in Table 3.

Table 2. Mass and Transportation Distances of the Substitute Materials and Ash.

Scenario	Material	Q_T^i	d_T^i , km	Q_u^{TR}	Q_{CP}^{TR}
S1-FF	• Commercial fertilizer (t)	24,830	100		
	• Limestone (t)	23,470	100		
	• Ash (t)			55,700	66,880
S2-LC	• Sand (t)	50,360	50		
	• Geofabric (m ²)	29,283	–		
	• Ash (t)			31,440	31,440
S3-RC	• Sand (t)	31,440	50		
	• Gravel (t)	76,010	50		
	• Crushed stone (t)	27,780	10		
	• Ash (t)			58,450	58,450
S4-RS	• Lime (t)	19,960	50		
	• Ash (t)			58,450	58,450
S0-LF	• Ash (t)			93,580	93,580

Table 3. Distances Between Ash Generating Units and Collection Points in the Regional Optimization Scenarios.

Distance (km)	Ash Generating Units Studied							
	Metsä Simpele	UPM Kaukas	Stora Enso Imatra	UPM Kymi	Stora Enso Anjalakoski	Karhula Heating Plant	Hovinsaari CHP	Hyötyvoimala CHP
Local Scenario (SL)	0	0	0	0	0	0	0	0
Regional Scenario (SR)	61	17	27	21	9	44	42	6
Case-study area scenario (SA)	120	47	85	56	64	78	76	60

Cost of Spreading the Materials in the Forest

The cost of spreading was calculated as follows:

$$C_S^{tr} = Q_S^i \cdot c_S \quad (6)$$

where Q_S^i is the mass of material i to be spread, t ; and c_S is the specific cost of spreading, €/t. The specific cost of aerial spreading was 60 €/t for ash and 200 €/t for commercial fertilizer and limestone, while the cost of ground spreading was 50 €/t for ash and 130 €/t for artificial fertilizer and limestone [19].

Cost of Materials

The cost of each material used in the study was calculated as follows:

$$C_i = Q_i \cdot c_i \quad (7)$$

where Q_i was the mass of the material i consumed [16], t ; and c_i was the price of material i in €/t (Table 4).

Waste Tax

All waste deposited in landfills is a subject to waste tax. As of 2015, the waste tax was 55 €/t [27]. The total cost paid as the waste tax was calculated as follows:

$$C_{LF}^{tr} = Q_{LF}^{tr} \cdot c_{WT} \quad (8)$$

where Q_{LF}^{tr} is the mass of ash landfilled, t ; and c_{WT} is the waste tax, €/t.

Cost of Landfill Maintenance

Disposal of ash in the landfills requires the use of machinery as well as further maintenance including leachate treatment and landfill closure. The gate fee that waste management companies charge for disposal of ash was taken into consideration in the current study because there was insufficient data available about the

cost of landfill maintenance. The cost used in the study was 45 €/t [28]. However, a cost variation between 15–55 €/t [28] was incorporated into the sensitivity analysis.

Equalization of Prices across Different Years

The prices used in the current study originated from multiple sources that were published in different years. The prices were equalized using the consumer price index recorded by the Finnish Statistics Services [29]. The prices were normalized to the year 2014. The 2015 prices were used as such. The correction calculations were performed as follows:

$$c_{i,2014} = c_{i,x} \cdot (1 + CPI_{x+1}) \cdot \dots \cdot (1 + CPI_{2014}) \quad (9)$$

where $c_{i,x}$ is the price of material i in year X ; and CPI_{x+1} and CPI_{2014} is the consumer price index starting from year $X + 1$ until year 2014. The results are presented in Table 5.

Selection of the Evaluation Criterion

Net present value (NPV) was used to compare the scenarios involved in this study. The alternative criteria that are often employed in CBA, such as benefit-cost ratio, internal rate of return, or payback time, were

Table 4. Prices of Materials Used in the Study.

Material	C_i , €/t	Reference
Commercial fertilizer	206	[23]
Limestone	26.5	[24]
Geofabric	2 ^a	assumed using prices available online
Sand	2.8	[25]
Gravel	6.5	[25]
Crushed stone	6.4 ^b	[25,26]
Lime	30	Estimated based on [24]

^aUnit €/m²;

^bAverage value from data presented in the references.

Table 5. Specific and Normalized Prices Used in the Current Study.

Scenario	Specific Price	Year X	Normalized Price
Rental of a single vehicle (€/h)	70	2014	70
CAPex of a granulation unit (€/unit)			
Equipment	136.0×10^3	2012	139.4×10^3
Personnel	45.0×10^3	2012	46.1×10^3
Maintenance	2.0×10^3	2012	2.1×10^3
Insurance	5.0×10^3	2012	5.1×10^3
Sampling and quality control	10.0×10^3	2012	10.3×10^3
OPex of a granulation unit			
Water (€/m ³)	1.3	2012	1.3
Electricity (€/MWh)	37.1	2015	37.1
Heat (€/MWh)	20.0	2012	20.5
Materials			
Commercial fertilizer (€/t)	206	2004	249
Limestone (€/t)	26.5	2012	27.1
Geofabric (€/m ²)	2.0	2015	2.0
Sand (€/t)	2.8	2014	2.8
Gravel (€/t)	6.5	2014	6.5
Crushed stone (€/t)	6.4	2014	6.4
Lime (€/t)	30.0	2012	30.8

deemed to be unsuitable for the comparison of mutually exclusive projects [20]. Since the costs and benefits were calculated for one year and investment costs were converted into annual payments, a simplified equation of the NPV for each scenario was used:

$$NPV = \frac{B - C}{(1 + i)} \quad (10)$$

where B is benefits of each scenario within one year;

C is the cost of each scenario within one year; and i is the social discount rate, which was assumed to be 5% [20]. The NPV of each utilization scenario was compared with that of the Baseline Scenario: landfilling the ash.

Weighting of the LCA Results

According to the ISO 14044 standard [30], there is no scientific basis for aggregating the life cycle impact assessment (LCIA) results into a single value. Nevertheless, weighting using the expert values gathered by a panel method is widely practiced [31]. Eskola *et al.* [32] interviewed a number of practitioners and engineers to rank the environmental impacts originating from earthworks in Finland. Their rankings were applied in the present study, which also includes the utilization of ash in earthworks. The areas of environmental concern in the study by Eskola *et al.* [32] partly differed from those included in the LCA study that was previously performed [16]. Table 6 lists the weighing factors for the impact categories covered in the current study as well as the corresponding names used by Eskola *et al.* [32].

The weighting factors were incorporated in the study to obtain a single value as follows:

$$LCA_w = \frac{\sum_i^n (WF_i \cdot LCIA_i)}{\sum_i^n WF_i}, \% \quad (11)$$

where WF_i is the weighting factor of an impact category, i , (Table 6); and $LCIA_i$ is the results of the LCIA for an impact category i presented as relative change [16], %.

Table 6. Factors Used for Weighting LCIA Results.

Impact Category (IC)	Weighting Factor (WFi)	Area of Concern According to Eskola <i>et al.</i> (1999)
Ecotoxicity potential (ETP)	66.9	Heavy metals to soil
Carcinogenic human toxicity potential (HTP _c)	66.9	Heavy metals to soil
Non-carcinogenic human toxicity potential (HTP _{non-c})	66.9	Heavy metals to soil
Resource depletion potential (RDP)	66.6a	Raw materials and fuels consumption
Global warming potential (GWP)	50.6	CO ₂ to air
Terrestrial eutrophication potential (TEP)	49.5	NO _x to air
Acidification potential (AP)	46.2b	SO ₂ and NO _x to air
Photochemical ozone formation potential (POFP)	39.9	VOC to air
Marine eutrophication potential (MEP)	39.4	N to water
Freshwater eutrophication potential (FEP)	38.6	COD to water

^aCalculated as the mean of the factors of raw material and fuel consumptions.

^bCalculated as the weighted mean of the factors of SO₂ and NO_x using the characterization factors from the acidification potential impact category [33,34].

RESULTS

Overall Results

The results of the economic analysis are presented in Figure 3 as relative changes of the NPV of each recycling scenario in relation to the NPV of the baseline scenario, ash landfilling. Furthermore, the contribution of each cost and benefit category to the overall NPV change is shown. As can be seen, all scenarios led to an increase in the NPV. The largest impact was almost 60% in the case of S1-FF when a part of fly ash and

bottom ash was utilized to fertilize and neutralize forest substituting commercial fertilizers and limestone.

The increase was mainly due to the fact that, within this scenario, the cost of distributing fertilizers and limestone in forest (45%) was avoided, as so was the cost of fertilizer (27%), and, to a lesser extent, landfilling tax and the cost of landfill maintenance (25%). The cost granulate, transport, and spread ash resulted in a NPV reduction of 20%. However, the additional costs associated with ash recycling were smaller than the benefits of eliminating industrial fertilizer and limestone procurement, transportation, and spreading.

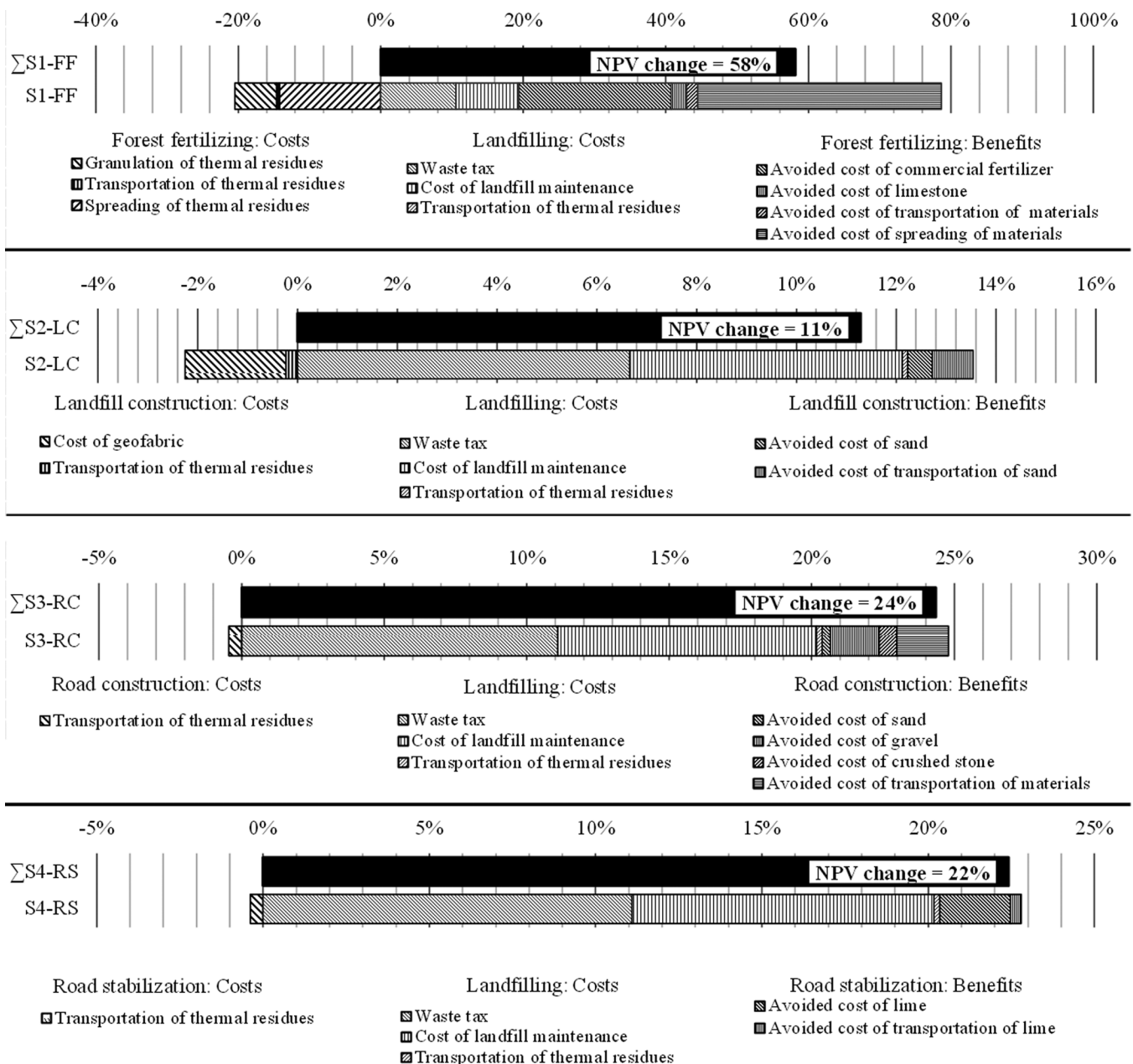


Figure 3. Overall change of the NPV of alternative scenarios studied in relation to the NPV of the baseline scenario.

The increase of the NPV in the other scenarios ranged from 11% in S2-LC to 24% in S3-RC, which was 2-5 times lower than that of S1-FF. In terms of S2-LC, 90% of the NPV increase was the result of avoiding the need to landfill the ash used construct the landfills. The cost of ash transport and the supplementary geofabric cost (19.9% of the NPV change) were, in combination, a little greater than the benefit of avoided sand acquisition (11.5% of the NPV change). Thus, construction of landfill from sand was more beneficial than ash recycling, while the economic effect was insignificant. Similarly to S2-LC, the majority of the overall NPV increase in the S3-RC and S4-RS scenarios (81–88%) resulted from preventing the ash landfilling cost. Nevertheless, as opposed to the S2-LC, the advantages of avoiding the costs of acquiring substitute materials and transportation (11–18% of the NPV change) considerably exceeded the added cost of ash recycling (1.7–1.9% of the NPV change), making ash more attractive from an economic perspective.

Regional Optimization

The results of the economic analysis of regional optimization are presented in Figure 4 in terms of the NPVs of each scenario. Overall, the results were relatively consistent in terms of the transportation distance and the number of ash pretreatment units, with the largest change in NPV being 3.1% in S1-FF. The average change in the NPV was 2% across the rest of the scenarios. In S2-LC, S3-RC, and S4-RS, the NPV was inversely proportional to the increase in transportation distance in the optimization scenarios. In S1-FF, the results were affected not only by the transportation distance, as was the case in the other scenarios, but also by the number of granulation units required for ash pretreatment. This resulted in a non-linear change in the NPV between different regional optimization scenarios. An optimal combination for S1-FF was achieved in the regional scenario (SR) where only two granulation units were required, and the transportation distance to the final utilization place was two times higher than that in the local scenario (SL). However, a further increase in the transportation distance in the case study

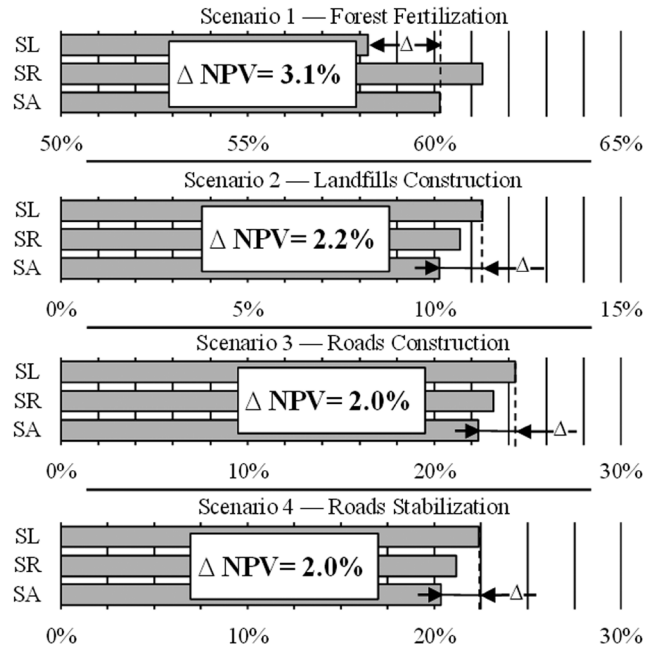


Figure 4. The NPV of regional optimization scenarios.

area scenario (SA) resulted in a lower NPV than that in the SR, even though the number of granulation units required was one.

Sensitivity Analysis

The best- and worst-case scenarios were modeled within the sensitivity analysis as a means of evaluating how possible changes in the system affected the outcomes. Table 7 presents the parameters that were employed in the sensitivity analysis along with their values. The cost of landfill maintenance and the price of commercial fertilizer were included in the analysis since these parameters were the most significant according to the CBA results.

The results of the analysis are presented in Figure 5. The difference between the best-case and the worst-case scenarios ranged from 3.6% NPV in S2-LC to 5.7% NPV in S1-FF. More than 90% of the variation in S1-FF was related to the uncertainty of the fertilizer price, whereas most of the variation in the other scenarios was related to the uncertainty of the landfill maintenance cost.

Table 7. Parameters and the Values Used in the Sensitivity Analysis.

Parameter	Scenario Affected	Expected Value	Best-case Scenario	Worst-case Scenario
Cost of landfill maintenance (€/t)	all	45	55	15
Price of commercial fertilizer (€/t)	S1-FF	249	338	186

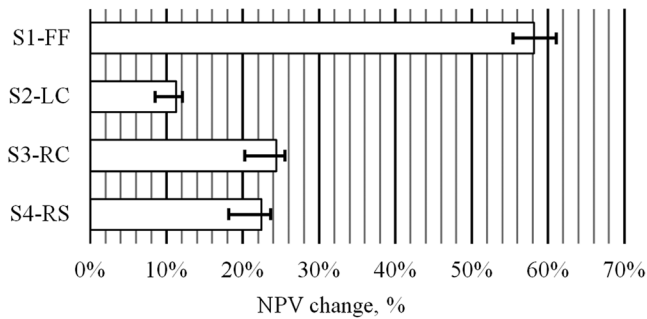


Figure 5. Results of the sensitivity analysis.

RECOMMENDATIONS

In the present study, a systematic assessment of 4 alternative recycling approaches for ash originating from eight industrial plants located within the case study area was conducted. The economic analysis was conducted via a cost-benefit analysis method. The environmental assessment was performed by weighting the results of an LCA that was previously conducted by the authors. Finally, the results of the economic analysis and the environmental assessment were combined.

The results of the cost-benefit analysis and the weighted life cycle assessment of the alternative uti-

lization scenarios are depicted in Figure 6. The economic performance is plotted on the X-axis as the net present value (NPV), while the environmental impact is presented on the Y-axis. The results are presented the relative changes attained as a result of the implementation of a certain recycling scenario compared to the baseline scenario of landfilling. The results indicate that neither of the alternative methods studied was superior in both the reduction of environmental impact and a better economic performance. Nevertheless, all scenarios resulted in an increase in the NPV. In terms of the environmental impact, all scenarios, with the exception of S2-LC, reduced the negative impact on the environment.

Economically, the utilization of 55,700 t of fly ash and bottom ash to fertilize and neutralize 176 km² of forest was the most attractive recycling method with an increased NPV of 58%. In terms of the remaining scenarios, the NPV increase was 11% in S2-LC where 35,140 t of bottom ash and slag were used to build 0.146 km² of landfills, 24% in S3-RC and 22% in S4-RS where 58,450 t of fly ash was used to build 11 km of roads or to stabilize weak soil for the construction of 3.8 km of roads respectively.

With regards to the environmental impact, the larg-

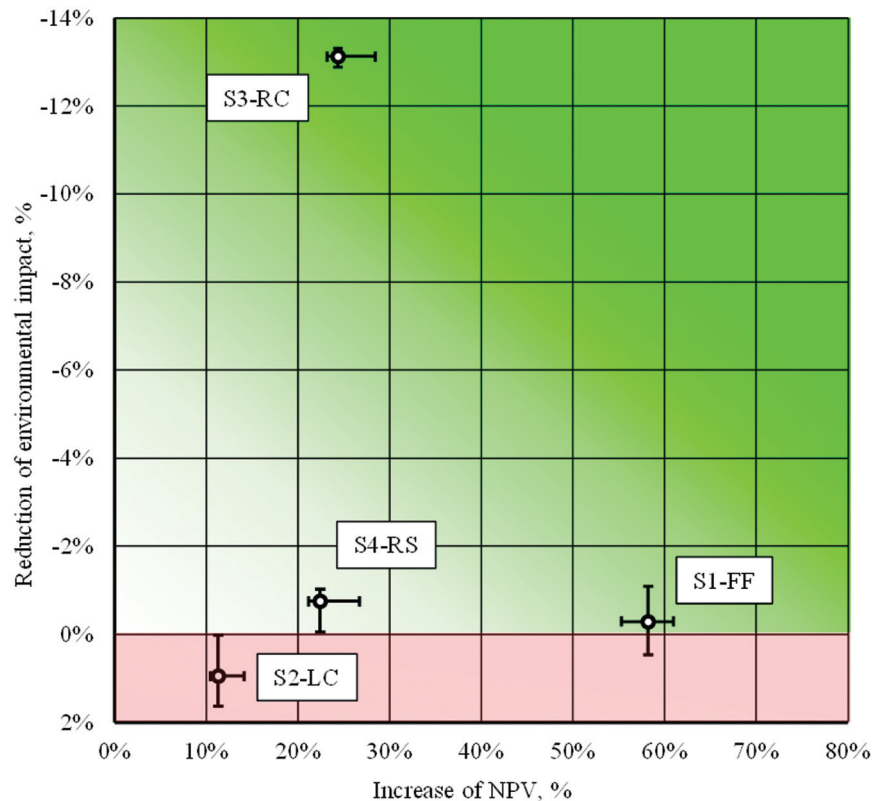


Figure 6. Combination of life cycle assessment and cost-benefit analysis results.

est reduction in environmental impact of 13% was achieved in scenario S3-RC. This was because scenario S3-RC avoided the need to acquire and transport large amount of commercial fertilizer and limestone and, therefore, reduced emissions. Moreover, utilization of ash for road construction reduces the amount of machinery required to build the road in comparison to the construction of a conventional road. Finally, reduced leaching of toxic substances through a pavement layer due to the prevention of precipitation did not increase the environmental impact. On the contrary, the use of the same amount of fly ash in S4-RS decreased the environmental impact of only 1%. The difference between S3-RC and S4-RS was caused by the difference in the road structures and the different substitute materials. S1-FF only slightly reduced the environmental impact by 0.3%. In the scenarios, there was a large reduction of the environmental impact due to prevented release of pollutants caused by the manufacturing of industrial fertilizers; however, high leaching of heavy metals from ash applied on a ground surface offset this positive impact. S2-LC was the least environmentally sound recycling approach having additional impact on the environment of 1%. Despite the toxicological impact of leaching heavy metals from ash was lower in S2-LC than it was in S1-FF and S4-RS, the impact that was avoided by acquiring substitute product was considerably smaller, yielding in an overall negative value.

Taking into consideration the findings of the economic and environmental assessments, the following recovery route for recycling the ash generated in the case study area is recommended:

1. Recycle fly ash and bottom ash for fertilization and neutralization of forest since the requirements governing the content of heavy metals in ash are the strictest;
2. Recycle fly ash in road construction and bottom ash in landfill construction where the quality of the ash does not meet the requirements for forest fertilization;
3. Recycle fly ash in road stabilization where the quality of the ash does not meet the requirements for road construction;
4. Recycle boilers slag in landfill construction;
5. Landfill the residues which are not applicable for use in any of the recycling methods studied;
6. Consider regionally centralized ash recycling processes as opposed to locally centralized systems.

ACKNOWLEDGMENTS

The research was conducted as a part of the ARVI research project, which was co-funded by Tekes, industrial companies, and research institutes. The authors are grateful to the representatives of the companies that provided us with data about ash amounts and composition.

REFERENCES

1. Z. T. Yao, X. S. Ji, P. K. Sarker, J. H. Tang, L. Q. Ge, M. S. Xia, and Y. Q. Xi, "A comprehensive review on the applications of coal fly ash," *Earth-Science Rev.*, vol. 141, pp. 105–121, Feb. 2015. <http://dx.doi.org/10.1016/j.earscirev.2014.11.016>
2. R. S. Blissett and N. A. Rowson, "A review of the multi-component utilisation of coal fly ash," *Fuel*, vol. 97, pp. 1–23, Jul. 2012. <http://dx.doi.org/10.1016/j.fuel.2012.03.024>
3. M. Ahmaruzzaman, "A review on the utilization of fly ash," *Prog. Energy Combust. Sci.*, vol. 36, no. 3, pp. 327–363, Jun. 2010. <http://dx.doi.org/10.1016/j.peccs.2009.11.003>
4. S. V. Vassilev, D. Baxter, L. K. Andersen, and C. G. Vassileva, "An overview of the composition and application of biomass ash. Part 1. Phase—mineral and chemical composition and classification," *Fuel*, vol. 105, pp. 40–76, 2013. <http://dx.doi.org/10.1016/j.fuel.2012.09.041>
5. D. Hoornweg and P. Bhada-Tata, "What a waste. A global review of solid waste management," World Bank, Washington, 2012.
6. R. Iyer and J. Scott, "Power station fly ash—A review of value-added utilization outside of the construction industry," *Resour. Conserv. Recycl.*, vol. 31, no. 3, pp. 217–228, Mar. 2001. [http://dx.doi.org/10.1016/S0921-3449\(00\)00084-7](http://dx.doi.org/10.1016/S0921-3449(00)00084-7)
7. S. Wang, "Application of solid ash based catalysts in heterogeneous catalysis," *Environ. Sci. Technol.*, vol. 42, no. 19, pp. 7055–7063, 2008. <http://dx.doi.org/10.1021/es801312m>
8. American Coal Ash Association, "Coal Combustion Product (CCP) Production & Use," 2014.
9. Y. Niu, H. Tan, and S. Hui, "Ash-related issues during biomass combustion: Alkali-induced slagging, silicate melt-induced slagging (ash fusion), agglomeration, corrosion, ash utilization, and related countermeasures," *Prog. Energy Combust. Sci.*, vol. 52, pp. 1–61, Oct. 2016. <http://dx.doi.org/10.1016/j.peccs.2015.09.003>
10. A. James, R. Thring, S. Helle, and H. Ghuman, "Ash Management Review—Applications of Biomass Bottom Ash," *Energies*, vol. 5, no. 12, pp. 3856–3873, Oct. 2012. <http://dx.doi.org/10.3390/en5103856>
11. S. V. Vassilev, D. Baxter, L. K. Andersen, and C. G. Vassileva, "An overview of the composition and application of biomass ash. Part 2. Potential utilisation, technological and ecological advantages and challenges," *Fuel*, vol. 105, pp. 19–39, 2013. <http://dx.doi.org/10.1016/j.fuel.2012.10.001>
12. K. Korpijärvi and U.-M. Mroueh, "Energiantuotannon tuhkien jalostaminen maarakennuskäyttöön," in *Uusiomateriaalien käyttö maarakentamisessa*, J. Inketöinen and E. Alasaarela, Eds. Ympäristöministeriö, 2010.
13. K. Korpijärvi, "Status of Ash Use and Legislation in Finland," no. January. 2012.
14. Finnish Forest Industries, "Email communication." 2014.
15. C. Fischer, M. Lehner, and D. L. McKinnon, "Overview of the use of landfill taxes in Europe," 2012.
16. I. Deviatkin, J. Havukainen, and M. Horttanainen, "Comparative life cycle assessment of thermal residues recovery methods," *J. Clean. Prod.*, vol. submitted, 2016.
17. D. James and C. Predo, "Principles and Practice of Cost-Benefit Analysis," in *Cost-Benefit studies of natural resource management in Southeast Asia*, D. James and H. A. Francisco, Eds. Singapore: Springle Science+Business Media, 2015, pp. 11–46. http://dx.doi.org/10.1007/978-981-287-393-4_2

18. A. Boardman, D. Greenberg, A. Vining, and D. Weimer, *Cost-benefit analysis: concepts and practice*, 4th ed. Upper Saddle River: Prentice Hall, 2010.
19. S. Pekkala, "Puun ja turpeen seospolton vaikutus tuhkan hyötykäyttökohteisiin," Lappeenranta University of Technology, 2012.
20. Nordic Council of Ministers, "Nordic guideline for cost-benefit analysis in waste management," Copenhagen, 2007.
21. U.-M. Mroueh, P. Eskola, and J. Laine-ylijoki, "Life-cycle impacts of the use of industrial by-products in road and earth construction," *Waste Manag.*, vol. 21, no. 3, pp. 271–277, Jun. 2001. [http://dx.doi.org/10.1016/S0956-053X\(00\)00100-8](http://dx.doi.org/10.1016/S0956-053X(00)00100-8)
22. M. Tiainen, "Voimalaitostuhkan Hyödyntämismahdollisuudet. Case: Kouvolan seutu," Lappeenranta University of Technology, 2014.
23. A. Korpilahti, "Tuhkan kuljetus ja levitys metsään," Metsäteho Oy, 2004.
24. "Kalkkitaulukko, nopeavaikutteinen." 2012.
25. Noormarkun Murske Oy, "Hinnasto," 2014. [Online]. Available: <http://www.noormarkunmurske.fi/hinnasto.html>. [Accessed: 21-Aug-2015].
26. EGSTONE Oy, "Hinnasto," 2015. [Online]. Available: http://sami-helin.com/index.php?option=com_content&view=article&id=50:murskeen-hinnasto&catid=36:sivuja&Itemid=143. [Accessed: 21-Aug-2015].
27. Valtiovarainministeriö, "Laki jäteverolain muuttamisesta 1072/2014," 2014. [Online]. Available: <http://www.finlex.fi/fi/laki/alkup/2014/20141072>. [Accessed: 21-Aug-2015].
28. Kymenlaakson Jäte Oy, "Keltakankaan jätekeskuksen jätetaksa 2015," 2015.
29. Statistics Finland, "Annual changes of Consumer Price Index," 2015. [Online]. Available: http://pxnet2.stat.fi/PXWeb/pxweb/en/StatFin/StatFin_hin_khi/?tablelist=true. [Accessed: 21-Aug-2015].
30. SFS-EN ISO 14044, "Environmental management—Life cycle assessment—Requirements and guidelines (ISO 14044:2006)," 2006.
31. N. Itsubo, "Weighting," in *Life Cycle Impact Assessment*, 2015, pp. 301–330.
32. P. Eskola, U.-M. Mroueh, M. Juvankoski, and A. Ruotoistenmäki, "Maarakentamisen elinkaariarviointi," VTT, Espoo, 1999.
33. M. Posch, J. Seppälä, J. P. Hettelingh, M. Johansson, M. Margni, and O. Jolliet, "The role of atmospheric dispersion models and ecosystem sensitivity in the determination of characterisation factors for acidifying and eutrophying emissions in LCIA," *Int. J. Life Cycle Assess.*, vol. 13, pp. 477–486, 2008. <http://dx.doi.org/10.1007/s11367-008-0025-9>
34. J. Seppälä, M. Posch, M. Johansson, and J.-P. Hettelingh, "Country-dependent Characterisation Factors for Acidification and Terrestrial Eutrophication Based on Accumulated Exceedance as an Impact Category Indicator (14 pp)," *Int. J. Life Cycle Assess.*, vol. 11, pp. 403–416, 2006. <http://dx.doi.org/10.1065/lca2005.06.215>

Effective Removal of Copper (II) and Cadmium (II) by Adsorbent Prepared from Chitosan-modified Magnetic Biochar

QIXUAN SONG^{1,2}, BAOSHAN YANG^{1,2,*}, HUI WANG^{1,2,*}, SHIPENG XU¹ and YANAN CAO^{1,2}

¹School of Resources and Environment, University of Jinan, Jinan 250022, China

²Shandong Provincial Engineering Technology Research Center for Ecological Carbon Sink and Capture Utilization, Jinan 250022, China

ABSTRACT: A novel chitosan-modified magnetic biochar composite (CC-Fe) was synthesized by embedding Fe₂O₃ and assembling chitosan in two-step. The properties of CC-Fe were characterized systematically by elemental analysis, Brunauer-Emmett-Teller (BET) surface area, scanning electron microscopy (SEM), Fourier transform infrared spectroscopy (FT-IR), and batch sorption processes. The prepared adsorbent composite was comprised of magnetic particulates of Fe₂O₃ and multifunctional group, and thus exhibited high sorption capability to remove copper (II) or cadmium (II) from waste water. For both copper (II) and cadmium (II), CC-Fe demonstrated a higher sorption capability (98% and 97%) than the non-chitosan magnetic biochar (11% and 7%). The sorption experimental results showed that the composite is a potential sorbent to remove copper (II) and cadmium (II). Due to its excellent magnetic characteristic, the heavy metal-laden CC-Fe could be isolated again from treated solution and reused after the desorption treatment. The functional groups of CC-Fe made efforts to the removal of heavy metals.

1. INTRODUCTION

THE waste water containing heavy metal ions has always been a serious threat to environment owing to their bioaccumulation, nonbiodegradability and toxicity even at low concentrations (Liu *et al.* 2013). It has been a potential threat to human health by consuming the polluted farm produce which accumulate heavy metal through waste water. (Chen *et al.* 2015). Therefore, the removal of various heavy metals from the discharged waste water is crucial to the environment. In order to remove the heavy metal from the waste water, the treatment techniques including biological, chemical and physical methods have been applied in the waste control (Azizi *et al.* 2011). The methods of chemical precipitation, coagulation-flocculation, reverse osmosis, membrane filtration, and ion-exchange have been implemented and documented. (Lee *et al.* 2012; Kim *et al.* 2013; Googerdchian *et al.* 2012). Although these technologies have been extensively paid much attention, the high cost, huge energy consumption, or the production of considerable toxic waste hamper their application (Mohan and Pittman 2006). Adsorption

separation, as one high-efficiency and high-cost-effective treatment technology, is widely applied in the heavy metals removal from aqueous solution (Wang *et al.* 2013; Fan and Zhang 2015).

Biochar has been considered as one low cost-efficiency adsorbents with simple preparation method and demonstrated great potential in the elimination of organic and inorganic pollutants from aqueous solutions (Beesley *et al.* 2010). However, the biochar-based adsorbents are difficult to reuse and separate after the adsorption treatment. In order to solve the deficiency and enhance biochar adsorption capacity, magnetic biochar were widely studied. A novel magnetic biochar was developed to adsorb arsenic, phosphate, and organic pollutants (Zhang *et al.* 2013). Zhou *et al.* (2014) synthesized biochar-supported zerovalent iron to remove heavy metals, phosphate, and methylene blue from artificial polluted wastewater. However, the adsorption ability of magnetic biochar was often greatly decreased due to the varied functional structure. Therefore, it is important to develop one kind of modified/engineered magnetic and recover biochar adsorbent. Chitosan is an inexpensive, easily available, renewable, and non-toxic product of the shellfish processing industry and is one of the most abundant natural polysaccharide (Kitur *et al.* 2003). Due to the high reactivity and excellent chelation characteristic, chitosan and its derivatives

*Author to whom correspondence should be addressed.

Hui Wang (hwang_118@163.com) and Baoshan Yang (stu_yangbs@ujn.edu.cn), 86-531-82767237, University of Jinan, No. 336, West Road of Nan Xinzhuang, Jinan, Shandong Province, China, 250022

were explored and used as biosorbents in the treatment of heavy metals from environment (Wu *et al.* 2010; Wang and Chen 2014). Although chitosan materials show a superior adsorption capacity to inorganic and organic contaminants (Reddy and Lee 2013), the solubility and low stability are the main disadvantages for the applications of chitosan. Therefore, chitosan has often been used as a surface modification agent to impregnate onto supporting surfaces because of its high affinity toward various heavy metal ions (Pontoni and Fabbriano 2012).

In this study, we prepared a novel chitosan-modified magnetic biochar composite by assembling chitosan with magnetic biochar/Fe₂O₃. The main aims of this study were to: (1) explore the preparation of chitosan-modified magnetic biochar composite, (2) describe the characteristics of the developed adsorbents, and (3) determine the sorption property of the composite. The developed chitosan-modified magnetic biochar adsorbent is easily operational, separated, and reused after the adsorption treatments.

2. MATERIALS AND METHODS

2.1. Materials

Maize straw was collected from Jining, Shandong Province, China for the feedstock biomass of biochar-derived magnetic composite. Ferric chloride hexahydrate (FeCl₃·6H₂O), chitosan, and acetic acid glacial (CH₃COOH, ≥99.5 w%), which grade were analytical, were purchased from Aladdin Reagent Co. Ltd. Shanghai, China. Cu and Cd stock solution were prepared by making appropriate amount Cu(NO₃)₂·3H₂O (CAS: 7758-99-8) and CdCl₂·2.5H₂O (CAS: 10022-68-1) dissolved in 1000 mL of DI water to make sure the concentrations of Cu²⁺ and Cd²⁺ were 1 g L⁻¹, respectively. The stock solutions were kept at 4°C and diluted to working concentrations before the experiment.

2.2. Sorbent Preparation

2.2.1 Biochar Preparation

Corn straw was milled to pass through 20 mesh sieves and dried for 24 h at 105°C before further treatment. The powdered biomass was pyrolyzed using a muffle furnace (SXL-1008, Shanghai Shuli Instrument Co., China). The pyrolysis temperature was increased to 700°C at a heating rate of 10°C min⁻¹ and remained unchanged at 700°C for 3h. The obtained biochar were

grounded to pass through 0.5 mm sieve and washed four times with deionized (DI) water. Ultimately, the biochars were dried at 110°C for 24 h and stored in a desiccator for experiment use. The pristine biochar was denoted as BC.

2.2.2. Preparation of Biochar/Fe₂O₃ Composite

Corn straw was washed several times and milled to pass through a 20 mesh sieve. The average size of biomass was approximately 0.8 mm. Then, the biomass was immersed into the FeCl₃ solution which was prepared by dissolving 40 g of FeCl₃·6H₂O into 60 mL of deionized (DI) water for 2 h (Zhang *et al.* 2013). The biomass which was pre-treated was pyrolyzed at 700°C using a muffle furnace. Heating rate was adjusted to 10°C min⁻¹ and then maintained stable for 3 h at targeted temperature for complete carbonization. And the pyrolysis process was under limited oxygen condition. Subsequently, biochar/Fe₂O₃ composite produced from the pyrolysis was milled and sieved, and the proportion of 0.5–0.8 mm was used after the residual ash proportion was minimized. The composite was designated as C-Fe.

2.2.3. Preparation of Chitosan-modified Magnetic Biochar Adsorbent

To make the composite sample, 3 g of the magnetic biochar was then added to 100 mL of 2% acetic acid liquid containing 3 g of chitosan. The resulting solution was stirred for 30 min. Then the magnetic biochar-chitosan homogenous suspension was dropwise added into 900 mL of 1.2% NaOH solution and kept the solution for all night long. The magnetic biochar coated over chitosan was separated by an external magnet and then washed with DI water in order to wipe of the excess of NaOH and oven-dried at 70°C for 24 h. This sample was denoted as CC-Fe.

2.2.4. Preparation of Chitosan-modified Biochar

The manufacture method was almost similar to part 2.2.3 with the substitute of magnetic biochar with biochar. And the chitosan-modified biochar were marked as CC.

2.3. The Characterizations of the Novel Composites

Elemental analyse (C, N and H) of the synthetical

adsorbent were conducted using a CHN Elemental Analyzer via high temperature catalyzed combustion and the resulting CO₂, H₂ and NO₂ gases were measured through infrared detection, respectively. The (O + N)/C and H/C atomic ratios were measured to evaluate the polarity and aromaticity, respectively. Use the methods described in Ahmad *et al.* (2013) to determine the moisture, ash, mobile matter and residual matter contents.

Brunauer-Emmett-Teller (BET) surface area was measured from N₂ isotherms at 77 K using a Surface Area and Porosimetry Analyzer (Quantachrome, Quantasorb SI). Scanning electron microscope (SEM) images were collected using a JEOL JSM-6400 Scanning Microscope. Using a Fourier Transform Infra-red Spectrophotometer (FT-IR) (Varian 640-IR; Varian, Palo Alto, CA., USA), we examined functional group on the superficial layer of adsorbents. And the target absorbance was in the range of 4000–400 cm⁻¹. The adsorbents were then blended with KBr at a ratio of 1:100 (w/w) and pressed into film.

2.4. Adsorption Experiments

50 mL solution which contained 40 mg L⁻¹ Cd(II) (or Cu(II)) solution was mixed with 0.05 g adsorbent (BC, C-Fe, CC, and CC-Fe, respectively). The suspension solution was filtered through a 0.45 μm millipore filter after shaken in a horizontal oscillating table, for 24 h, and the filtrate was collected for the downward analysis. The concentrations of Cd(II) (or Cu(II)) in the collected liquid were determined with Air-acetylene Flame Atomic Adsorption Spectrophotometer (PerkinElmer 900T, USA). Adsorption capacity was determined using the difference of concentrations of Cd(II) or Cu(II) between the initial and final aqueous. The adsorption kinetic experiments of Cd(II) (or Cu(II)) on each adsorbent (BC, CC-Fe, CC, and C-Fe) were conducted in flasks containing 50 mL of 40 mg L⁻¹ Cd(II) (or Cu(II)) and 0.05 g adsorbent at room temperature (22 ± 0.5°C). The flasks were shaken in a horizontal oscillating table. And the samples were taken from flasks using pipette at predetermined time intervals (from 10 min to 24 h) and filtered. Then the concentrations of Cd(II) (or Cu(II)) in samples were measured.

Sorption isotherm experiments of Cd(II) and Cu(II) onto the adsorbents were obtained by mixing 50 mL of heavy metal solutions of diversified concentrations in the range of 40–250 mg L⁻¹ with 1 g L⁻¹ sorbent. On the basis of adsorption kinetics experiment, the adsorption equilibrium time was chosen at 24 h. After shaking

for 24 h, the solution were sampled and filtered immediately through 0.45 μm mipor filter. And then the concentrations of Cd(II) and Cu(II) in the filtrates were measured.

3. RESULTS AND DISCUSSION

3.1. Characterization of Adsorbent

3.1.1. Elemental Analysis

The elemental compositions of the four sorbents were summarized in Table 1. It showed that the pristine biochar contained the highest C content (67.39%), in contrast, C-Fe had the lowest C content (14.60%). Similar trend was also found for O content because of the addition of Fe. But the C content of the chitosan-modified biochar was increased. Moreover, chitosan contained extra N, which also resulted in the rise of N element of CC and CC-Fe. It is general to use the molar ratios of H/C and O/C (or (O + N)/C) to determine aromaticity and polarity, respectively (Uchimiya *et al.* 2010). Although H/C ratios of pristine biochar was the lowest (H/C = 0.05) among the four adsorbents, the BC exhibits higher aromaticity compared to other biochar composites (H/C = 0.15) (Chun *et al.* 2004). On the contrary, CC and CC-Fe had a relatively higher H/C ratio which suggested that there was some residue of the original organic matter. The higher H/C ratios of C-Fe may be due to the lower C content by magnetizing processes. Compared with CC (0.47) and CC-Fe (0.50), BC also had lower ratio of O/C (0.39), indicating that it is less hydrophilic on the surface of BC. It was also proven by the ratios of (O + N)/C, which indicated the polarity of the biochar composites (CC, C-Fe and CC-Fe) became higher than that of pristine biochar (BC). These increased polarity and decreased aromaticity of biochar composites may be because of the presence of hydroxyl polarity groups and amino or γ-Fe₂O₃ (Boamah *et al.* 2015; Zhang *et al.* 2013).

Table 1. Elemental Composition of Biochar (BC), Biochar/Fe₂O₃ (C-Fe), Chitosan-modified Biochar (CC), and Chitosan-modified Magnetic Biochar (CC-Fe).

Sample	C	H	N	O	H/C	O/C	(O+N)/C
BC	67.39	3.54	1.69	26.57	0.05	0.39	0.42
C-Fe	14.60	2.18	0.40	12.32	0.15	0.84	0.87
CC	45.21	4.47	3.75	21.08	0.10	0.47	0.55
CC-Fe	28.14	4.37	3.69	14.15	0.16	0.50	0.63

Table 2. Pore Volume and Surface Area of BC, C-Fe, CC, and CC-Fe.

Biochar	BET Surface Area (m ² /g)	Total Pore Volume (cm ³ /g)	Average Pore Diameter (nm)	Micropore Volume (cm ³ /g)	Micropore Diameter (nm)
BC	7.181×10^2	9.72×10^{-1}	2.71	6.47×10^{-1}	6.63×10^{-1}
C-Fe	2.32×10^2	2.28×10^{-1}	1.97	1.14×10^{-1}	8.9×10^{-1}
CC	4.44×10^1	2.48×10^{-2}	1.12	2.48×10^{-2}	6.37×10^{-1}
CC-Fe	3.99×10^1	2.02×10^{-2}	1.01	1.61×10^{-2}	5.57×10^{-1}

3.1.2. Surface Area and Specific Pore Size Distribution

Table 2 presents the pore structure and surface area characterization of BC, C-Fe, CC and CC-Fe. The BET surface areas of the BC ($718.1 \text{ m}^2 \text{ g}^{-1}$) were superior to the other three biochar composites (232 , 44.4 and $39.9 \text{ m}^2 \text{ g}^{-1}$ for C-Fe, CC and CC-Fe, respectively). The pore volume and surface area of CC and CC-Fe decreased dramatically after the modification of chitosan. It may be inferred that some of the pore of the biochar was blocked by the chitosan and thus N_2 had less affinity for surface adsorption. In addition, the comparison of CC with CC-Fe also suggested that magnetization process reduced the pore volume and surface area.

3.1.3. Scanning Electron Microscope Analysis

Surface characteristics of the biochars before and after modification were examined by SEM-EDS (Figure

1). Compared with the original biochars [Figure 1(a)], the SEM images of C-Fe can be clearly observed some bright points [Figure 1(b)], even some hexahedron [Figure 1(c)], which indicated the existence of ferric oxide. The high content of iron in the results of EDS [Figure 1(f)] attested the above conclusion. In addition, except for the bright particulates, the surface of CC-Fe composite became thicker and rougher because of the cover of the chitosan [Figure 1(d)].

3.1.4. Fourier Transform Infrared (FTIR) Analysis

FTIR spectra and spectroscopic assignment of BC, C-Fe, CC, and CC-Fe are exhibited in Figure 2. The peaks of BC occurring at the wavenumbers of 3438 cm^{-1} and 1590 cm^{-1} corresponded to OH stretching vibration (Vuković *et al.* 2010) and carbonyl/carboxyl C=O stretching vibration (Yan *et al.* 2014), respectively. The peak at $\sim 2790 \text{ cm}^{-1}$ is connected with $-\text{CH}_2$ stretching vibration. Meanwhile, the peaks at 1439

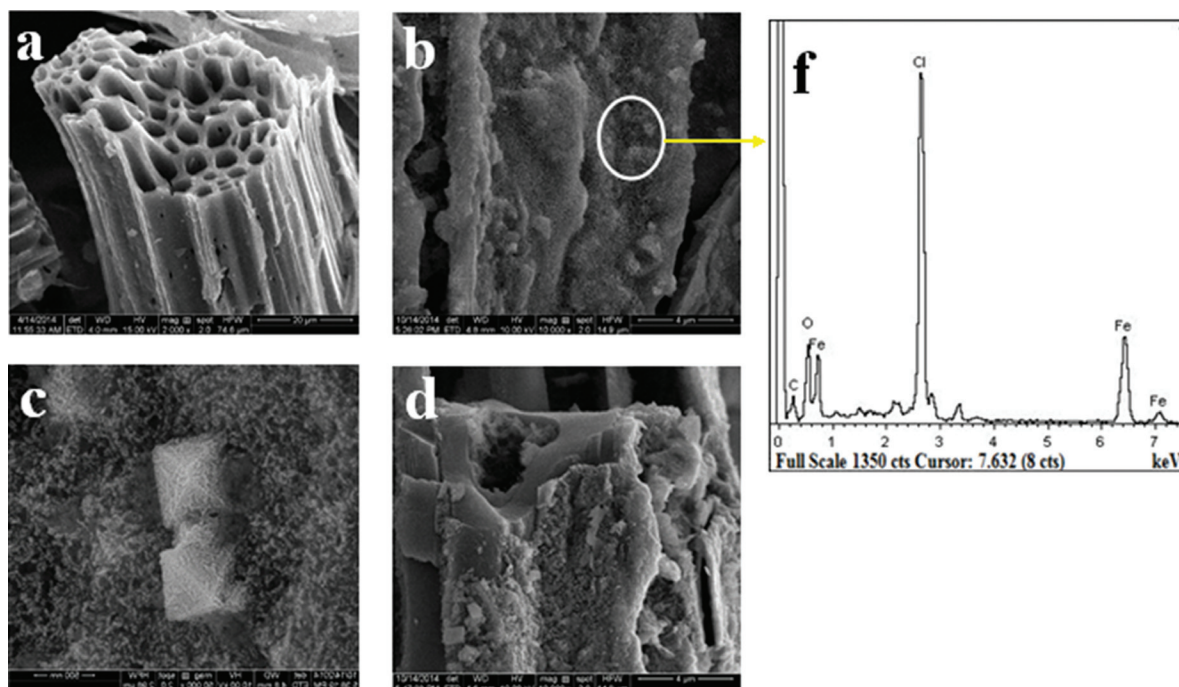


Figure 1. Scanning electron microscope (SEM) photographs of BC (a), C-Fe (b), CC (c) and CC-Fe (d); and (f) is EDS of C-Fe.

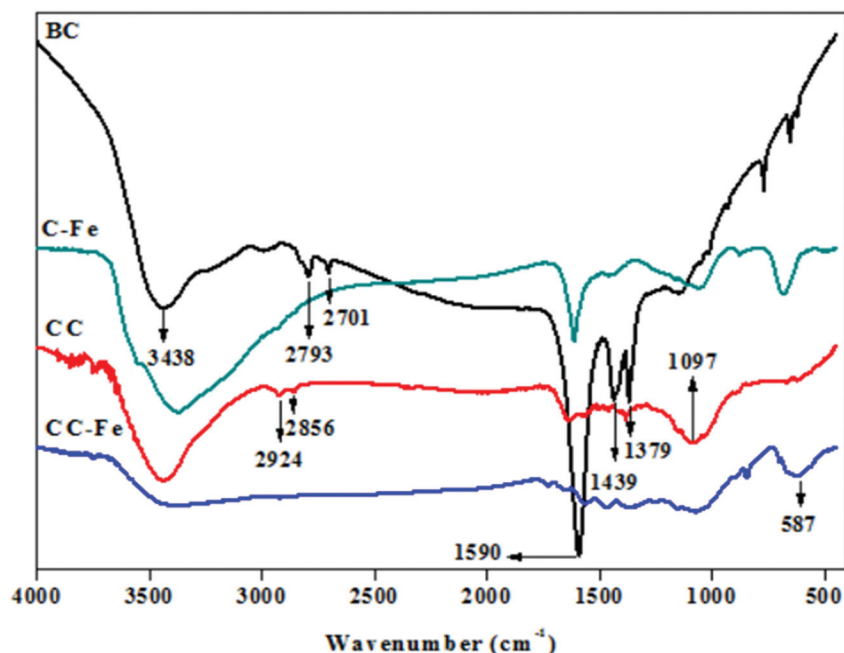


Figure 2. FT-IR spectra of BC, CC, CC-Fe and C-Fe.

cm^{-1} and 1379 cm^{-1} mainly corresponded to C-N stretching (Ma *et al.* 2014). With the same peaks of BC, C-Fe and CC-Fe have peaks at 3438 cm^{-1} and 1590 cm^{-1} which are assigned to the OH and C=O stretching vibration, respectively. Furthermore, the peak at 587 cm^{-1} is related to Fe-O characteristic band (Tarigh and Shemirani 2013), indicating Fe_2O_3 had adhered to BC and CC. C-Fe and CC-Fe have none peaks at $\sim 2790 \text{ cm}^{-1}$ indicating that the surface functional groups has changed after the magnetization of biochar compared with BC. In the spectrum of CC and CC-Fe, the peaks of 1590 cm^{-1} , 1439 cm^{-1} and 1379 cm^{-1} disappeared and the C-O stretching vibration bands at $\sim 1097 \text{ cm}^{-1}$ (Vuković *et al.* 2010) comes from amine after chitosan functionalized.

3.2. Adsorption of Cd(II) and Cu(II)

3.2.1. Adsorption Capability to Cd(II) and Cu(II)

Four adsorbents of BC, C-Fe, CC, and CC-Fe exhibited different efficiencies for Cd(II) and Cu(II) (Figure 3). The pristine biochar had a high adsorption capability to Cd(II) and Cu(II) (both almost 99%), but C-Fe which modified with magnetic property had a lower removal ratio of Cd(II) and Cu(II) (7% and 11%, respectively). In contrast, the CC and CC-Fe modified with chitosan showed good efficiency for the removal of Cd(II) and Cu(II) (97% and 98%, respectively). And these removal were higher than the previous researches

on the removal of Cd(II) and Cu(II) by adsorbents of kaolinite waste samples and limestone samples (Sdiri *et al.* 2012; Helios-Rybicka and Wójcik 2012). This meant that the removal of Cd(II) and Cu(II) by magnetic biochar adsorption sharply decreased while the high removal efficiency can be sustained by chitosan-modified magnetic biochar. These results were in consist with the removal of arsenic by the magnetic biochar (Zhang *et al.* 2013).

3.2.2. Adsorption Kinetics

Figure 4 showed the adsorption kinetics of Cd(II)

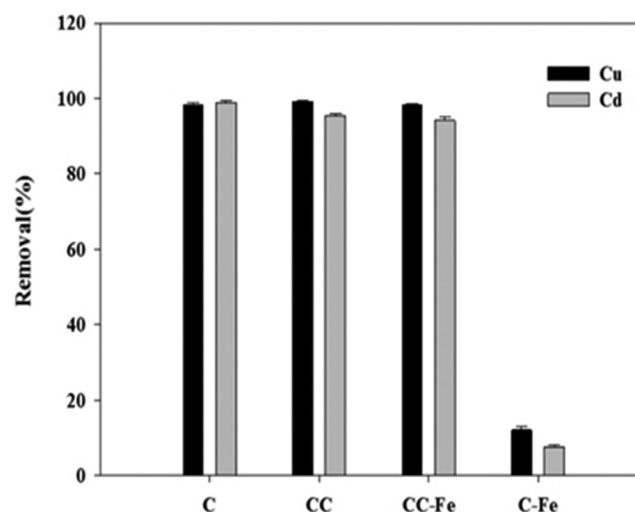


Figure 3. Effect of adsorbent on Cd(II) and Cu(II) removal.

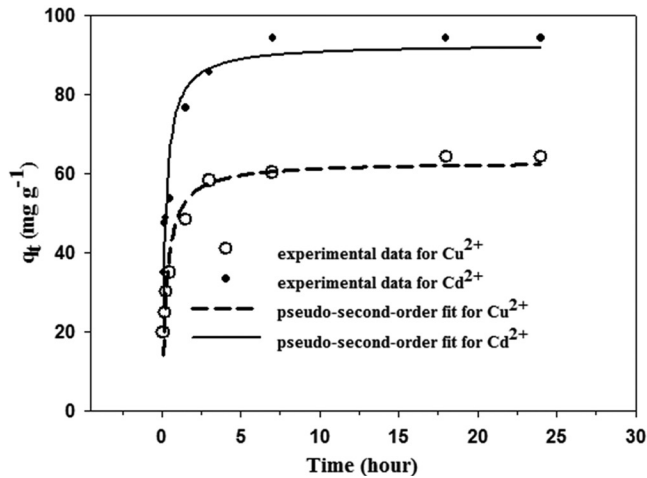


Figure 4. Adsorption kinetic for Cd(II) and Cu(II) on the CC-Fe composite.

and Cu(II) on CC-Fe which both reached sorption equilibrium within 7 h. At the beginning 3 h, the rate of Cd(II) and Cu(II) went through a rapid adsorption phase, and then leveled off. The relatively fast kinetics may be likely due to the easily accessible external surface sorption sites which could be occupied by Cd(II) and Cu(II) via physical sorption (Mohan *et al.* 2014). And specific and irreversible sorption may be the main cause of slow sorption phase (Ahmad *et al.* 2014). In this study, kinetic data which was collected by the adsorption kinetics of Cd(II) and Cu(II) were simulated by pseudo-first-order and pseudo-second-order models. The equations are listed as (Inyang *et al.* 2012):

First-order:

$$q_t = q_e(1 - e^{-k_1 t}) \quad (1)$$

Second-order:

$$q_t = \frac{k_1 q_e^2 t}{1 + k_1 q_e t} \quad (2)$$

Where q_e and q_t are the quantities of Cd(II) and Cu(II) adsorbed at equilibrium and at time t , respectively (mg g^{-1}), and k_1 (h^{-1}) and k_2 ($\text{g mg}^{-1} \text{h}^{-1}$) is pseudo first-order and pseudo second-order apparent

sorption rate constants, respectively. The fitting of the pseudo first-order Equation (1) is based on mononuclear adsorption, while pseudo second-order Equation (2) based on binuclear adsorption.

Table 3 presented the fitting data to the pseudo-first-order and the pseudo-second-order model. It showed that both of the two, models are suitable for Cd(II) adsorption, of which R^2 are 0.90 and 0.91, respectively. And the results showed both physisorption and chemisorption of Cd(II) on the adsorbent (Lu *et al.* 2012). However, the adsorption kinetics of Cu(II) fits pseudo-second-order model better ($R^2 = 0.93$) than the pseudo-first-order model ($R^2 = 0.85$), suggesting the chemisorption may dominate the sorption of Cd(II) by CC-Fe.

3.2.3. Sorption Isotherms

The sorption isotherms were generated by varying the ratio of sorbate to sorbent. Langmuir and Freundlich models (Inyang *et al.* 2012) were used to simulate the adsorption isotherms of Cu(II) and Cd(II) to the BC, CC and CC-Fe composites:

Langmuir:

$$q_e = \frac{K_L Q_m C_e}{1 + K_L C_e} \quad (3)$$

Freundlich:

$$q_e = K_F C_e^n \quad (4)$$

Where C_e is the concentration of the sorbate at equilibrium (mg L^{-1}); q_e is the amounts of Cd(II) and Cu(II) adsorbed at equilibrium (mg g^{-1}); Q_m represents the Langmuir maximum sorption amount (mg g^{-1}); K_L denotes the Langmuir adsorption capacity constant that connected with free energy (L mg^{-1}); K_F is the Freundlich adsorption constant that connected with the interaction bonding energies ($\text{mmol}^{(1-n)} \text{L}^n \text{kg}^{-1}$); and n denotes the Freundlich linearity index.

Table 4 shows the fitting parameters of Langmuir and Freundlich models. For Cd(II) and Cu(II) sorption

Table 3. Calculated Kinetics Parameters for Pseudo-First-order and Pseudo-second-order Models for the Adsorption of Cd(II) and Cu(II).

Metal	Pseudo-first-order			Pseudo-second-order		
	q_e (mg g^{-1})	K_1 (h^{-1})	R^2	q_e (mg g^{-1})	K^2 ($\text{g mg}^{-1} \text{h}^{-1}$)	R^2
Cu ²⁺	55.65 ± 3.023	2.94 ± 0.65	0.85	55.56 ± 0.156	0.01 ± 0.05	0.93
Cd ²⁺	87.62 ± 3.285	3.34 ± 0.51	0.90	83.68 ± 0.35	0.10 ± 0.0008	0.91

Table 4. Langmuir and Freundlich Isotherm Constants for Cd(II) and Cu(II) Adsorption onto Pristine Biochars (BC) and Biochar Composites (CC-Fe and CC).

Metal	Sorbent	Langmuir			Freundlich		
		Q_m (mg g ⁻¹)	K_L (L mg ⁻¹)	R^2	K_F (mg ¹⁻ⁿ L ⁿ g ⁻¹)	n	R^2
Cu ²⁺	BC	117.63 ± 2.95	2.46 ± 0.235	0.99	4.11 ± 0.287	0.28 ± 0.012	0.93
	CC-Fe	131.19 ± 5.26	0.13 ± 0.016	0.93	16.09 ± 0.188	0.38 ± 0.006	0.88
	CC	141.18 ± 1.510	0.19 ± 0.003	0.95	32.11 ± 0.763	0.26 ± 0.003	0.93
Cd ²⁺	BC	110.76 ± 1.92	20.91 ± 1.36	0.99	4.88 ± 0.244	0.21 ± 0.087	0.99
	CC-Fe	105.26 ± 0.90	0.11 ± 0.004	0.95	30.76 ± 0.772	0.25 ± 0.006	0.94
	CC	108.70 ± 0.002	0.38 ± 0.0025	0.86	53.61 ± 0.393	0.17 ± 0.001	0.85

on BC, both of the two models fit the experimental sorption data better ($R^2 > 0.93$). The Langmuir maximum sorption capacities (Q_m) of BC to Cd(II) and Cu(II) were about 110.76 mg g⁻¹ and 117.63 mg g⁻¹, respectively. As can be seen in the Table 4, the coefficient (R^2) of Langmuir model is higher than those of Freundlich model, which indicated that the adsorption of Cd(II) and Cu(II) onto adsorbents (CC and CC-Fe) were mainly driven by the Langmuir surface adsorption mechanisms. These results were consistent with the previous studied adsorption mechanisms of Cd(II) and Cu(II) by chemical adsorption on MNPs-EDTA and M-CNTs (Liu *et al.* 2013; Ihsanullah *et al.* 2015). And the Q_m of Cd(II) and Cu(II) sorption onto CC (108.70 mg g⁻¹ and 141.18 mg g⁻¹, respectively) was a little bit higher than CC-Fe (105.26 mg g⁻¹ and 131.19 mg g⁻¹, respectively). Compared with Cu(II) sorption on pristine biochar (BC), biochar composites (C-Fe and CC-Fe) had higher adsorption capacities, on the contrary, C-Fe and CC-Fe had lower Q_m of Cd(II). The possible reason is pristine biochar had a higher adsorption capacity to Cu(II) than Cd(II). And the BET analysis shows BC has the highest total pore volume and surface area followed by C-Fe, while CC and CC-Fe contain lower. However, BC, CC and CC-Fe have higher removal percentage of Cd(II) and Cu(II) than

C-Fe. It can be seen that the adsorption of Cd(II) and Cu(II) is not only connected with adsorbents surface area, but also with other properties which control the interaction between adsorbates and adsorbents. The comparison of the maximum adsorption capacities of CC-Fe toward Cd(II) and Cu(II) with those of other sorbents was shown in Table 5. A comparison of those values with that obtained in the current study showed that CC-Fe exhibited considerable capacities for copper and cadmium adsorption from aqueous solutions. The higher adsorption capacities of CC-Fe may be ascribed to both the multi-groups of biochar and chitosan. The chitosan covered on the surface of biochar adsorbed Cd(II) and Cu(II) via amino or hydroxyl groups in chitosan chains coordinated with heavy metal ions. Meanwhile, on the basis of the functional groups of the biochar, biochar uncoated chitosan also could make efforts to surface complexation and/or precipitation.

3.3. Magnetic Properties of Chitosan-modified Magnetic Biochar

A magnetic hysteresis curve for CC-Fe was used at 300°C to investigate its magnetic properties (Figure 5). The composite showed superparamagnetism properties and the saturation magnetization of CC-Fe was 9.5

Table 5. Comparison of the Cd(II) and Cu(II) Adsorption Capacities of CC-Fe and Different Adsorbents in the Literature.

Heavy Metal	Adsorbent	q_{max} (mg/g)	References
Cu ²⁺	Treating Fe ₃ O ₄ nano-particles with gum arabic	38.50	[30]
	Diatomite from Algeria	20.27	[31]
	Monodisperse chitosan-bound Fe ₃ O ₄ nano-particles	21.50	[32]
	Chitosan-modified magnetic biochar	131.19	This work
Cd ²⁺	Sodium hydroxide treated rice husk	20.24	[33]
	M-AC	15.90	[29]
	Crosslinked chitosan-clay beads	72.31	[34]
	Chitosan-modified magnetic biochar	105.26	This work

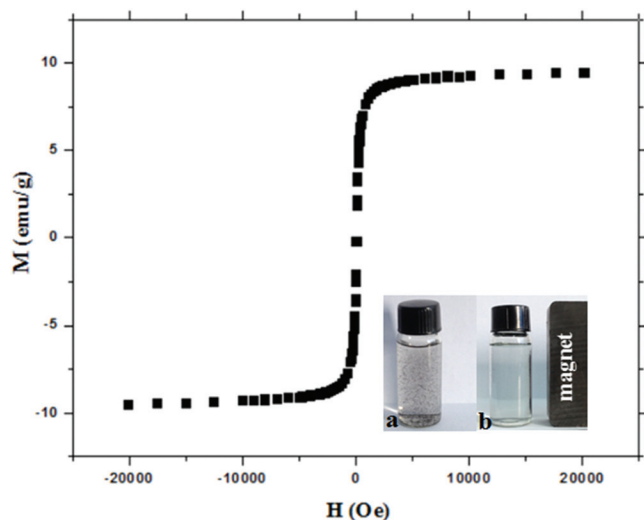


Figure 5. Magnetic hysteresis curve of CC-Fe.

emu/g which was very lower than that of pure Fe_2O_3 materials (76.0 emu/g) (Zhu *et al.* 2007). The reason may be the cover of chitosan decrease the magnetization. In addition, the small particle effect of a noncol-linear spin arrangement which appeared at the superficial layer, led to the attenuation of magnetic moment in Fe_2O_3 . However, the CC-Fe composite obviously showed a good magnetic property which made the adsorbent separated by a permanent magnet easily (Figure 5). The magnetic property of CC-Fe is crucially important for the potential recycling use in the removal of Cd(II) and Cu(II) from liquid solution.

4. CONCLUSIONS

In this work, chitosan-modified magnetic biochar was synthesized. And the CC-Fe was applied to remove heavy metals in aqueous solution. The CC-Fe not only could effectively remove Cd(II) and Cu(II) from aqueous solutions, but also can be separated easily by magnet due to its high magnetic response. The chitosan-modified magnetic biochar is a high efficiency and cost-effective adsorbent for the dislodge of Cd(II) and Cu(II). Biochar played the role as the skeleton and the functional groups of both chitosan and biochar may contribute to the removal. The recycling of the spent chitosan-modified magnetic biochar composite had great advantage over the traditional modified biochar adsorbents.

5. ACKNOWLEDGEMENTS

The study was supported by National Natural Science Foundation of China (31270586), Science and

Technology Development Plan of Shandong Province (2014GSF117029), and China Scholarship Council Foundation (201402000002).

6. REFERENCES

- A. Azizi, M. R. A. Moghaddam, M. Arami. Wood Waste from Mazandaran Wood and the Paper Industry as a Low Cost Adsorbent for Removal of a Reactive Dye. *J Residual Science and Technology*, 2011, 8(1). 21–28.
- A. Sdiri, T. Higashi, F. Jamoussi, S. Bouaziz. Effects of impurities on the removal of heavy metals by natural limestones in aqueous systems. *J Environ Manage*, 2012, 93 (1), 245–253. <http://dx.doi.org/10.1016/j.jenvman.2011.08.002>
- D. Mohan, A. Sarswat, Y.S. Ok, C.U. Pittman, Jr. Organic and inorganic contaminants removal from water with biochar, a renewable, low cost and sustainable adsorbent—A critical review. *Bioresour Technol*, 2014, 160, 191–202. <http://dx.doi.org/10.1016/j.biortech.2014.01.120>
- D. Mohan, C.U. Pittman, Jr. Activated carbons and low cost adsorbents for remediation of tri- and hexavalent chromium from water. *J Hazard Mater*, 2006, 137 (2), 762–811. <http://dx.doi.org/10.1016/j.jhazmat.2006.06.060>
- D.H.K. Reddy, S.-M. Lee. Application of magnetic chitosan composites for the removal of toxic metal and dyes from aqueous solutions. *Adv Colloid Interface Sci*, 2013, 201–202, 68–93. <http://dx.doi.org/10.1016/j.cis.2013.10.002>
- E. Helios-Rybicka, R. Wójcik. Competitive sorption/desorption of Zn, Cd, Pb, Ni, Cu, and Cr by clay-bearing mining wastes. *Appl Clay Sci*, 2012, 65–66, 6–13. <http://dx.doi.org/10.1016/j.clay.2012.06.006>
- F. Googerdchian, A. Moheb, R. Emadi. Lead sorption properties of nano-hydroxyapatite–alginate composite adsorbents. *Chem Eng J*, 2012, 200–202, 471–479. <http://dx.doi.org/10.1016/j.cej.2012.06.084>
- F.A. Ihsanullah, Al-Khalidi, B. Abusharkh, M. Khaled, M.A. Atieh, M.S. Nasser, T. Laoui, T.A. Saleh, S. Agarwal, I. Tyagi, V.K. Gupta. Adsorptive removal of cadmium(II) ions from liquid phase using acid modified carbon-based adsorbents. *J Mol Liq*, 2015, 204, 255–263. <http://dx.doi.org/10.1016/j.molliq.2015.01.033>
- F.C. Wu, R.L. Tseng, R.S. Juang. A review and experimental verification of using chitosan and its derivatives as adsorbents for selected heavy metals. *J Environ Manage*, 2010, 91 (4), 798–806. <http://dx.doi.org/10.1016/j.jenvman.2009.10.018>
- F.S. Kittur, A.B.V. Kumar, L.R. Gowda, R.N. Tharanathan. Chitosan analysis by a pectinase isozyme of *Aspergillus niger*—A non-specific activity. *Carbohydr Polym*, 2003, 53 (2), 191–196. [http://dx.doi.org/10.1016/S0144-8617\(03\)00042-0](http://dx.doi.org/10.1016/S0144-8617(03)00042-0)
- G.D. Tarigh, F. Shemirani. Magnetic multi-wall carbon nanotube nanocomposite as an adsorbent for preconcentration and determination of lead (II) and manganese (II) in various matrices. *Talanta*, 2013, 115, 744–750. <http://dx.doi.org/10.1016/j.talanta.2013.06.018>
- G.D. Vuković, A.D. Marinković, M. Čolić, M.Đ. Ristić, R. Aleksić, A.A. Perić-Grujić, P.S. Uskoković. Removal of cadmium from aqueous solutions by oxidized and ethylenediamine-functionalized multi-walled carbon nanotubes. *Chem Eng J*, 2010, 157 (1), 238–248. <http://dx.doi.org/10.1016/j.cej.2009.11.026>
- H. Lu, W. Zhang, Y. Yang, X. Huang, S. Wang, R. Qiu. Relative distribution of Pb^{2+} sorption mechanisms by sludge-derived biochar. *Water Res*, 2012, 46 (3), 854–862. <http://dx.doi.org/10.1016/j.watres.2011.11.058>
- H. Zhu, D. Yang, L. Zhu, H. Yang, D. Jin, K. Yao. A facile two-step hydrothermal route for the synthesis of gamma- Fe_2O_3 nanocrystals and their magnetic properties. *J Mater Sci*, 2007, 42 (22), 9205–9209. <http://dx.doi.org/10.1007/s10853-007-1887-0>
- J. Wang, C. Chen. Chitosan-based biosorbents: modification and application for biosorption of heavy metals and radionuclides. *Bioresour Technol*, 2014, 160, 129–141. <http://dx.doi.org/10.1016/j.biortech.2013.12.110>
- J. Yan, L. Han, W. Gao, S. Xue, M. Chen. Biochar supported nanoscale zerovalent iron composite used as persulfate activator for removing trichloroethylene. *Bioresour Technol*, 2014, 175C, 269–274.
- L. Beesley, E. Moreno-Jimenez, J.L. Gomez-Eyles. Effects of biochar

- and greenwaste compost amendments on mobility, bioavailability and toxicity of inorganic and organic contaminants in a multi-element polluted soil. *Environ Pollut*, 2010, 158 (6), 2282–2287. <http://dx.doi.org/10.1016/j.envpol.2010.02.003>
- L. Pontoni, M. Fabbri. Use of chitosan and chitosan-derivatives to remove arsenic from aqueous solutions—A mini review. *Carbohydr Res*, 2012, 356, 86–92. <http://dx.doi.org/10.1016/j.carres.2012.03.042>
- M. Ahmad, A.U. Rajapaksha, J.E. Lim, M. Zhang, N. Bolan, D. Mohan, M. Vithanage, S.S. Lee, Y.S. Ok. Biochar as a sorbent for contaminant management in soil and water: A review. *Chemosphere*, 2014, 99, 19–33. <http://dx.doi.org/10.1016/j.chemosphere.2013.10.071>
- M. Ahmad, S.S. Lee, A.U. Rajapaksha, M. Vithanage, M. Zhang, J.S. Cho, S.E. Lee, Y.S. Ok. Trichloroethylene adsorption by pine needle biochars produced at various pyrolysis temperatures. *Bioresour Technol*, 2013, 143, 615–622. <http://dx.doi.org/10.1016/j.biortech.2013.06.033>
- M. Inyang, B. Gao, Y. Yao, Y. Xue, A.R. Zimmerman, P. Pullammanappallil, X. Cao. Removal of heavy metals from aqueous solution by biochars derived from anaerobically digested biomass. *Bioresour Technol*, 2012, 110, 50–56. <http://dx.doi.org/10.1016/j.biortech.2012.01.072>
- M. Safa, M. Larouci, B. Meddah, P. Valemens. The sorption of lead, cadmium, copper and zinc ions from aqueous solutions on a raw diatomite from Algeria. *Water Sci Technol*, 2012, 65, 1729–1737. <http://dx.doi.org/10.2166/wst.2012.183>
- M. Uchimiya, L.H. Wartelle, I.M. Lima, K.T. Klasson. Sorption of deisopropylatrazine on broiler litter biochars. *J Agric Food Chem*, 2010, 58 (23), 12350–12356. <http://dx.doi.org/10.1021/jf102152q>
- M. Zhang, B. Gao, S. Varnosfaderani, A. Hebard, Y. Yao, M. Inyang. Preparation and characterization of a novel magnetic biochar for arsenic removal. *Bioresour Technol*, 2013, 130, 457–462. <http://dx.doi.org/10.1016/j.biortech.2012.11.132>
- P.O. Boamah, Y. Huang, M. Hua, Q. Zhang, J. Wu, J. Onumah, L.K. Sam-Amoah, P.O. Boamah. Sorption of heavy metal ions onto carboxylate chitosan derivatives—A mini-review. *Ecotoxicol Environ Saf*, 2015, 116, 113–120. <http://dx.doi.org/10.1016/j.ecoenv.2015.01.012>
- S.A. Kim, S. Kamala-Kannan, K.-J. Lee, Y.-J. Park, Shea, P.J. Shea, W.-H. Lee, H.-M. Kim, B.-T. Oh. Removal of Pb(II) from aqueous solution by a zeolite–nanoscale zero-valent iron composite. *Chem Eng J*, 2013, 217, 54–60. <http://dx.doi.org/10.1016/j.cej.2012.11.097>
- S.S. Banerjee, D.H. Chen. Fast removal of copper ions by gum arabic modified magnetic nano-adsorbent, *J Hazard Mater*, 2007, 147, 792–799. <http://dx.doi.org/10.1016/j.jhazmat.2007.01.079>
- S.-M. Lee, C. Laldawngliana, D. Tiwari. Iron oxide nano-particles-immobilized-sand material in the treatment of Cu(II), Cd(II) and Pb(II) contaminated waste waters. *Chem Eng J*, 2012, 195–196, 103–111. <http://dx.doi.org/10.1016/j.cej.2012.04.075>
- T. Wang, W. Liu, L. Xiong, N. Xu, J.R. Ni. Influence of pH, ionic strength and humic acid on competitive adsorption of Pb(II), Cd(II) and Cr(III) onto titanate nanotubes. *Chem Eng J*, 2013, 215–216, 366–374. <http://dx.doi.org/10.1016/j.cej.2012.11.029>
- U. Kumar, M. Bandyopadhyay. Sorption of cadmium from aqueous solution using pretreated rice husk. *Bioresour Technol*, 2006, 97, 104–109. <http://dx.doi.org/10.1016/j.biortech.2005.02.027>
- X. D. Fan, X. K. Zhang. Adsorption of Heavy Metals by Adsorbents from Food Waste Residue. *J Residuals Science & Technology*, 2015, 12, 155–158. <http://dx.doi.org/10.12783/issn.1544-8053/12/S1/22>
- Y. Chen, H. X. Zhao, Z. H. Xie, H. Y. Huang, S. Y. Zang, B. Lian. Heavy Metal Pollution Characteristics in the Kaili Coal Mining Region, Guizhou Province, China. *J Residuals Science & Technology*, 2015, 12 (sp 1), 123–131.
- Y. Cho, S. Jang, Y. Kim, S. Komarneni, S. Kim. Uptake of cadmium, copper, and lead by microporous synthetic Na-birnessite. *J Porous Mater*, 2011, 18, 125–131. <http://dx.doi.org/10.1007/s10934-010-9430-0>
- Y. Chun, G.Y. Sheng, C.T. Chiou, B.S. Xing. Compositions and sorptive properties of crop residue-derived chars. *Environ Sci Technol*, 2004, 38 (17), 4649–4655. <http://dx.doi.org/10.1021/es035034w>
- Y. Liu, M. Chen, Y. Hao. Study on the adsorption of Cu(II) by EDTA functionalized Fe₃O₄ magnetic nano-particles. *Chem Eng J*, 2013, 218, 46–54. <http://dx.doi.org/10.1016/j.cej.2012.12.027>
- Y. Ma, W.J. Liu, N. Zhang, Li, Y.S., Jiang, H., Sheng, G.P., 2014. Polyethylenimine modified biochar adsorbent for hexavalent chromium removal from the aqueous solution. *Bioresour. Technol.* 169, 403–408. <http://dx.doi.org/10.1016/j.biortech.2014.07.014>
- Y. Zhou, B. Gao, A.R. Zimmerman, H. Chen, M. Zhang, X. Cao. Biochar-supported zerovalent iron for removal of various contaminants from aqueous solutions. *Bioresour Technol*, 2014, 152, 538–542. <http://dx.doi.org/10.1016/j.biortech.2013.11.021>
- Y.C. Chang, D.H. Chen. Preparation and adsorption properties of mono-disperse chitosan-bound Fe₃O₄ magnetic nanoparticles for removal of Cu(II) ions. *J Colloid Interface Sci*, 2005, 283, 446–451. <http://dx.doi.org/10.1016/j.jcis.2004.09.010>

Modifications of Concentrations of Plant Macronutrient Ions in Digestate from Anaerobic Digestion during Nitrification Processes

KENJI TAKEMURA, RYOSUKE ENDO*, TOSHIO SHIBUYA and YOSHIAKI KITAYA
Graduate School of Life and Environmental Sciences, Osaka Prefecture University, Osaka, 599-8531, Japan

ABSTRACT: The goal of this study was to establish a system for converting digestate from anaerobic digestion processes into liquid fertilizer for soilless culture. Modifications of concentrations of plant macronutrient ions during nitrification processes were investigated with digestate from a simulated municipal organic waste. Concentrations of phosphate and calcium ions in the nitrified digestate increased; the rates of increase were $15.3 \text{ mg L}^{-1} \text{ d}^{-1}$ and $17.6 \text{ mg L}^{-1} \text{ d}^{-1}$, respectively. Moreover, concentrations of macronutrient ions, except for magnesium, in the nitrified digestate were similar to those in a standard nutrient solution that is commonly applied to soilless culture.

INTRODUCTION

ANAEROBIC digestion is one of the most promising biomass conversion technologies [1,2,3]. With this technology, micro-organisms gradually decompose organic matter (e.g., carbohydrates, proteins and fats) via anaerobic processes which are basically hydrolysis, acidogenesis, acetogenesis and methanogenesis, into biogas and digestate [4,5,6]. Biogas can be used as a source of renewable energy [7,8], and the digestate can potentially be used as a fertilizer for extensive agricultural fields [9]. However, in large cities and their suburbs, there is typically not enough area to apply the digestate. Additionally, transportation of the digestate to distant agricultural fields is unrealistic because of the high associated costs [10]. For these situations, it will be necessary to develop other utilization methods for efficient use of the digestate [9,11]. In this study, we propose a system for converting digestate from anaerobic digestion processes into liquid fertilizer that can be applied to soilless horticultural crops, which can be grown feasibly in urban areas. Soilless culture is receiving increasing attention in sustainability studies because the plants can be grown in greenhouses at high yields and with more efficient use of water and fertilizers; such crops also allow for mechanization of maintenance tasks and disease control (e.g., [12]).

When anaerobic digestate is used as liquid fertilizer in soilless culture, one type of problem encountered is that it contains an excess amount of ammonium ions (NH_4^+) [11,13,14] which were produced by degradation of proteins in anaerobic conditions [15]. This will lead to toxicity in many plant species, although the NH_4^+ toxicity can be alleviated by co-provisioning of nitrate ions (NO_3^-) [16,17]. Additionally, the growth media used in soilless culture cannot support the conversion of NH_4^+ into NO_3^- ; for example, with coconut fiber and rockwool, which are common substrates for soilless culture, hardly any of the NH_4^+ was nitrified [18]. Therefore, it is necessary to convert NH_4^+ into NO_3^- in the digestate before applying the material to soilless culture, and nitrification (biological conversion of NH_4^+ into NO_3^-) has been widely used for this purpose [19,20]. Botheju *et al.* reported that about 75% of NH_4^+ -N in digestate was removed in a sequential batch reactor process primarily through the conversion of NH_4^+ -N into NO_3^- -N [13]. However, research on the nitrification of digestate with other nitrification processes (e.g., fixed bed reactors, moving bed biofilm reactors) is limited.

In order to assess the effectiveness of nitrification processes as treatment methods for anaerobic digestate that is to be applied to soilless culture, it is necessary to know modifications of concentrations of plant nutrient ions in it during nitrification processes, which are absorbed by plants primarily as inorganic ions [21]. Zhang *et al.* reported that the phosphorus (P) in the di-

*Author to whom correspondence should be addressed.
E-mail: endo@envi.osakafu-u.ac.jp, Tel. & Fax. +81-72-254-9668

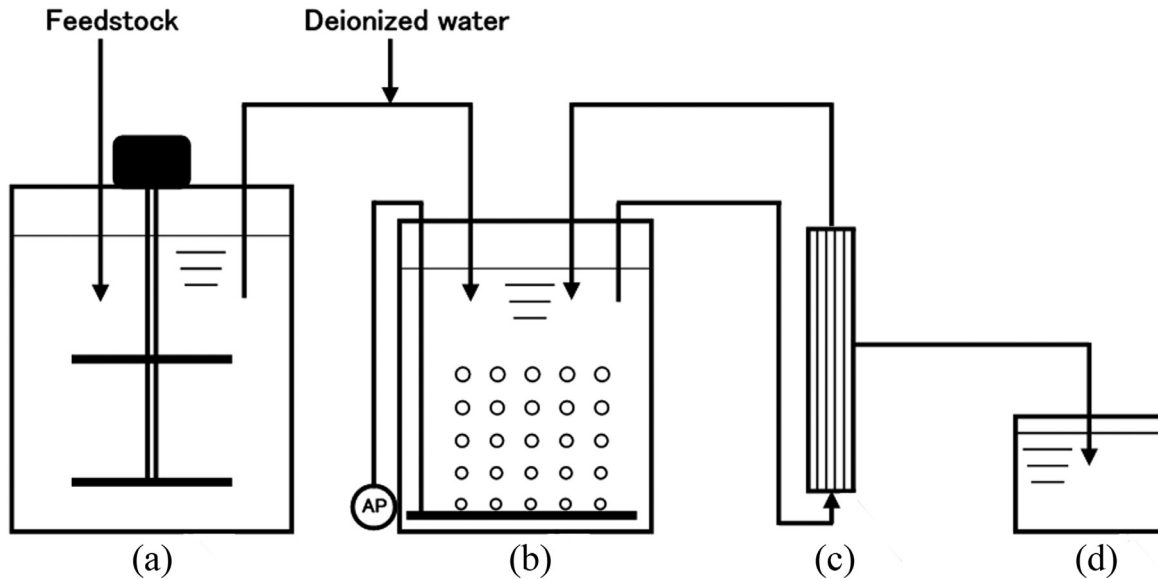


Figure 1. Schematic diagram of the experimental set-up. (a) Anaerobic digester (mesophilic continuously stirred tank type, 200 L, water temperature of $37.0 \pm 1.0^\circ\text{C}$). The feedstock for this reactor was a simulated organic fraction of municipal solid waste that was diluted 3 times with deionized water. (b) Moving bed biofilm reactor (150 L, water temperature of $21.5 \pm 1.0^\circ\text{C}$, dissolved oxygen at $2.5 \pm 1.0 \text{ mg L}^{-1}$). The feedstock for this reactor was digestate from the anaerobic digestion that was diluted 3 times with deionized water. (c) Membrane filtration apparatus (a pore size of $0.20 \mu\text{m}$). (d) Effluent storage tank (300 L, ambient temperature). AP indicates the air pump.

gestate was released into the solution as phosphate ions by lowered pH levels when hydrochloric acid (HCl) was added [22]. Mehta and Batstone reported that additions of HCl, which reduced the pH of the digestate, were associated with the release of ionic species of P, calcium (Ca), and magnesium (Mg) [23]. According to these studies, we hypothesize that concentrations of phosphate, calcium and magnesium ions will be increased by the lowered pH levels induced by nitrification together with conversion of NH_4^+ into NO_3^- , during nitrification processes of the digestate.

In the present study, modifications of concentrations of plant macronutrient ions during nitrification of digestate from anaerobic digestion of municipal organic waste were investigated, using a moving bed biofilm reactor (hereinafter called “MBBR”) which is known to be efficient for NH_4^+ -N removal and stable under high or variable conditions [24]. In addition, concentrations of plant macronutrient ions in the nitrified digestate were compared with those in a standard nutrient solution. Moreover, as the nitrified digestate must be filtered prior to practical usage as liquid fertilizer in soilless culture to ensure chemical stability and prevent clogging in the fertilizer supply system, and because liquid fertilizer is usually used at pH values ranging from 5.5 to 6.5, influences of filtrate pH levels on the concentrations of plant macronutrient ions in the nitrified digestate were also assessed.

MATERIALS AND METHODS

Moving Bed Biofilm Reactor

The schematic diagram of the experimental set-up is shown in Figure 1. A MBBR with a total liquid volume of 150 L [Figure 1(b)] was used in this study. Cubic polyolefin carriers (Figure 2, Sekisui Chemi-



Figure 2. Cubic polyolefin carriers ($10 \text{ mm} \times 10 \text{ mm} \times 10 \text{ mm}$) used in this equipment.

cal, Japan) with sizes of 10 mm were added to the system, and these occupied 20% of the total liquid volume. A diffuser placed at the bottom of the reactor was used for the oxygen supply and to mix the materials in the reactor. The reactor was inoculated with waste activated sludge (150 L) that was collected from a community sewage treatment facility located in Osaka, Japan. Feedstocks of 15 L were fed into the MBBR once a day for five days each week. The nitrified digestate in the MBBR was continuously removed and fed into the membrane filtration apparatus at volumes of 9 L d⁻¹ (during three days of feedstock addition) or 4.5 L d⁻¹ (two days when the feedstock was not fed into the MBBR and two days during feedstock addition) [Figure 1(c)], Toyobo Engineering, Japan). In addition, a volume of the nitrified digestate equal to 6 L was removed once a day for five days each week before each feedstock addition for stable operation of the MBBR and the membrane filtration apparatus. Thus, on a weekly basis, a total of 75 L of feedstock were added to the MBBR, 45 L of the nitrified digestate were removed for experimental work, and 30 L of the nitrified digestate were removed to keep the system stable. The module type used in the membrane filtration apparatus was a hollow fiber membrane with a pore size of 0.20 μm, and it was made of polyvinylidene fluoride. The reactor was operated at 21.5 ± 1.0°C, and dissolved oxygen (DO) was maintained at 2.5 ± 1.0 mg L⁻¹ in the system.

Feedstock for the MBBR

The feedstock for the MBBR was digestate obtained from an anaerobic digester (a mesophilic continuously stirred tank type digester operated at a water temperature of 37.0 ± 1.0°C), and a total liquid volume of 200 L was used [Figure 1(a)]. The feedstock was diluted 3 times with deionized water before feeding it into the MBBR. The digester started operation in synchrony with the MBBR and was inoculated with 200 L of digestate that came from an anaerobic digestion plant that treats animal manure and food wastes; the plant is located in Kyoto, Japan. The feedstock for the digester was termed a “simulated organic fraction of municipal solid waste” (hereinafter called “simulated OFMSW”) following a previous report (Table 1, [25]). The simulated OFMSW was diluted 3 times with deionized water and pulverized before feeding it into the digester. Aliquots of this material (5 L) were then fed into the system’s digester once a day for five days each week.

Table 1. The Composition of the Simulated Organic Fraction of Municipal Solid Waste.

Materials		Proportion of a Net Weight Basis (%)
Fruit	Apple	10
	Grapefruit (rind)	5
	Orange (rind)	5
	Banana (rind)	10
Vegetable	Cabbage	12
	Potato	12
	Carrot	12
Meat and Fish	Meat	5
	Fish (with bone)	5
	Egg	4
Staple Food	Rice	10
	Bread	5
	Noodle	2.5
	Chinese noodle	2.5

Chemical Analyses

Concentrations of total nitrogen (T-N) and organic nitrogen (Org-N), pH, and DO were measured in accordance with Standard Methods for the Examination of Water and Wastewater [26]. Concentrations of macronutrient ions were analyzed by using an ion chromatograph (LC-10A, Shimadzu, Japan) equipped with a Shim-pack IC-A3 column (anion) and Shim-pack IC-SC1 column (cation) that employed an electric conductivity detector. The oven temperature was 40°C. Eluents included p-hydroxybenzoic acid/bis-tris (anion) and sulfuric acid (cation). Eluent flow rates were set to 1.5 mL min⁻¹ (anion) and 1.2 mL min⁻¹ (cation). The injected sample volume was 1 mL.

Calculation Method for Change Rates of Concentrations of Macronutrient Ions in the MBBR

Concentrations of macronutrient ions, T-N, and Org-N in the digestate, the diluted digestate, and the nitrified digestate were periodically analyzed after day 53. Many of the samples showed steady values after day 168. In this situation, concentrations of macronutrient ions, T-N, and Org-N immediately after feeding and a day after feeding the diluted digestate into the MBBR were calculated from Equations (1) and (2) by using the values from day 168, day 175, and day 189, respectively. Moreover, change rates were calculated from Equation (3).

$$Con_{st} = \frac{(Con_{in} \times Vol_{in} + Con_{ef} \times Vol_{re})}{Vol_M} \quad (1)$$

$$Con_{en} = Con_{ef} \quad (2)$$

$$Con_{cr} = \frac{Con_{en} - Con_{st}}{T} \quad (3)$$

where Con_{st} (mg L^{-1}) represents the concentrations of macronutrient ions, T-N, and Org-N in the MBBR immediately after the diluted digestate was fed into the reactor; Con_{in} (mg L^{-1}) represents the concentrations in the diluted digestate; Vol_{in} is the quantity of diluted digestate fed into the MBBR (15 L); Con_{ef} (mg L^{-1}) represents the concentrations in the nitrified digestate that was removed before each feeding of the diluted digestate; Vol_{re} is the total liquid volume of the MBBR immediately after the nitrified digestate was withdrawn (135 L); Vol_M is the total liquid volume of the MBBR (150 L); Con_{en} (mg L^{-1}) represents the concentrations a day after the feeding in the MBBR; Con_{cr} ($\text{mg L}^{-1} \text{d}^{-1}$) represents the change rates of concentrations in the MBBR; and T is the time (d).

Influences of pH on Concentrations of Phosphate and Calcium Ions in a Mixed Solution of the Diluted Digestate and Nitrified Digestate with or without Filtration

Influences of decreases in the pH on concentrations of phosphate and calcium ions were assessed by adding nitric acid to a mixed solution of the diluted digestate and nitrified digestate; the mixed solution was prepared in the same volumetric ratio (1:9) as that used in the MBBR (hereinafter called “the mixed solution”). The mixed solution (50.0 mL) was added to a beaker and was stirred by using a magnetic stirrer (200 rpm). A known amount of nitric acid (6.9 wt%) was then added to the mixed solution every 120 min. The pH of the mixed solution was measured immediately before each addition of the nitric acid. At the same time, a sample was collected and concentrations of phosphate and calcium ions in the sample were analyzed.

In the filtration procedures, the mixed solution was filtered through a 0.45- μm pore diameter membrane filter (Advantec, Japan) according to Standard Methods [26]. Influences of decreases in the pH on concentrations of phosphate and calcium ions in the filtrate of the mixed solution were also assessed by adding nitric acid (1.0 wt%) to the filtrate.

Influences of pH on Concentrations of Macronutrient Ions in the Filtrate of the Nitrified Digestate

Influences of increases in the pH on concentrations of macronutrient ions in the filtrate of the nitrified digestate were assessed by adding sodium hydroxide (1.0 wt%) to the filtrate. The filtrate of nitrified digestate was collected from the membrane filtration apparatus. Other experimental procedures were the same as above.

Statistical Analyses

Pearson’s correlation analysis and simple regression analysis were used to evaluate the correlations between data sets. In addition, paired t -tests were used to evaluate the significance of differences between data sets. Calculations were carried out by using the software “Statcel 3” (Yanai 2011). $P < 0.05$ was considered statistically significant.

RESULTS AND DISCUSSION

Concentrations of the nitrogen forms in the MBBR immediately after the diluted digestate was fed into it and a day after the feeding are shown in Table 2. The concentrations of T-N decreased significantly. The decrease rate was $9 \text{ mg L}^{-1} \text{d}^{-1}$ which might be because of uptake by biofilm communities, stripping of ammonia, etc., and this decrease corresponded to 1.7% of the concentration of T-N immediately after feeding of the diluted digestate. The concentrations of NH_4^+ -N also decreased significantly, and the decrease rate was $24 \text{ mg L}^{-1} \text{d}^{-1}$. At the same time, the concentrations of NO_3^- -N increased significantly, and the increase rate was $25 \text{ mg L}^{-1} \text{d}^{-1}$. In addition, regarding Org-N, no significant differences were detected between concentrations immediately after the feeding of the diluted digestate and a day after the feeding; the concentrations of nitrite-N (NO_2^- -N) both immediately after the feeding of the diluted digestate and a day after the feeding were N.D. (not detected). These results indicate that the increase of NO_3^- -N concentrations over the course of a day were mainly due to the conversion of NH_4^+ -N into NO_3^- -N. The increase of NO_3^- -N throughout each day corresponded to 83% of the NH_4^+ -N added by the diluted digestate, which was a little more than the value (about 75%) reported by Botheju *et al.* [13].

Concentrations of phosphate, potassium, calcium and magnesium ions in the MBBR immediately after

Table 2. Concentrations of the Various Forms of Nitrogen in the MBBR Immediately After Feeding of the Diluted Digestate and a Day After the Feeding.

	T-N (mg L ⁻¹)	NH ₄ ⁺ -N (mg L ⁻¹)	NO ₃ ⁻ -N (mg L ⁻¹)	NO ₂ ⁻ -N (mg L ⁻¹)	Org-N (mg L ⁻¹)
Concentrations in the MBBR immediately after feeding of diluted digestate	535 ± 6	85 ± 6	227 ± 14	N.D. ^b	223 ± 21
Concentration in the MBBR a day after the feeding	527 ± 7	61 ± 8	253 ± 15	N.D.	213 ± 24
<i>P</i> value ^a	0.006	0.011	0.004	–	0.084

Each value represents a mean ± standard error ($n = 3$).

^a*P* values were calculated by using a paired *t*-test.

^bN.D., not detected.

the diluted digestate was fed into the system and a day after the feeding are shown in Table 3. There was no significant difference in regards to the potassium ions, while the concentrations of phosphate and calcium ions increased significantly; the increase rates were 15.3 mg L⁻¹d⁻¹ and 17.6 mg L⁻¹d⁻¹, which corresponded to 11.1% and 9.3% of that immediately after feeding of the diluted digestate, respectively. These increases will be advantageous for plant growth because plants absorb essential nutrients primarily as inorganic ions [21].

Results of the experiment performed to assess influences of pH on concentrations of phosphate and calcium ions in the mixed solution are shown in Figure 3. Concentrations of phosphate and calcium ions increased following the decrease of pH values, and statistically significant correlations were observed between pH values and concentrations of phosphate and calcium ions (Pearson's correlation coefficients (r) = -0.97 for both ions); regression coefficients were -17.9 and -23.5, respectively.

As previously mentioned, in the MBBR, nitrification of digestate was advanced (the concentration of NH₄⁺-N decreased at the rate of 24 mg L⁻¹ d⁻¹, whereas the concentration of NO₃⁻-N increased at the rate of 25 mg L⁻¹ d⁻¹). The nitrification promotes a decrease of pH (2 moles of H⁺ released by converting each mole of NH₄⁺ into NO₃⁻) [27]. Practically, in the MBBR,

the pH of 5.9–6.1 immediately after feeding of the diluted digestate decreased to 4.0–4.2 a day after the feeding. In addition, results of the experiment to assess influences of pH on concentrations of phosphate and calcium ions indicated that these concentrations increased following the decrease of pH values. According to these results, increase of concentrations of phosphate and calcium ions in the MBBR might have been caused by the decrease of pH values following nitrification processes. In literatures [27,28,29], it was reported that dissolution of phosphate driven by acidification induced by nitrification could be dominant among other biological and chemical reactions (e.g., uptake by microorganisms).

According to the regression coefficients between pH values and concentrations of phosphate and calcium ions in the laboratory beaker experiment, the increases of concentrations were estimated to be 34.0 mg L⁻¹ and 44.7 mg L⁻¹, respectively, when the pH values decreased from 5.9–6.1 to 4.0–4.2. These values were larger than those in the MBBR (15.3 mg L⁻¹ and 17.6 mg L⁻¹). These differences might have been caused by differences of biological uptake, adsorption, etc. [30,31,32] but more studies are needed.

Moreover, the results of the experiment that was performed to assess the effects of pH on concentrations of phosphate and calcium ions in the filtrate of the mixed solution are shown in Figure 4. In the fil-

Table 3. Concentrations of Macronutrient Ions in the MBBR Immediately After Feeding of the Diluted Digestate and a Day After the Feeding.

	Phosphate ions (mg L ⁻¹)	Potassium ions (mg L ⁻¹)	Calcium ions (mg L ⁻¹)	Magnesium ions (mg L ⁻¹)
Concentrations in the MBBR immediately after feeding of diluted digestate	137.9 ± 11.9	270.2 ± 19.4	189.0 ± 22.3	N.D. ^b
Concentration in the MBBR a day after the feeding	153.2 ± 13.2	274.8 ± 20.5	206.6 ± 24.7	N.D.
<i>P</i> value ^a	0.007	0.073	0.018	–

Each value represents a mean ± standard error ($n = 3$).

^a*P* values were calculated by using a paired *t*-test.

^bN.D., not detected.

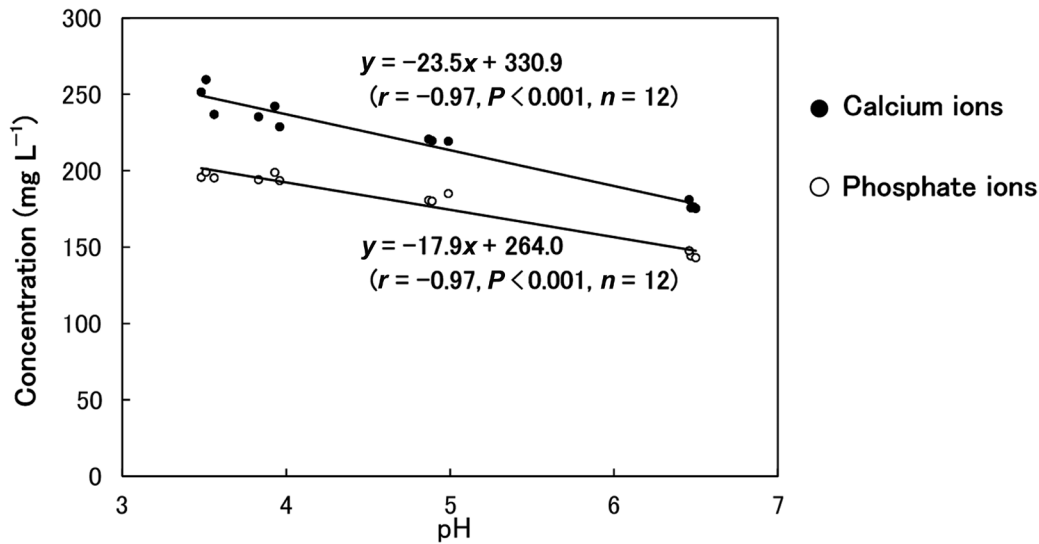


Figure 3. Simple regression analysis between pH values and concentrations of phosphate or calcium ions in a mixed solution of the nitrified digestate and the diluted digestate in the same volume ratio as in the MBBR (9:1). The pH was reduced by adding nitric acid (6.9 wt%) to the samples. x , pH values; y , concentration of phosphate or calcium ions; and r , Pearson's correlation coefficient.

trate, statistically significant correlations were also observed between the pH values and concentrations of phosphate and calcium ions ($r = -0.95$ and $r = -0.58$, respectively). The regression coefficients for phosphate and calcium were -9.5 and -1.5 , respectively. According to the regression coefficients for the mixed solution and for the filtrate, the ratios of the increasing concentrations of phosphate and calcium ions in the filtrate against those in the mixed solution for the same decrease of pH were 53.1% and 6.4%, respectively. These results indicate that the increase of calcium ions

following the decrease of pH in the mixed solution was mainly the result of ionization of the materials remaining on the filter (pore size; $0.45 \mu\text{m}$), while the increase of phosphate ions was the result of both ionization of the materials remaining on the filter and those in the filtrate.

Concentrations of macronutrient ions in the nitrified digestate and a standard nutrient solution used for soilless culture (Enshi-shoho, [33,34,35]) are shown in Table 4. Concentrations of macronutrient ions in the nitrified digestate were similar to the Enshi-shoho

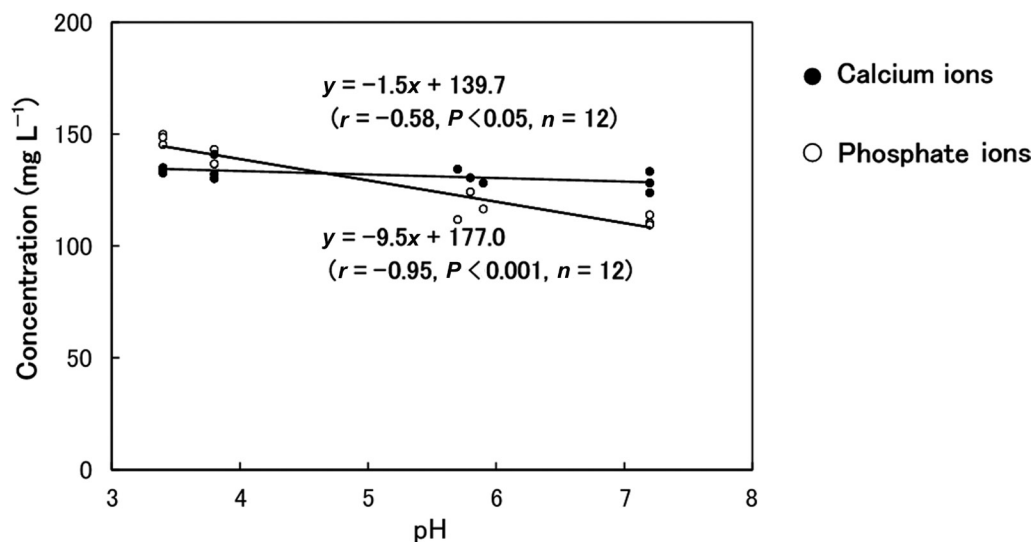


Figure 4. Simple regression analysis between pH values and concentrations of phosphate or calcium ions in a filtrate of the mixed solution of the nitrified digestate and the diluted digestate in the same volume ratio as in the MBBR (9:1). The pH was reduced by adding nitric acid (1.0 wt%) to the samples. x , pH values; y , concentration of phosphate or calcium ions; and r , Pearson's correlation coefficient.

Table 4. Concentrations of Macronutrient Ions in the Nitrified Digestate and the Standard Nutrient Solution Used for Soilless Culture (Enshi-shoho).

	N ^a (meq L ⁻¹)	P ^b (meq L ⁻¹)	K (meq L ⁻¹)	Ca (meq L ⁻¹)	Mg (meq L ⁻¹)
Nitrified digestate	18.1 ± 1.1	4.7 ± 0.4	7.0 ± 0.5	10.3 ± 1.2	N.D. ^c
Standard nutrient solution used for soilless culture (Enshi-shoho)	16.0	4.0	8.0	8.0	4.0

Each value of nitrified digestate represents a mean ± standard error ($n = 3$).

^aN, Nitrate forms.

^bP, Phosphate forms.

^cN.D., not detected.

except for magnesium. The results of the experiment performed to assess the effects of pH on concentrations of macronutrient ions in the filtrate of the nitrified digestate showed that there were no significant differences ($n = 3$) between the concentrations of macronutrient ions at pH 4.1 (the initial pH) and those at pH 4.9 and 5.8 that were increased by the addition of sodium hydrate, except for at pH 5.8 regarding potassium ions. The concentration of potassium ions increased significantly, and the increase corresponded to 2.2% of the initial concentration. These results indicate that the concentrations of macronutrient ions in the filtrate of the nitrified digestate were also similar to the Enshi-shoho except magnesium in the same pH range as that in liquid fertilizers usually used for soilless culture.

Overall, the results of this study indicate that concentrations of phosphate and calcium ions were increased together with conversion of NH_4^+ into NO_3^- , during nitrification of the digestate from anaerobic digestion, and the filtrate of the nitrified digestate could be a viable substitute for standard nutrient solutions in soilless culture if the macronutrients are supplemented with magnesium.

ACKNOWLEDGMENTS

The authors are grateful for financial support from the Industry-University-Government Cooperation Research Project of Osaka Prefecture University and the Hitachi Zosen Corporation. This research was also partly supported by the Japan Society for Promotion of Science (JSPS Grants-in-Aid for Scientific Research, 15K12246 and 26520311).

REFERENCES

- Edwards, J., Othman, M., Burn, S., "A review of policy drivers and barriers for the use of anaerobic digestion in Europe, the United States and Australia", *Renewable and Sustainable Energy Reviews*, Vol. 52, 2015, pp. 815–828. <http://dx.doi.org/10.1016/j.rser.2015.07.112>
- Kumaran, P., Hephzibah, D., Sivasankari, R., *et al.*, "A review on industrial scale anaerobic digestion systems deployment in Malaysia: Opportunities and challenges", *Renewable and Sustainable Energy Reviews*, Vol. 56, 2016, pp. 929–940. <http://dx.doi.org/10.1016/j.rser.2015.11.069>
- Carrere, H., Antonopoulou, G., Affes, R., *et al.*, "Review of feedstock pretreatment strategies for improved anaerobic digestion: From lab-scale research to full-scale application", *Bioresour. Technology*, Vol. 199, 2016, pp. 386–397. <http://dx.doi.org/10.1016/j.biortech.2015.09.007>
- Mao, C., Feng, Y., Wang, X., *et al.*, "Review on research achievements of biogas from anaerobic digestion", *Renewable and Sustainable Energy Reviews*, Vol. 45, 2015, pp. 540–555. <http://dx.doi.org/10.1016/j.rser.2015.02.032>
- Negri, M., Bacenetti, J., Fiala, M., *et al.*, "Evaluation of anaerobic degradation, biogas and digestate production of cereal silages using nylon-bags", *Bioresour. Technology*, Vol. 209, 2016, pp. 40–49. <http://dx.doi.org/10.1016/j.biortech.2016.02.101>
- Feng, L., Kou, H., Zhang, X., *et al.*, "The research of corrected first order kinetics on hydrolysis and biogas generation in batch anaerobic digestion", *Journal of Residuals Science and Technology*, Vol. 12 No. 4, 2015, pp. 249–255. <http://dx.doi.org/10.12783/issn.1544-8053/12/4/8>
- Uddin, W., Khan, B., Shaukat, N., *et al.*, "Biogas potential for electric power generation in Pakistan: A survey", *Renewable and Sustainable Energy Reviews*, Vol. 54, 2016, pp. 25–33. <http://dx.doi.org/10.1016/j.rser.2015.09.083>
- Hijazi, O., Munro, S., Zerhusen, B., *et al.*, "Review of life cycle assessment for biogas production in Europe", *Renewable and Sustainable Energy Reviews*, Vol. 54, 2016, pp. 1291–1300. <http://dx.doi.org/10.1016/j.rser.2015.10.013>
- Monlau, F., Sambusiti, C., Ficara, E., *et al.*, "New opportunities for agricultural digestate valorization: current situation and perspectives", *Energy and Environmental Science*, Vol. 8, 2015, pp. 2600–2621. <http://dx.doi.org/10.1039/C5EE01633A>
- Li, X., Guo, J., Dong, R., *et al.*, "Properties of plant nutrient: Comparison of two nutrient recovery techniques using liquid fraction of digestate from anaerobic digester treating pig manure", *Science of the Total Environment*, Vol. 544, 2016, pp. 774–781. <http://dx.doi.org/10.1016/j.scitotenv.2015.11.172>
- Endo, R., Yamashita, K., Shibuya, T., *et al.*, "Use of methane fermentation digestate for hydroponic culture: Analysis of potential inhibitors in digestate to cucumber seedling", *Eco-Engineering*, Vol. 28, No. 3, 2016 (in press).
- Lee, S., Lee, J., "Beneficial bacteria and fungi in hydroponic systems: Types and characteristics of hydroponic food production methods", *Scientia Horticulturae*, Vol. 195, 2015, pp. 206–215. <http://dx.doi.org/10.1016/j.scienta.2015.09.011>
- Botheju, D., Svalheim, Ø., Bakke, R., "Digestate nitrification for nutrient recovery", *The Open Waste Management Journal*, Vol. 3, 2010, pp. 1–12. <http://dx.doi.org/10.2174/1876400201003010001>
- Möller, K., Müller, T., "Effects of anaerobic digestion on digestate nutrient availability and crop growth: A review", *Engineering in Life Sciences*, Vol. 12, No. 3, 2012, pp. 242–257. <http://dx.doi.org/10.1002/elsc.201100085>

15. Tampio, E., Ervasti, S., Paavola, T., *et al.*, “Anaerobic digestion of autoclaved and untreated food waste”, *Waste Management*, Vol. 34, 2014, pp. 370–377. <http://dx.doi.org/10.1016/j.wasman.2013.10.024>
16. Britto, D. T., Kronzucker, H. J., “NH₄⁺ toxicity in higher plants: a critical review”, *Journal of Plant Physiology*, Vol. 159, 2002, pp. 567–584. <http://dx.doi.org/10.1078/0176-1617-0774>
17. Hachiya, T., Watanabe, C. K., Fujimoto, M., *et al.*, “Nitrate addition alleviates ammonium toxicity without lessening ammonium accumulation, organic acid depletion and inorganic cation depletion in *Arabidopsis thaliana* shoots”, *Plant and Cell Physiology*, Vol. 53, No. 3, 2012, pp. 577–591. <http://dx.doi.org/10.1093/pcp/pcs012>
18. Miyata, H., Ikeda, H., “Behavior of nitrogen in the media supplied with the aqueous phase produced by methane fermentation as liquid fertilizer”, *Soil Science and Plant Nutrition*, Vol. 52, 2006, pp. 135. <http://dx.doi.org/10.1111/j.1747-0765.2006.t01-8-x>
19. Ahn, Y.-H., “Sustainable nitrogen elimination biotechnologies: A review”, *Process Biochemistry*, Vol. 41, 2006, pp. 1709–1721. <http://dx.doi.org/10.1016/j.procbio.2006.03.033>
20. Li, J., Meng, J., Li, J., *et al.*, “The effect and biological mechanism of COD/TN ratio on nitrogen removal in a novel upflow microaerobic sludge reactor treating manure-free piggery wastewater”, *Bioresour. Technology*, Vol. 209, 2016, pp. 360–368. <http://dx.doi.org/10.1016/j.biortech.2016.03.008>
21. Taiz, L., Zeiger, E. 2010. *Plant physiology fifth edition*, Sunderland: Sinauer Associates, Inc.
22. Zhang, T., Bowers, K. E., Harrison, J. H., *et al.*, “Releasing phosphorus from calcium for struvite fertilizer production from anaerobically digested dairy effluent”, *Water Environment Research*, Vol. 82, No. 1, 2010, pp. 34–42. <http://dx.doi.org/10.2175/106143009X425924>
23. Mehta, C. M., Batstone, D. J., “Nutrient solubilization and its availability following anaerobic digestion”, *Water Science and Technology*, Vol. 67, No. 4, 2013, pp. 756–763. <http://dx.doi.org/10.2166/wst.2012.622>
24. Levstek, M., Plazl, I., “Influence of carrier type on nitrification in the moving-bed biofilm process”, *Water Science and Technology*, Vol. 59, No. 5, 2009, pp. 875–882. <http://dx.doi.org/10.2166/wst.2009.037>
25. Sasaki, H., Li, Y.-Y., Seki, K., *et al.*, “Effects of hydraulic retention time and loading rate on high-solids thermophilic methane fermentation of the organic fraction of municipal solid waste”, *Journal of Japan Society on Water Environment*, Vol. 22, No. 12, 1999, pp. 983–989. <http://dx.doi.org/10.2965/jswe.22.983>
26. APHA, AWWA, WEF. 2012. *Standard Methods for the Examination of Water and Wastewater twenty second edition*, Washington, D. C.: American Public Health Association, American Water Works Association, Water Environment Federation.
27. Daumer, M. L., Béline, F., Guiziou, F., *et al.*, “Influence of pH and biological metabolism on dissolved phosphorus during biological treatment of piggery wastewater”, *Biosystems Engineering*, Vol. 96, No. 3, 2007, pp. 379–386. <http://dx.doi.org/10.1016/j.biosystemseng.2006.11.011>
28. Daumer, M. L., Béline, F., Guiziou, F., *et al.*, “Effect of nitrification on phosphorus dissolving in a piggery effluent treated by a sequencing batch reactor”, *Biosystems Engineering*, Vol. 96, No. 4, 2007, pp. 551–557. <http://dx.doi.org/10.1016/j.biosystemseng.2007.01.001>
29. Berzins, A., Petrina, Z., Nikolajeva, V., *et al.*, “Characteristics of a ceramic carrier after wastewater treatment process in the model column cascade with ethanol addition”, *The Open Biotechnology Journal*, Vol. 9, 2015, pp. 76–84. <http://dx.doi.org/10.2174/1874070701509010076>
30. Yuan, Z., Pratt, S., Batstone, D. J., “Phosphorus recovery from wastewater through microbial processes”, *Current Opinion in Biotechnology*, Vol. 23, 2012, pp. 878–883. <http://dx.doi.org/10.1016/j.copbio.2012.08.001>
31. Ramasahayam, S. K., Guzman, L., Gunawan, G., *et al.*, “A comprehensive review of phosphorus removal technologies and processes”, *Journal of Macromolecular Science, Part A: Pure and Applied Chemistry*, Vol. 51, 2014, pp. 538–545. <http://dx.doi.org/10.1080/10601325.2014.906271>
32. Fan, X. D., Zhang, X. K., “Adsorption of heavy metals by adsorbents from food waste residue”, *Journal of Residuals Science and Technology*, Vol. 12, Supplement 1, 2015, pp. 155–158. <http://dx.doi.org/10.12783/issn.1544-8053/12/S1/22>
33. Tanaka, S., Ito, T., Ochi, Y., *et al.*, “The effect of calcium concentration and osmotic pressure of nutrient solution on cucumber downy mildew in a water culture system” *Acta Horticulturae*, Vol. 548, 2001, pp. 581–589. <http://dx.doi.org/10.17660/ActaHortic.2001.548.72>
34. Japan Greenhouse Horticulture Association, Hydroponic Society of Japan. 2012. *All about Hydroponics*, Tokyo: Seibundo Shinkosha (in Japanese).
35. Zhang, Y., Kiriwa, Y., Nukaya, A., “Influence of nutrient concentration and composition on the growth, uptake patterns of nutrient elements and fruit coloring disorder for tomatoes grown in extremely low-volume substrate”, *The Horticulture Journal*, Vol. 84, No. 1, 2015, pp. 37–45. <http://dx.doi.org/10.2503/hortj.MI-003>

Effect of Sludge Conditioning Temperature on the Thickening and Dewatering Performance of Polymers

ZE YAN¹, BANU ÖRMECI^{1,*} and JINLI ZHANG²

¹*Department of Civil and Environmental Engineering, Carleton University, Ottawa ON, K1S 5B6, Canada*

²*Department of Chemical Engineering and Technology, Tianjin University, Tianjin 300072, China*

ABSTRACT: The objective of this study was to investigate the impact of sludge conditioning temperature on the optimum polymer dose, and thickening and dewatering performance of polymers used for sludge conditioning. Thickening and dewatering performance was investigated at 10°C, 35°C, 50°C, 60°C, and 100°C using filtration, capillary suction time (CST), and settling tests and zeta potential measurements. A high molecular weight and medium-high cationic charge polyacrylamide polymer (Zetag 8160) was used to condition sludge. Results showed that 50°C was the sludge temperature that resulted in the best settling, thickening and dewatering using the least amount of polymer, and 35°C was also effective.

1. INTRODUCTION

THE cost of sludge management constitutes approximately half of the cost of wastewater treatment [1], and the quantities continue to increase as new wastewater treatment plants are built and the existing ones are upgraded to keep up with the growing population and stricter regulations. Sludge thickening and dewatering play a key role in reducing the treatment and final disposal costs at wastewater treatment plants. Cationic polymers are used for both thickening and dewatering processes, and the optimization of their use would substantially improve the performance of these processes. Both under-dosing and over-dosing lead to poor settling and dewatering, and therefore it is important to use polymers at the optimum dose [2]. Moreover, polymers are one of the most expensive chemicals used for wastewater treatment, and using polymers at the optimum dose and under optimum conditions would help to achieve major savings for wastewater treatment plants.

To maximize the polymer efficiency and minimize the polymer use, several parameters can be optimized including operational parameters, sludge characteristics and environmental conditions. These include mixing used during conditioning [3,4], shear exposure after conditioning [5], polymer type and chemistry [6],

pH [7], metal ions [8], ionic effects [9,10], extracellular polymers [11] as well as sludge temperature. It has been known that cold temperatures are not ideal for conditioning but there have not been extensive studies on the effect of sludge temperature on sludge conditioning, thickening and dewatering. Polymers are typically dosed at room temperature; however, wastewater and sludge temperatures may vary largely based on the seasonal variations and the treatment processes used at treatment plants.

Heating sludge is very costly and therefore it is not typically used to improve conditioning unless heating is part of the treatment process. In recent years, there has been a major interest in the use of new and innovative thermal processes for sludge pre-treatment, treatment or dewatering. These processes include thermal and thermochemical hydrolysis [12], incineration [13], wet air oxidation [14], and super-critical water oxidation [15,16]. The thermal processes require sludge temperatures to be increased to mid (25–55°C), high (55–100°C), or very high (>100°C) temperatures in pressurized systems, and a step-wise temperature increase in the process can potentially be used to improve the performance of thickening and dewatering, which would also improve the performance of thermal processes. This approach would not add any additional costs for heating sludge before conditioning. At higher temperatures, water molecules are more active and it is easier to break the particle-particle and the particle-liquid interactions [17].

The objective of this study was to investigate the

*Author to whom correspondence should be addressed.
Professor and Canada Research Chair, 1125 Colonel By Drive, Ottawa ON, K1S 5B6, Canada. Phone: +1 (613) 5202600, ext. 4144, Fax: +1 (613) 5203951, E-mail: banu.ormeci@carleton.ca

impact of sludge temperature on the optimum polymer dose and conditioning of wastewater sludge, and improve the performance of settling, thickening and dewatering processes by using the optimum temperature required for conditioning. The sludge temperature range selected for the study was 10–100°C, which can be employed at wastewater treatment plants without the need for non-pressurized systems.

2. MATERIALS AND METHODS

2.1. Preparation of Sludge Samples

Anaerobically digested sludge samples were collected from a wastewater treatment plant in Ontario, Canada once a week. The plant digests mixed primary and secondary sludge under mesophilic temperatures. Sludge samples were stored in a refrigerator, and samples were brought to room temperature before use. A hot plate was used to increase the temperature of samples to 10°C, 35°C, 50°C, 60°C, and 100°C in 2 L glass beakers while being stirred at 200 rpm. After reaching the target temperature, sludge samples were conditioned with polymer as explained below.

2.2. Preparation of Polymer Stock Solution

The polymer used in this study was Zetag 8160 (BASF), which is a polyacrylamide, medium-high cationic charge, high-molecular-weight polymer that is in granular solid form. This was also the polymer that was used at the treatment plant for sludge dewatering. The polymer stock solution was prepared at a concentration of 0.5% using a jar tester (PB-700 Jartester, Phipps & Bird Inc., USA). Five g of Zetag 8160 polymer was mixed with 1 L of deionized water, and stirred for first 5 min at 200 rpm followed by 55 min at 125 rpm. A hand-held blender was used to break up the remaining polymer clumps and the polymer stock solution was left for maturation.

2.3. Conditioning of Sludge Samples with Polymer

Sludge samples of 200 mL volume were spiked with polymer and mixed in 500 mL beakers using a jar tester apparatus (PB-700 Jartester, Phipps & Bird Inc., USA). Polymer doses were selected to cover the under-dose, optimum dose and over-dose polymer ranges, rapidly injected into the sludge samples, and mixed at 200 rpm for 2 min and 30 sec. After conditioning, sludge samples were used for the settling, filtration, capillary

suction time (CST) and zeta potential tests as explained below. All experiments were run in triplicate and the average values are shown in the figures. Polymer doses are reported as g/kg DS (dry solids).

2.4. Evaluation of Thickening and Dewatering Performance

2.4.1. Capillary Suction Time (CST) Test

Capillary suction time (CST) test was used to evaluate the dewaterability of sludge samples after conditioning with polymer. CST test measures the time it takes for filtered water to travel between two sensors, and shorter CST times indicate better filtration properties. A CST tester (Type 319 Multi-CST, Triton Electronics Ltd., England) was used with the CST paper (No. 17 chromatography grade paper cut into 7 cm × 9 cm, Whatman PLC), and the protocol outlined in the Standard Methods [18] was followed.

2.4.2. Filtration Test

Conditioned sludge samples of 200 mL were filtered for 3 minutes using 55 mm-diameter coarse filters (Fisher Scientific Ltd.) and a vacuum pump. Filtrate volume and total solids concentration of the cake remaining on the filter were measured after filtration. Total solids concentration of the cake was determined following the protocol in the Standard Methods [18].

2.4.3. Zeta Potential Test

After the filtration tests, 10 mL of the filtrate from each sample was used for measuring the zeta potential. The filtrate samples were diluted by 10 times and 10 particles were tracked to get the average zeta potential measurement for each sample. Zeta potential measurements were performed using a zeta meter (Zeta-Meter System 4.0, GENEQ Inc.) operated at the default cell parameters of 200 V and 25°C. Samples that were conditioned and dewatered at higher temperatures were cooled down to 25°C before the zeta potential measurements.

2.4.4. Settling Test

Settling tests were carried out in 100 mL graduated cylinders in triplicate. 100 mL of the conditioned sludge sample was transferred to each graduated cylinder and the height of the interface between the solid

and the liquid phases was recorded for 30 minutes. The final height of the interface indicates the settling and thickening performance of the conditioned sludge. After the settling curves were established, the slopes of the lines before the inflection point (first 60 seconds) were used to calculate the settling velocities.

3. RESULTS AND DISCUSSION

3.1. Sludge Conditioning at 10°C

Figure 1 illustrates the results from the CST and filtration tests after conditioning sludge at 10°C by adding the Zetag 8160 polymer. In the under-dose range, filtrate volume and cake solids concentration increased gradually as the polymer dose approached the optimum dose. At the same time, a decrease in CST was observed which indicated water was rapidly released from conditioned sludge. At or around the optimum dose, the filtrate volume and cake solids reached their maximum values and CST reached its minimum value. In the over-dose range, deterioration in filterability was observed which was indicated by an increase in CST and decreases in filtrate volume and cake solids. Based on the results illustrated in Figure 1, optimum polymer dose at 10°C was determined to be 19.5 ± 0.7 g/kg DS (dry solids) with a CST of 20.0 ± 0.6 s, filtrate volume of 143 ± 5 mL, and cake solids of 7.7 ± 0.3 %.

The results from the zeta potential measurements are shown in Figure 2. Zeta potential is the electric potential of the particle and the surrounding double layer at the slipping plane and indicates the magnitude of the

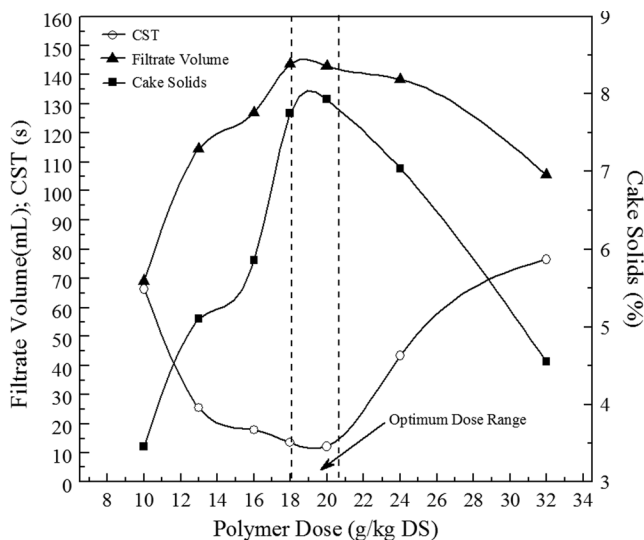


Figure 1. CST, filtrate volume and cake solids at 10°C in the under-dose, optimum dose, and over dose ranges.

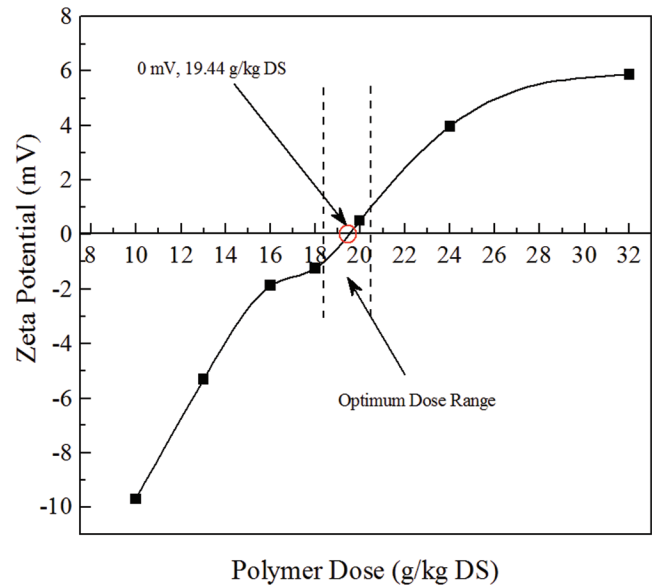


Figure 2. Zeta potential measurements at 10°C at increasing polymer doses.

attraction-repulsion forces between particles. A strong negative or positive charge would indicate the stability of the particles in the solution, and at or around the optimum polymer dose zeta potential approaches zero [19,20]. Sludge particles are negatively charged and therefore zeta potential values are negative in the under-dose range. Increasing the cationic polymer dose gradually decreases the magnitude of the negative zeta potential, and the zeta potential reaches a value of zero at the optimum dose. When the optimum dose is exceeded, zeta potential values obtain a positive charge that increase in magnitude with continuing polymer addition. The zeta potential measurements illustrated in Figure 2 point to an optimum dose of 19.44 g/kg DS, which is in accord with the optimum dose determined with the CST and filtration tests.

Settling test results showing the settling behaviour and the final interface height of the samples are presented in Figure 3 and Table 1. The initial height of the solids-liquid interface was 17.8 cm for all samples. All samples settled rapidly in the first minute; however, the sample that was conditioned at 20 g/kg DS had the highest settling velocity (6.5 cm/min) compared to the samples that were conditioned at lower or higher polymer doses. Differences in the settling height of the interfaces were clearly seen in the first 5 minutes. The height of the final interface was lowest (9.1 cm) for the sludge sample conditioned at 20 g/kg DS indicating the best settling and compaction of solids among the doses tested. At polymer doses lower or higher than 20 g/kg DS, the height of the final interface gradually increased and

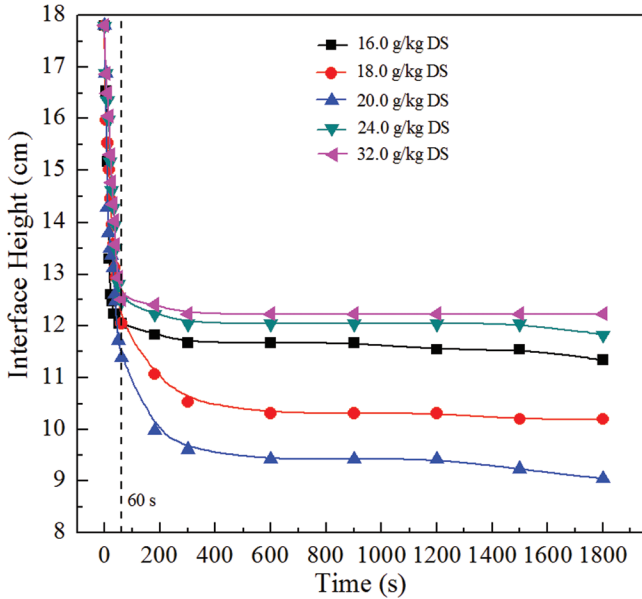


Figure 3. Settling test results at 10°C after 30 minutes of settling.

was 11.8 cm at 24 g/kg DS and 10.2 cm at 18 g/kg DS. These results indicated that 20 g/kg DS was the optimum polymer dose among the doses tested.

3.2. Sludge Conditioning at 35°C

Sludge conditioning experiments were repeated at 35°C using the same polymer. Based on the results of the filtration and CST tests, the optimum polymer dose range emerged as 19.3 ± 1.4 g/kg DS (Figure 4), which resulted in 13.9 ± 0.4 s of CST, 161 ± 2 mL of filtrate volume and $11.0 \pm 0.3\%$ of cake solids. The zeta potential values of the particles in the filtrate samples are shown in Figure 5. The polymer dose where the zeta potential reached a neutral value was around 19.41 g/kg DS, which confirms the optimum dose range determined with the filtration and CST tests (Figure 4).

Figure 6 illustrates the settling test results from sludge samples conditioned at 35°C. Increasing the polymer dose improved the settling characteristics of sludge, and the lowest interface height (7.2 cm) after

Table 1. Final Interface Heights (30 minutes) and Average Settling Velocities (60 s) at 10°C.

Polymer Dose (g/kg DS)	Final Interface Height (cm)	Settling Velocity (cm/min)
16.0	11.3	5.8
18.0	10.2	5.8
20.0	9.1	6.5
24.0	11.8	5.2
32.0	11.9	5.3

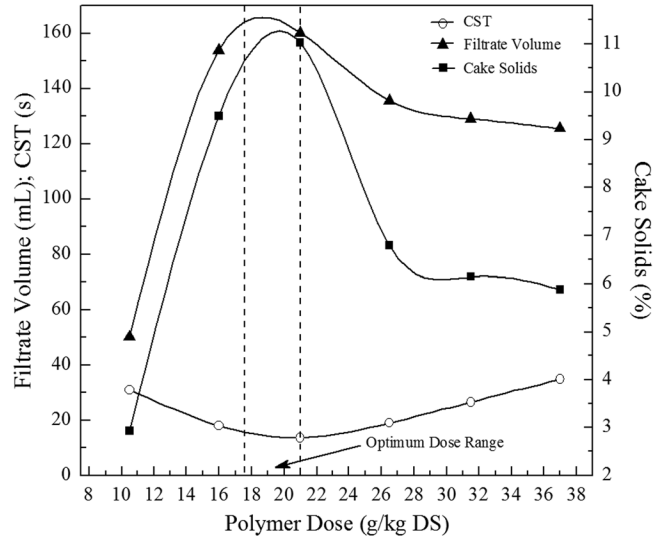


Figure 4. CST, filtrate volume and cake solids at 35°C in the under-dose, optimum dose, and over dose ranges.

30 min. of settling was observed at the polymer dose of 21 g/kg DS, which is in agreement with results shown in Figures 4 and 5. The adjacent lower and higher polymer doses were 16 g/kg DS and 26.5 g/kg DS, and the interface height corresponded to 7.5 cm and 8.8 cm at these doses.

Table 2 illustrates the calculated average settling velocities as well as the final interface heights recorded at each dose. The fastest settling (10.5 cm/min) occurred at 21 g/kg DS, which was the optimum dose. When the polymer dose was lower or higher than 21 g/kg DS, settling velocities decreased proportional to the increase or decrease in the polymer dose.

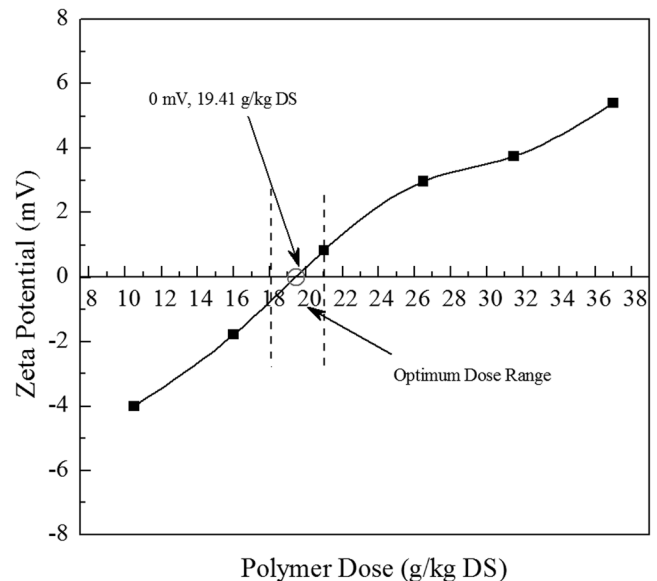


Figure 5. Zeta potential measurements at 35°C at increasing polymer doses.

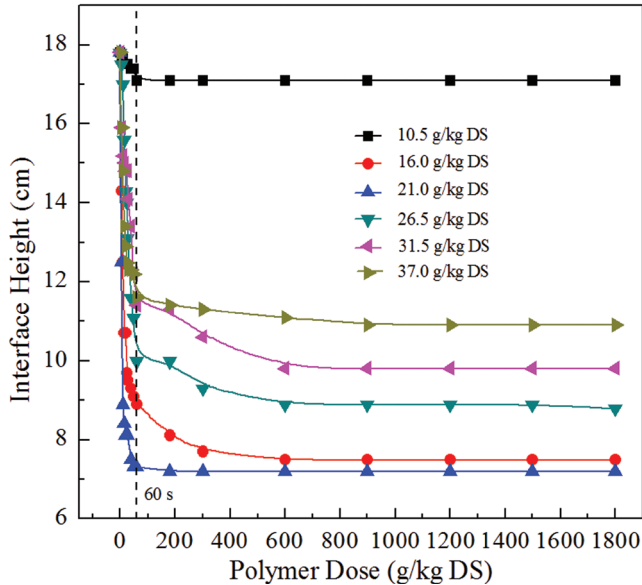


Figure 6. Settling test results at 35°C after 30 minutes of settling.

3.3. Sludge Conditioning at 50°C

Figure 7 illustrates the results from the filtration and CST tests after conditioning sludge at 50°C. The lowest CST (11.8 ± 0.6 s) and the highest filtrate volume (165 ± 3 mL) and cake solids (11.5 ± 0.4 %) were measured at 19.2 ± 0.9 g/kg DS. Zeta potential measurements also indicated the optimum dose as 19.40 g/kg DS where a neutral value for the zeta potential was achieved (Figure 8).

Figure 9 illustrates the settling performances of conditioned sludge samples at 50°C in the dose range of 10–27 g/kg DS. Among the doses tested, the best settling performance was observed at 20 g/kg DS, which resulted in the lowest interface height. At polymer doses lower or higher than 20 g/kg DS, settling characteristics of sludge deteriorated and resulted in a higher interface height. The calculated settling velocities and the final interface heights are reported in Table 3. The highest settling velocity, 12.6 cm/min, was obtained at

Table 2. Final Interface Heights (30 minutes) and Average Settling Velocities (60 s) at 35°C.

Polymer Dose (g/kg DS)	Final Interface Height (cm)	Settling Velocity (cm/min)
10.5	17.1	0.7
16.0	7.5	8.9
21.0	7.2	10.5
26.5	8.8	7.8
31.5	9.8	6.4
37.0	10.9	6.2

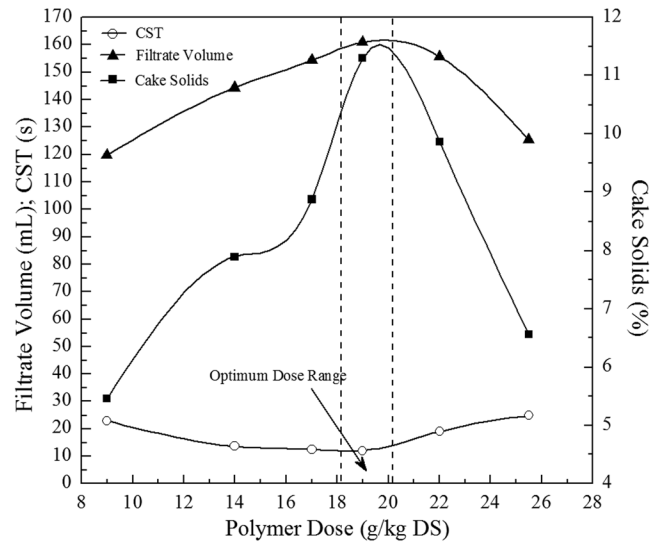


Figure 7. CST, filtrate volume and cake solids at 50°C in the under-dose, optimum dose, and over dose ranges.

the polymer dose of 20 g/kg DS, and this corresponded to the lowest interface height of 5.4 cm.

3.4. Sludge Conditioning at 60°C

Figure 10 illustrates the results from the filtration and CST tests after conditioning sludge at 60°C. The optimum dose range was identified as 26.5 ± 1.5 g/kg DS, with CST of 12.3 ± 0.5 s, the filtrate volume of 146 ± 3 mL and the cake solids of 7.7 ± 0.3 %. These results showed a deterioration in sludge filtration compared to the results obtained at 50°C. Heating

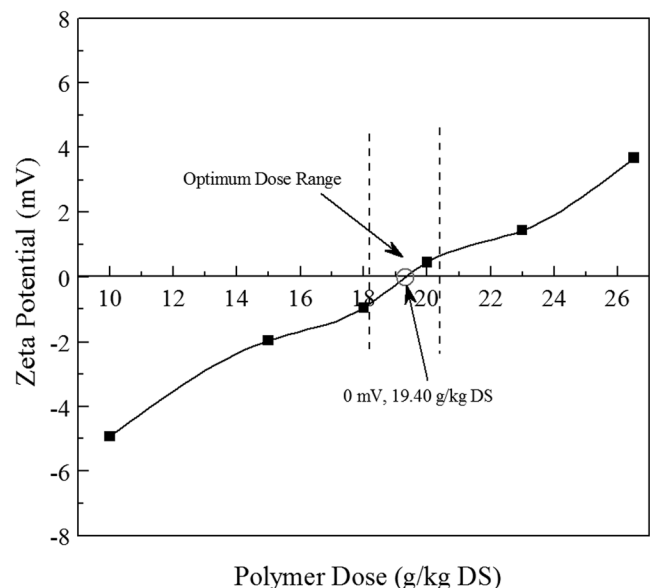


Figure 8. Zeta potential measurements at 50°C at increasing polymer doses.

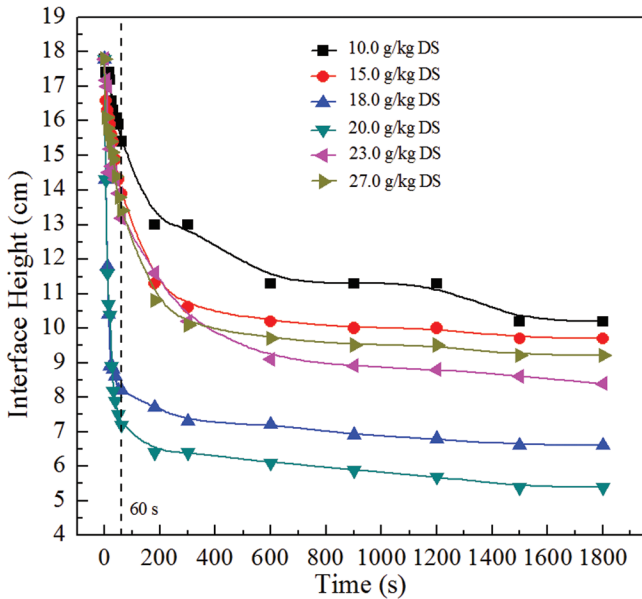


Figure 9. Settling test results at 50°C after 30 minutes of settling.

at these higher temperatures started dissolving solids and breaking up large particles, which increased the polymer demand due to the generation of more negatively charged surfaces.

As the zeta potential results show in Figure 11, a higher polymer dose (26.5 g/kg DS) was needed to neutralize the zeta potential at 60°C. At 20 g/kg DS, which was the optimum dose for the temperatures lower than 50°C, the zeta potential value was approximately -1.5 mV. With increasing temperatures, the binding between the polymer and sludge particles weakens and the efficiency of flocculation decreases [21]. Therefore, more polymer is needed to achieve the same level of conditioning and flocculation at higher temperatures.

Results from settling tests at 60°C are shown in Figure 12 and Table 4. Among the doses tested, 26.5 g/kg DS resulted in the highest settling velocity (5.8 cm/min) and the lowest interface height (10.7 cm). Presence of large quantities of bubbles was also observed during settling. Compared to other temperatures

Table 3. Final Interface Heights (30 minutes) and Average Settling Velocities (60 s) at 50°C.

Polymer Dose (g/kg DS)	Final Interface Height (cm)	Settling Velocity (cm/min)
10.0	10.2	2.4
15.0	9.7	3.9
18.0	6.6	9.6
20.0	5.4	12.6
23.0	8.4	4.6
27.0	9.2	4.4

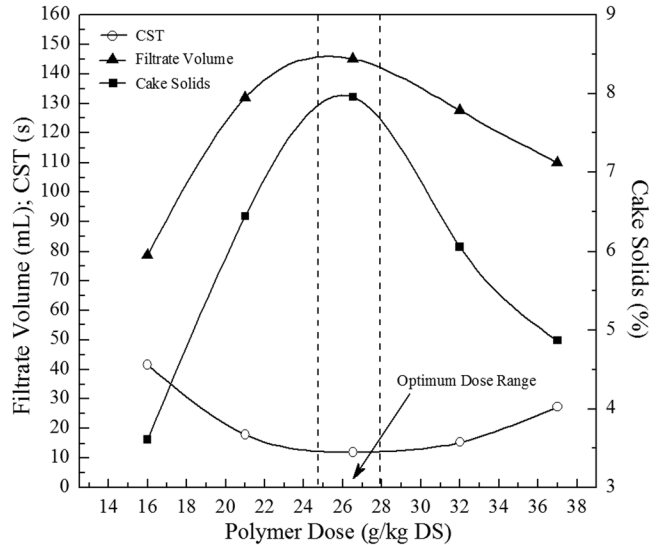


Figure 10. CST, filtrate volume and cake solids at 60°C in the under-dose, optimum dose, and over dose ranges.

(e.g., 35°C and 50°C), both the settling velocity and the height of the interface got worse at 60°C in spite of adding more polymer. The binding ability of polyacrylamide is decreased after around 60°C [22] which can also explain the decreased effectiveness of the polymer and the higher polymer doses required at higher temperatures.

3.5. Sludge Conditioning at 100°C

The polymer doses required for sludge conditioning at 100°C were drastically higher (Figure 13). The opti-

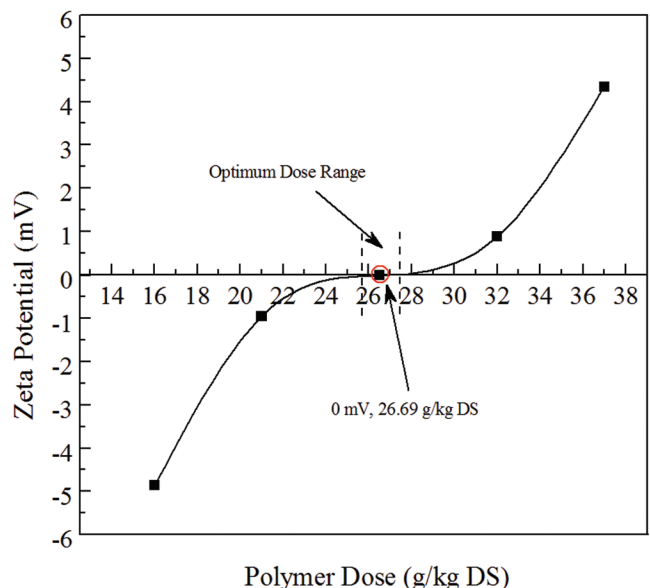


Figure 11. Zeta potential measurements at 60°C at increasing polymer doses.

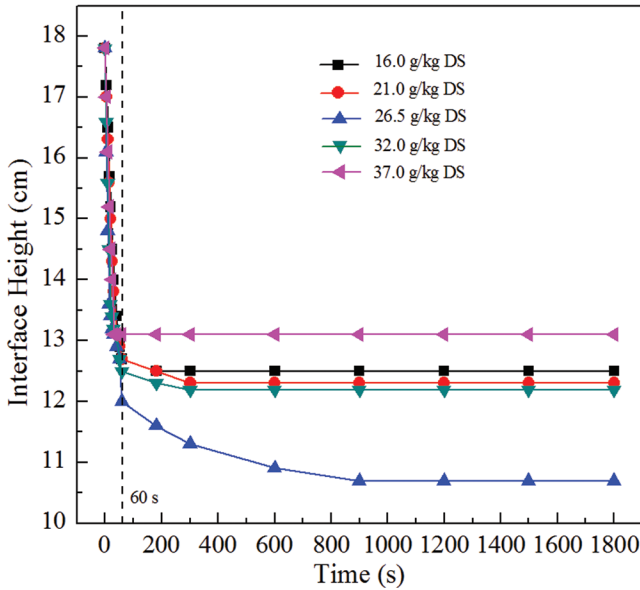


Figure 12. Settling test results at 60°C after 30 minutes of settling.

imum dose at this temperature was 38.5 ± 1.2 g/kg DS, which was almost double the dose at 50°C. In the optimum dose range, CST was 12.8 ± 0.3 s, filtrate volume was 149 ± 3 mL, and cake solid concentration was 7.9 ± 0.3 %. Increasing the sludge temperature, increased the polymer demand of the sample.

Figure 14 illustrates that the zeta potential results. At the starting polymer dose of 15 g/kg DS, the zeta potential was approximately -10 mV, which was 5 times more than the zeta potential values measured around 15 g/kg DS at other temperatures tested. Increasing the polymer dose decreased the magnitude of the zeta potential, but even at the highest polymer dose of 55 g/kg DS, charge neutralization was not achieved. The filtration based tests indicated an optimum dose of 38.5 g/kg DS, but the zeta potential at this dose was still -4 mV. This can be explained by the different temperatures that the measurements were carried at. The CST and filtration tests were conducted with sludge at 100°C but the zeta potential measurements had to be done at 25°C due to the constraint of the zeta-meter. The solubility

Table 4. Final Interface Heights (30 minutes) and Average Settling Velocities (60 s) at 60°C.

Polymer Dose (g/kg DS)	Final Interface Height (cm)	Settling Velocity (cm/min)
16.0	12.5	5.1
21.0	12.3	5.1
26.5	10.7	5.8
32.0	12.2	5.3
37.0	13.1	4.7

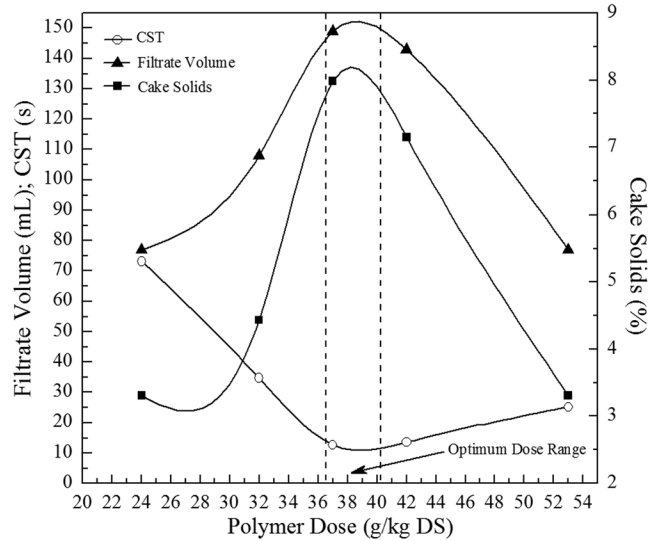


Figure 13. CST, filtrate volume and cake solids at 100°C in the under-dose, optimum dose, and over dose ranges.

of acrylamide sharply increases after 50°C [23], and therefore when the temperature of filtrate is decreased from 100°C to 25°C, zeta potential measurements will underestimate the quantity and effectiveness of the dissolved polymer in the solution. This would explain the negative zeta potential of -4 mV at the optimum dose of 38.5 g/kg DS at 100°C.

The settling test results at 100°C are illustrated in Figure 15 and Table 5. The lowest height of the interface (7.9 cm) and the highest settling velocity (4 cm/min) was observed at 37 g/kg DS, which was also the optimum dose determined by the filtration tests.

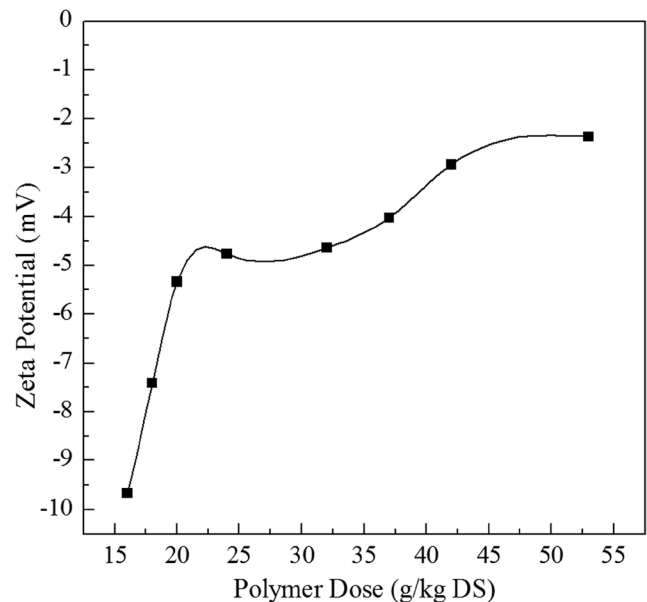


Figure 14. Zeta potential measurements at 100°C at increasing polymer doses.

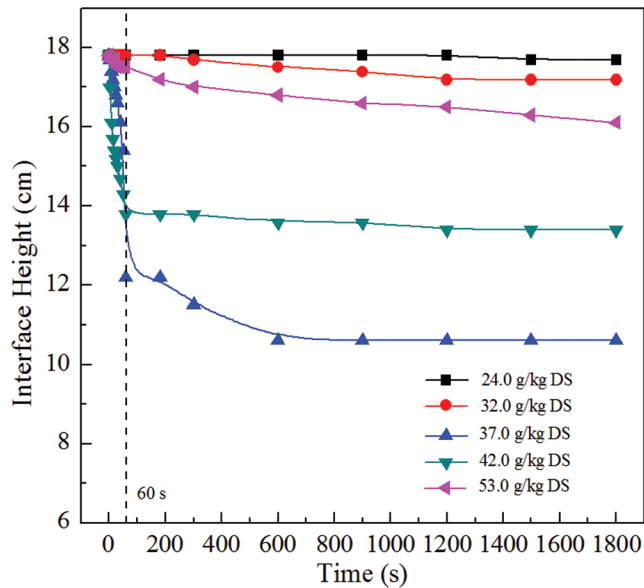


Figure 15. Settling test results at 100°C after 30 minutes of settling.

3.6. Comparison of Conditioning Performance at Different Temperatures

Table 6 presents the optimum dose, CST, filtrate volume, cake solids, and settling velocity obtained at each temperature tested (10°C, 35°C, 50°C, 60°C and 100°C) to provide a comparison of results. The optimum dose required to condition the sludge was very similar (19.2–19.5 g/kg DS) at 10, 35, and 50°C; however, the ability of sludge to release its water was significantly different. Increasing the temperature until 50°C improved the thickening and filtration characteristics of conditioned sludge, and the highest filtrate volume (165 mL), cake solids (11.5%) and settling velocity (12.6 cm/min) were observed at 50°C. Increasing the sludge temperature further to 60°C and 100°C not only increased the polymer demand substantially, but also decreased the ability of sludge to release its water. The optimum polymer dose was 26.5 g/kg DS at 50°C, and 38.5 g/kg DS at 100°C. At 100°C, the filtrate volume was reduced to 149 mL and the settling velocity was only 4 cm/min.

Table 5. Final Interface Heights (30 minutes) and Average Settling Velocities (60 s) at 100°C.

Polymer Dose (g/kg DS)	Final Interface Height (cm)	Settling Velocity (cm/min)
24.0	17.7	0.1
32.0	17.2	0.1
37.0	7.9	4.0
42.0	13.4	3.8
53.0	16.1	0.3

Changes in sludge temperature impacts the sludge characteristics as well as the polymer characteristics. A modest increase in sludge temperature (35–50°C) is likely to decrease the viscosity and improve the filtration characteristics of sludge. In addition, temperature increases the solubilization of extracellular polymers and DNA, which result in the improvement of sludge surface characteristics such as surface charge [24]. It was previously reported that higher temperatures lead to changes in the structure, density and chemical composition of flocs which influence the settleability and desorptivity [25,26,27]. Higher temperatures also impact the activity of polymers by decreasing their rate of formation and viscosity and increasing their hydrolysis into soluble compounds [27,28,29]. The results of this research show that temperatures up to 50°C improved the dewaterability of sludge but higher temperatures lead to deterioration in sludge dewaterability likely due to the destruction of flocs and sludge network. This study did not include sludge temperatures higher than 100°C since these systems would require pressurized vessels and would not be easily employable at full-scale treatment plants. At temperatures higher than 150°C during hydrothermal treatment (carbonization) of sludge, the decomposition of extracellular polymers was reported to destroy their binding with water and release this water resulting in better dewaterability [24].

4. CONCLUSIONS

In this study, temperature was found to be an impor-

Table 6. Summary of Results at Each Temperature.

T (°C)	Optimum Dose (g/kg DS)	CST (s)	Filtrate Volume (mL)	Cake Solids (%)	Settling Velocity (cm/min)
10	19.5 ± 0.7	20.0 ± 0.6	143 ± 5	7.7 ± 0.3	6.5
35	19.3 ± 1.4	13.9 ± 0.4	161 ± 2	11.0 ± 0.3	10.5
50	19.2 ± 0.9	11.8 ± 0.6	165 ± 3	11.5 ± 0.4	12.6
60	26.5 ± 1.5	12.3 ± 0.5	146 ± 3	7.7 ± 0.3	5.8
100	38.5 ± 1.2	12.8 ± 0.3	149 ± 3	7.9 ± 0.3	4.0

tant factor that impacts sludge conditioning, optimum polymer dose, and thickening and dewatering performance. A wide range of sludge temperatures (10°C, 35°C, 50°C, 60°C and 100°C) were tested. In the temperature range of 10°C to 50°C, the polymer dose required for conditioning was similar but resulted in different thickening and dewatering performance. The best results were observed at 50°C, where the highest filtrate volume, cake solids and settling velocity were obtained at a polymer dose of 19.2 g/kg DS. Thickening and dewatering performance was also very good at 35°C. Increasing the sludge temperature further to 60°C and 100°C increased the polymer demand up to 38.5 g/kg DS and deteriorated the thickening and dewatering performance. The results of this research show that sludge conditioning at 35–50°C can significantly improve treatment performance and result in savings for treatment plants. There would be no additional cost for heating sludge at wastewater treatment plants where thermal treatment processes (e.g., thermal hydrolysis, wet oxidation, super critical water oxidation) are used, and a step-wise temperature increase before thickening or dewatering can be easily incorporated in the treatment train.

5. ACKNOWLEDGMENT

The authors thank the Ontario-China Research and Innovation Fund (OCRIF) for financial support provided for this project.

6. REFERENCES

- Nowak, O., 2006. Optimizing the Use of Sludge Treatment Facilities at Municipal WWTPs. *Journal of Environmental Science and Health Part A*, 41(9):1807–17. <http://dx.doi.org/10.1080/10934520600778986>
- Al Momani, F.A., Örmeci, B., 2014. Optimization of polymer dose based on residual polymer concentration in dewatering supernatant. *Water Air Soil Pollut.* 255, 2154–2165. <http://dx.doi.org/10.1007/s11270-014-2154-z>
- Werle, C., Novak, J., Knocke, W., and Sherrard, J., 1984. Mixing Intensity and Polymer Sludge Conditioning. *J. Environ. Eng.*, 110 (5), 919–934. [http://dx.doi.org/10.1061/\(ASCE\)0733-9372\(1984\)110:5\(919\)](http://dx.doi.org/10.1061/(ASCE)0733-9372(1984)110:5(919))
- Novak, J. T. and Lynch, D. P., 1990. The effect of shear on conditioning: Chemical requirements during sludge dewatering. *Water Science and Technology*, 22 (12), 117–124.
- Örmeci, B. and Ahmad, A., 2009. Measurement of additional shear during sludge conditioning and dewatering. *Water Research*, 43 (13), 3249–3260. <http://dx.doi.org/10.1016/j.watres.2009.04.049>
- Murray, A., Örmeci, B., 2008. Impact of polymer-sludge interaction on rheogram peaks and optimum dose determination. *Water Science and Technology*. 57 (3), 389–394. <http://dx.doi.org/10.2166/wst.2008.018>
- Amuda, O. S. and Amoo, I. A., 2007. Coagulation/flocculation process and sludge conditioning in beverage industrial wastewater treatment. *Journal of Hazardous Materials*. 141 (3), 778–783. <http://dx.doi.org/10.1016/j.jhazmat.2006.07.044>
- Park, C., Muller, C. D., Abu-Orf, M. M. and Novak, J. T., 2006. The Effect of Wastewater Cations on Activated Sludge Characteristics: Effects of Aluminum and Iron in Floc. *Water Environment Research*. 78 (1), 31–40. <http://dx.doi.org/10.2175/106143005X84495>
- Shi, Y., Yang, J., Yu, W., Zhang, S., Liang, S., Song, J., Xu, Q., Ye, N., He, S., Yang, C., Hu, J., 2015. Synergetic conditioning of sewage sludge via Fe²⁺/persulfate and skeleton builder: Effect on sludge characteristics and dewaterability. *Chemical Engineering Journal*. 270, 572–581. <http://dx.doi.org/10.1016/j.cej.2015.01.122>
- Zhang, X., Lei, H., Chen, K., Liu, Z., Wu, Han, Liang, H., 2012. Effect of potassium ferrate (K₂FeO₄) on sludge dewaterability under different pH conditions. *Chemical Engineering Journal*. 210, 467–474. <http://dx.doi.org/10.1016/j.cej.2012.09.013>
- Houghton, J. I. and Stephenson, T., 2002. Effect of influent organic content on digested sludge extracellular polymer content and dewaterability. *Water Research*. 36 (14), 3620–3628. [http://dx.doi.org/10.1016/S0043-1354\(02\)00055-6](http://dx.doi.org/10.1016/S0043-1354(02)00055-6)
- Neyens E. and Baeyens J., 2003. A review of thermal sludge pretreatment processes to improve dewaterability. *Journal of Hazardous Materials*. 98 (1-3), 51–67. [http://dx.doi.org/10.1016/S0304-3894\(02\)00320-5](http://dx.doi.org/10.1016/S0304-3894(02)00320-5)
- Werthera, J. and Ogadab, T., 1999. Sewage sludge combustion. *Progress in Energy and Combustion Science*. 25 (1), 55–116. [http://dx.doi.org/10.1016/S0360-1285\(98\)00020-3](http://dx.doi.org/10.1016/S0360-1285(98)00020-3)
- Bertanza G, Galessi R, Menoni L, Salvetti R, Slavik E, Zanaboni S., 2015. Wet oxidation of sewage sludge: full-scale experience and process modeling. *Environ Sci Pollut Res Int*. 22(10), 7306–16. <http://dx.doi.org/10.1007/s11356-014-3144-9>
- Griffith, J. W. and Raymond D. H., 2002. The first commercial supercritical water oxidation sludge processing plant. *Waste Management*. 22(4):453–9. [http://dx.doi.org/10.1016/S0956-053X\(02\)00029-6](http://dx.doi.org/10.1016/S0956-053X(02)00029-6)
- Qian, L., Wang, S., Xu, D., Guo, Y, Tang, X, and Wang, L., 2015. Treatment of sewage sludge in supercritical water and evaluation of the combined process of supercritical water gasification and oxidation. *Bioresour Technol*. 176, 218–224. <http://dx.doi.org/10.1016/j.biortech.2014.10.125>
- Hii, K., Baroutain, S., Parthasarathy, R., et al., 2014. A review of wet air oxidation and Thermal Hydrolysis technologies in sludge treatment. *Bioresour Technol*. 155, 289–299. <http://dx.doi.org/10.1016/j.biortech.2013.12.066>
- APHA, American Public Health Association, American Water Works Association, and the Water Environment Federation 2005 Standard Methods for the Examination of Water and Wastewater. 21th Ed., Washington, D. C.
- Dentel, S. and Abu-Orf, M. M., 1993. Application of the streaming current detector in sludge conditioner selection and control. *Water Science & Technology*. 28(1), 169–179.
- López-Maldonado, E.A., Oropeza-Guzman, M.T., Jurado-Baizaval, J.L., Ochoa-Teran, A., 2014. Coagulation–flocculation mechanisms in wastewater treatment plants through zeta potential measurements. *Journal of Hazardous Materials*. 279, 1–10. <http://dx.doi.org/10.1016/j.jhazmat.2014.06.025>
- Meid, J., Dierkes, F., Cui, J., 2012. Mechanical properties of temperature sensitive microgel/polyacrylamide composite hydrogels— from soft to hard fillers. *Soft Matter*. 8, 4254–4263. <http://dx.doi.org/10.1039/c2sm06868k>
- Sakohara, S., Ochiai, E., Kusaka, T., 2007. Dewatering of activated sludge by thermosensitive polymers. *Separation and Purification Technology*. 56 (3), 296–302. <http://dx.doi.org/10.1016/j.seppur.2007.02.004>
- Uğuzodoğan, E., Denkbaz, E.B., Kabasakal, O.S., 2013. Investigation of temperature sensitivity behaviors of water soluble polyacrylamides. *Journal of Applied Polymer Science*. 127 (6), 4374–4384. <http://dx.doi.org/10.1002/app.38008>
- Wang, L. and Li, A. (2015) Hydrothermal treatment coupled with mechanical expression at increased temperature for excess sludge dewatering: The dewatering performance and the characteristics of products. *Water Research*. 68, 291–303. <http://dx.doi.org/10.1016/j.watres.2014.10.016>

25. Dignac, M. F., Urbain, V., Rybacki, D., Ruchet, A. (1988) Chemical description of extracellular polymers: Implications on activated sludge floc structure. *Water, Science & Technology*. 38 (8-9), 45–53. [http://dx.doi.org/10.1016/S0273-1223\(98\)00676-3](http://dx.doi.org/10.1016/S0273-1223(98)00676-3)
26. Chundakkadu, K. and Van Loosdrecht, C. M. (1999) Effect of temperature on storage polymers and settleability of activated sludge. *Water Research*. 33 (10), 2374–2382. [http://dx.doi.org/10.1016/S0043-1354\(98\)00445-X](http://dx.doi.org/10.1016/S0043-1354(98)00445-X)
27. Sawalha, O., and Scholz, M. (2012) Impact of temperature on sludge dewatering properties assessed by the capillary suction time. *Industrial & Engineering Chemistry Research*, 51, 2782–2788. <http://dx.doi.org/10.1021/ie202381r>
28. Feng, L., Wang, H., Chen, Y., and Wang, Q. (2009) Effects of solids retention time and temperature on waste activated sludge hydrolysis and short-chain fatty acids accumulation under alkaline conditions in continuous flow reactors. *Bioresource Technology*. 100 (1), 44–49. <http://dx.doi.org/10.1016/j.biortech.2008.05.028>
29. Joönsson, K. and Jansen, J. C. (2006) Hydrolysis of return sludge for production of easily biodegradable carbon: effect of pre-treatment, sludge age, and temperature. *Water Science & Technology*. 53 (12), 47–54. <http://dx.doi.org/10.2166/wst.2006.405>

Copper (II) Removed from Aqueous Solutions by Aminated Bagasse Pith

XINLIANG LIU^{1,2,*}, CONG GAO¹, CHEN LIANG^{1,2}, SHUANGXI NIE^{1,2} and SHUANGFEI WANG^{1,*}

¹College of Light Industry and Food Engineering, Guangxi University, Nanning 530004, P.R. China

²Guangxi Key Laboratory of Clean Pulp & Papermaking and Pollution Control, Nanning 530004, P.R. China

ABSTRACT: The paper investigated the heavy metal ions adsorption by bio-adsorbent obtained from modifying bagasse pith. The bagasse pith, a main solid bio-waste from sugar and pulp industry, was treated by epichlorohydrin and diethylenetriamine. The pith before and after modification were analyzed to characterize its structure change by Fourier Transform Infrared Spectroscopy and Scanning Electron Microscope. It shown that numbers of minor fragments cohere to the surface of fibrous bundle of modified pith. The carboxyl groups has been introduced with the change of substitutional groups in aromatic skeletal of lignin on surface of pith. The kinetics and thermo-dynamic properties were studied. The results shown the adsorption process are well described by Langmuir isotherm and pseudo-2nd order model. It is considered that the bagasse pith, a renewable bio-waste, would be modified to treat the waste water polluted by heavy metal in further studies.

1. INTRODUCTION

WATER pollution is a worldwide environmental problem, especially in waste water polluted by heavy metal ions discharged from the industrial waste. These metals, such as Cu, Pb, Cr and Zn, are toxic. Their presence could cause some diseases [1–4]. For restoration, a lot of effective methods are used to remove polluted ions [5,6]. Among those methods, adsorption is one of the economical and efficient methods. Recently, low cost materials such as renewable and biodegradable byproducts or wastes from agriculture attract researchers' attention as their physic-chemical properties. Some of them, such as tree fern, sawdust, rice bran, wheat bran, corncobs, etc., have been modified to remove heavy metals [5,7–9].

Bagasse pith, a main solid waste from sugar and pulp industry, contains lignin, hemicellulose and cellulose. Thus, it contains hydroxyl, carboxyl and carbonyl groups [10], which are the efficacious functional groups for ions sorption. In addition, bagasse pith has the unique physical structure. Based on Lee's study, the pith consists of numerous parenchyma cells with

bundles of small fibers in the inner pith [11]. It is reported that small quantity cellulose fibers and a regular shape of spongy particle are in bagasse pith, which enhanced its specific surface. In earlier studies, bagasse pith has been used to prepare activated carbon or dye adsorbent [12–14]. However, there is seldom study on the modified pith and its adsorption for heavy metal ions removal. In the previous, we found the cellulose and lignin, the main constituents of bagasse pith, could be modified to be good ions adsorbents [15].

The present study was focused on the modification of bagasse pith and its adsorption ability for Cu(II). The equilibrium, kinetics and thermodynamic property of modified pith were investigated.

2. METHODS

2.1. Materials

Bagasse pith was supplied by Nanning Sugar Industry Co., Ltd. China. It was washed by distilled water and dried at room temperature. The main compositions of bagasse pith were cellulose 38.10% (w/w, the same as below), lignin 25.93%, hemicellulose 24.23%, ash 1.28%, alcohol-benzene soluble 2.28% and 1% NaOH soluble 28.34%. All chemicals, were obtained from commercial sources. 300 mg/L Cu(II) were prepared by CuCl₂ and its initial pH is 5.52.

*Authors to whom correspondence should be addressed.

Postal Address: College of Light Industry and Food Engineering, Guangxi University, Nanning 530004, P.R. China; Tel: +8615977760717 Fax: +86 771 3237097
E-mail: xinliang.liu@hotmail.com; sfwang@gxu.edu.cn

2.2. Methods

2.2.1. Preparation of Modified Bagasse Pith

Modified bagasse pith was produced by the reference. [16] and then aminated with diethylenetriamine cross linked by formaldehyde. Bagasse pith (2 g) was added into flask with 100 mL NaOH (10%, w/w) and 10 mL ethanol (75%, w/w). Then, 10 mL of epichlorohydrin was added into this mixture in 30 min, and stirred at 60°C for 4h. Then, the product was filtered by G2 glass filter and washed by distilled water. The epoxy-bagasse pith was obtained, and dried (at 50°C).

Add epoxy-bagasse pith (2 g), NaOH (10%, 15 mL), and diethylenetriamine (5 mL) are added into a flask. Then, drop formaldehyde (5 mL) into the heated mixture at 80°C in 30 min, and reaction 3 h. After that, the modified bagasse pith was filtered and washed by distilled water.

2.2.2. Sorption

The adsorption experiments were processed at room temperature (25°C). 0.5 g modified bagasse pith and 200 mL Cu(II) ion solution (300 mg/L) were added in to the flask. The aqueous solutions were taken with membrane (0.45 μm). The Atomic Absorption Spectrometer (TAS-990AFG) was used to measured the concentrations. The adsorption was calculated by Equation (1),

$$q_t = \frac{V(C_0 - C_t)}{w} \quad (1)$$

where q_t is the adsorption capacity. C_0 is the concentration of metal ions at time 0, and C_t (mg/L) is the concentration of metal ions at time t . and V is the volume (L) of solution, and w is the mass (g) of adsorbent.

2.2.3. Mechanism Study

0.5 g modified bagasse pith and 200 mL Cu(II) ion solution (300 mg/L) were added in to the flask. To change the initial pH of solution, NaOH (1 mol/L) and HCl (1 mol/L) solution were added.

The pH and electricity conductivity of solution were also determined during adsorption processed at initial pH 6.5.

2.2.4. Characterization

FTIR (Fourier Transform Infrared spectroscopy of

PerkinElmer BXII spectrum) was used by using KBr pellets, by a. SEM (Scanning electron microscope of Hitachi S-3400N) was to analyze the surface changes of the pith before and after modification.

3. RESULTS AND DISCUSSION

3.1. The Morphology Analysis

The pith component consists of numerous big hollow cavities, which decreases bulk density [11]. Most are the parenchyma cell with bundles of small fibers in the inner pith. The most of the cells are in regular shape as spongy. Some cellulose fibers in small size are embedded. All of these could improve its surface strength. To increase the bagasse pulp quality, the pith, the density of which is 220 kg/m³ [17] should be depithed, as the cells of pith are usually in tiny shape (length < 0.4 mm) with thin wall [18]. Thus, after it has been treated by the depithing machine, most parenchyma cells were ruptured with fibrous bundle separated.

In Figure 1, the morphology of fragment pith Figure 1(a) is in the shape of layer with smooth surface before modification, while it presents the convex-concave folds of the surface [in Figure 1(b)]. It would be the effects of cross-link by the epichlorohydrin or formaldehyde. Numbers of minor fragments cohere to the surface of fibrous bundle of modified pith comparing the morphology before [Figure 1(c)] and after [see in Figure 1(d)] modification. Thus, it indicated the surface chemical component of pith would take part in the reactions.

3.2. FTIR Spectroscopy

The main chemical compositions of bagasse pith contains cellulose, lignin and hemicellulose etc. Thus, there are abundant of hydroxyl, aldehyde, carboxyl, methoxy, phenyl and ether bonds existed in pith.

Based on the assignments given in literatures [19–21], common features as well as particular vibrations were found. In Figure 2, main bands in all samples can be assigned to: absorption of alcoholic hydroxyl groups and phenolic hydroxyl groups are at 3421 cm⁻¹ and 3450–3500 cm⁻¹. C–H stretching of methylene and methine groups are at 2900–2945 cm⁻¹. Methoxyl groups stretching in lignin are at 2848 cm⁻¹. C=O stretching vibration in carboxyl are at 1734 cm⁻¹. The characteristic peaks of aromatic skeletal are at 1426, 1513, and 1603 cm⁻¹. Band at 1428 cm⁻¹ indicated aldehyde group vibration and –CH₂ symmetric bending

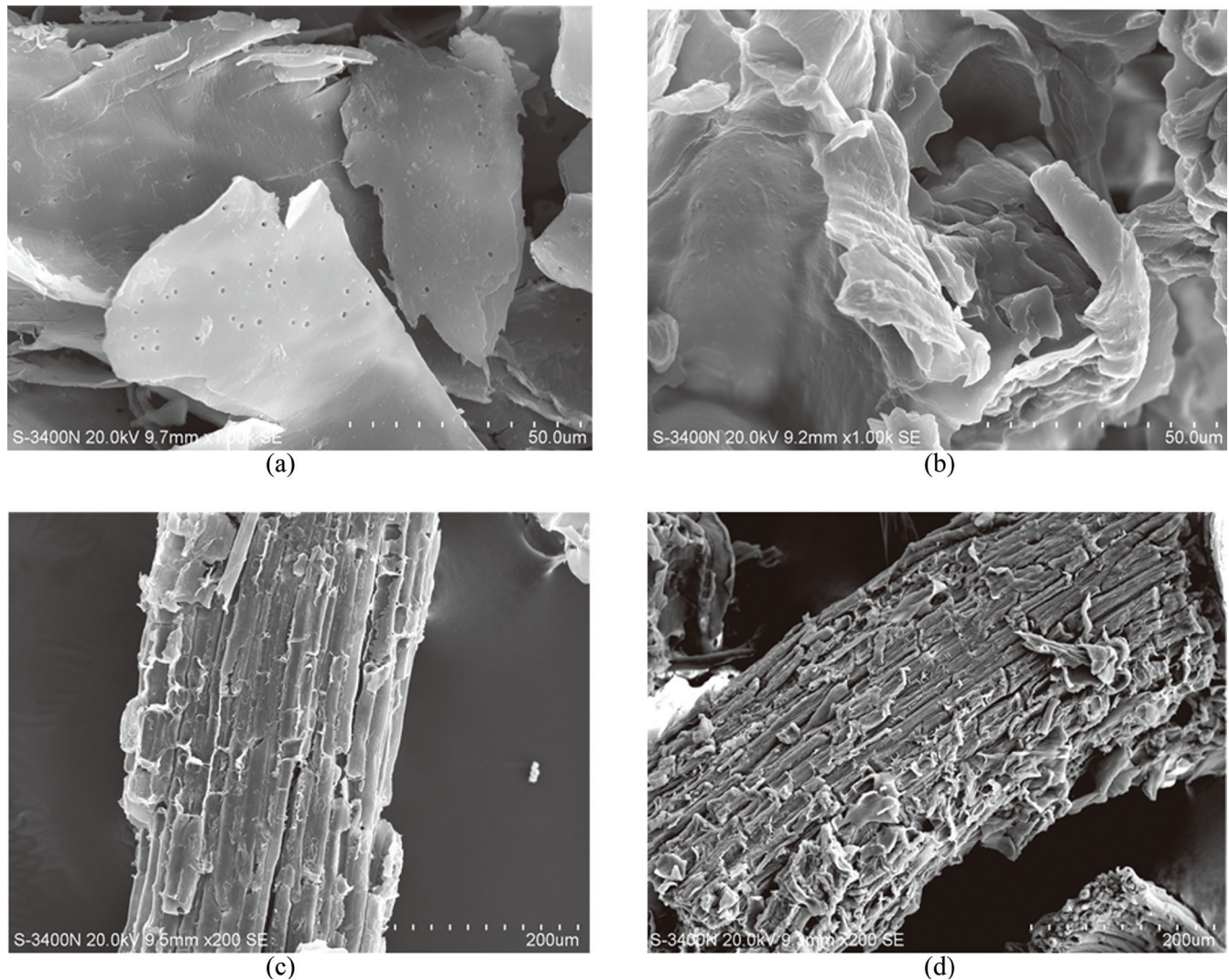


Figure 1. The morphology of bagasse pith and aminated epoxy-pith: the fragment of pith before (a) and after (b) modification, the fibrous bundle of pith before (c) and after (d) modification.

vibration. The band relates to bending vibration of the structure C–H at 1376 cm^{-1} . The bands indicates the cellulose ring breathing with C–O stretching at 1327 and 1250 cm^{-1} . Bandrelates to anti symmetric bridge C–O–C stretching in cellulose, lignin or hemicellulose at 1167 cm^{-1} . The band at 1111 cm^{-1} indicades C–H in-plane deformation for syringyl type in structure of lignin, and band at 1050 cm^{-1} for guaiacyl type. Another bandcorresponded to lone aryl C–H out plane wagging at 899 cm^{-1} .

The modified pith, the peaks disappear at 1734 cm^{-1} and rise at 1654 cm^{-1} with red shifting at 1636 cm^{-1} , which means the carboxyl takes part in a chemical reaction of hydrolysis and amination. The C–N vibration leads the intensity increasing at 1465 cm^{-1} . Bands weaken at 1376 , 1253 and 900 cm^{-1} suggested that the substitutional groups of aromatic skeletal in lignin on

surface of pith would be changed. The N–H vibration makes the bands red shift at 1165 cm^{-1} , and blue shift at 1111 and 1050 cm^{-1} . Thus, it can be concluded that the distribution of chemical structures, such as hydroxyl, carboxyl, methoxy, phenyl and so on, has been changed by modification on surface of fragment pith.

3.3. Influence of Solution Initial pH

The adsorption property of adsorbents is sensitive to pH . The optimal pH of sorption experiment was processed at initial pH from 1 to 7.5 in Cu(II) solution (300 mg/L), and the result is as shown in Figure 3. With the pH increasing from 2 to 6, the sorption capacities were increased from 4.23 mg/g to 61.45 mg/g for modified pith, but the sorption capacities were increased from 4.22 mg/g to 18.64 mg/g for pith. The amino group as

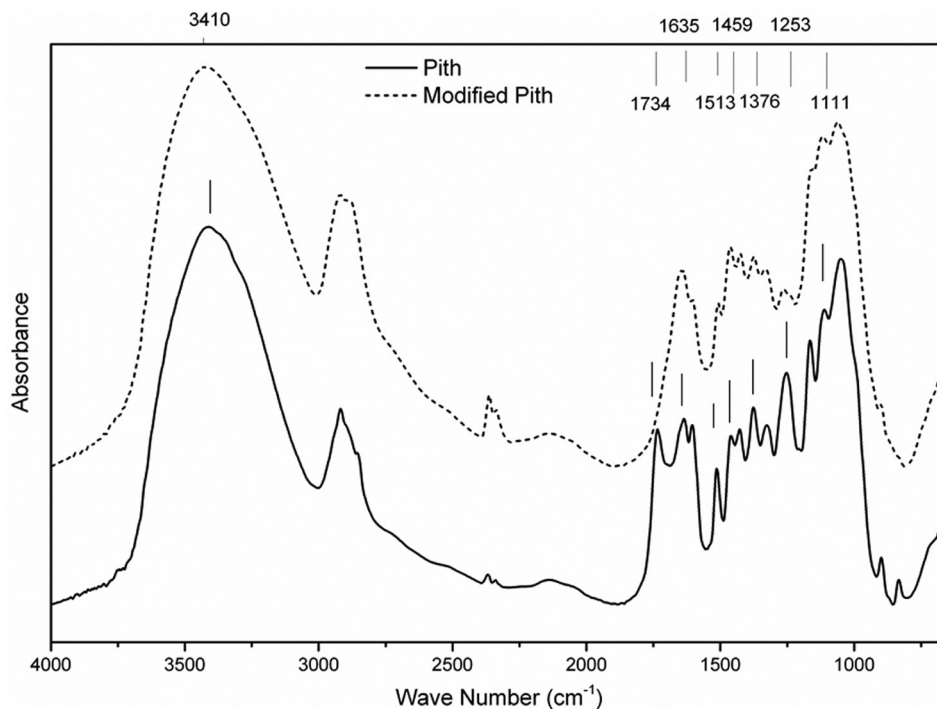


Figure 2. The FTIR of bagasse pith before and after modification.

the functional groups for adsorption accompanied by stoichiometric release of protons with the pH changing. [22,23]. While pH of the solution approached 8, the colloidal suspension occurred. Thus, the pH was chosen between 6 and 7 in the experiments.

The pH of the solutions would be changed with adsorption processing characterized by the described by the electricity conductivity. The relation between pH and electricity conductivity was investigated. As shown in Figure 4, the electricity conductivity decreases from 1.29 ms down to 0.96 ms with pH decreased

from 5.26 to 4.86 at first 40min. It indicated that amine and carboxyl groups were be introduced on the surface of pith, which improved its adsorption capability [24]. This would be explained by two steps of adsorption. In first step, more active sites were available, which could trap or adsorb more metal ions. Carbonyl groups or amine groups release hydrogen ion by ion exchange, which made pH and electricity conductivity decrease rapidly in this step. In the second step, the he active sites are exhausted on the surface of adsorbent, resulting in the ions move to interior of adsorbent and attach

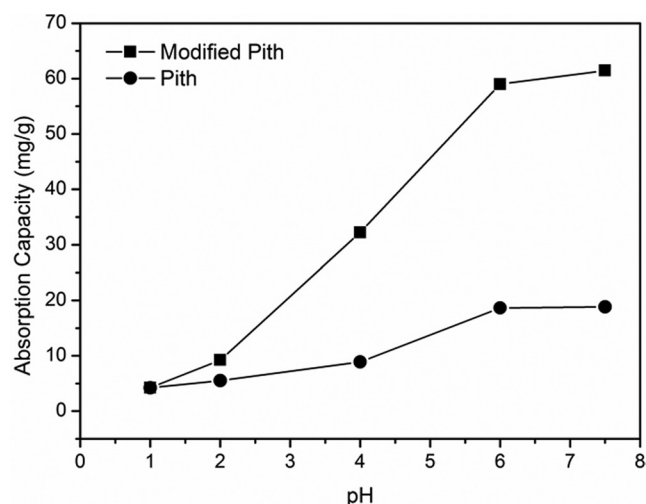


Figure 3. The initial pH effect on the adsorption of pith and modified pith.

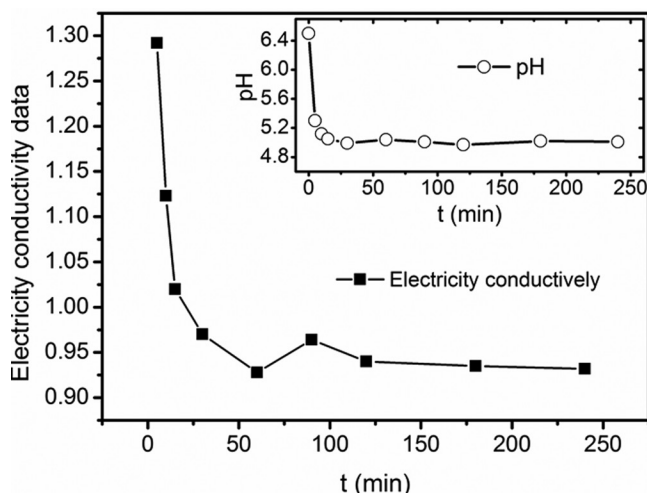


Figure 4. The electricity conductivity and pH of the solutions changes during adsorption.

Table 1. The Values of Parameters and Correlation Coefficient for Each Isotherm Model.

T/K	Langmuir Isotherm				Freundlich Isotherm		
	a_L (L/mg)	K_L (L/g)	R^2	R_L	K_F (mg/g)	$1/n$	R^2
303	0.05337	5.0967	0.99445	0.6046	14.24911	0.3879	0.95079
313	0.0673	6.8239	0.99406	0.6149	16.49019	0.3866	0.96106
323	0.09821	10.668	0.99633	0.6416	21.56541	0.3630	0.92121

to the interior sites. The adsorption rate was limited. Thus, pH and electricity conductivity tends to be level.

3.4. Isotherm Models Investigations

The isotherm were analyzed by Freundlich and Langmuir isotherm models at various temperatures. Langmuir model is a monolayer adsorption model, and it can be wrote as [25,26],

$$q_e = \frac{K_L C_e}{1 + a_L C_e} \quad (2)$$

where q_e (mg/g) is amount adsorbed at equilibrium. C_e (mg/L) is the concentration at equilibrium. a_L (L/mg) and K_L (L/g) are constant.

The adsorption system would be described as ‘favourable’ or ‘unfavourable’, which could be discussed by evaluating the proposed dimensionless separation factor, R_L , from the Langmuir Isotherm. It can be wrote as:

$$R_L = \frac{1}{1 + a_L C_{ref}} \quad (3)$$

Where, a_L is the constant of Langmuir. C_{ref} is the reference fluid-phase concentration of adsorbate (mg/l) [26].

If $R_L > 1$, it means the adsorption is unfavourable. If $1 > R_L > 0$, the adsorption is considered to be favourable. If $R_L = 0$, the adsorption would be irreversible.

Freundlich isotherm, a multilayer adsorption model, is as [15,26],

$$q_e = K_F C_e^{1/n} \quad (4)$$

where K_F is the parameter related to intensity of adsorption, q_e is the adsorption capacity (mg/g).

n means the distribution of active sites and strength of the sorption process. K_F indicates the sorption capacity. When n is greater than 1, the surface density could make the bond energies increase. When n is below 1, the surface density could make the bond energies decrease. When n is equal to 1, the bond energies does not depend on the surface density, and all surface sites are equivalent. Thus, if n between 1 and 10, it is beneficial for sorption [26].

The parameter values and correlation coefficient values are compared as shown in Figures 5(a) and 5(b).

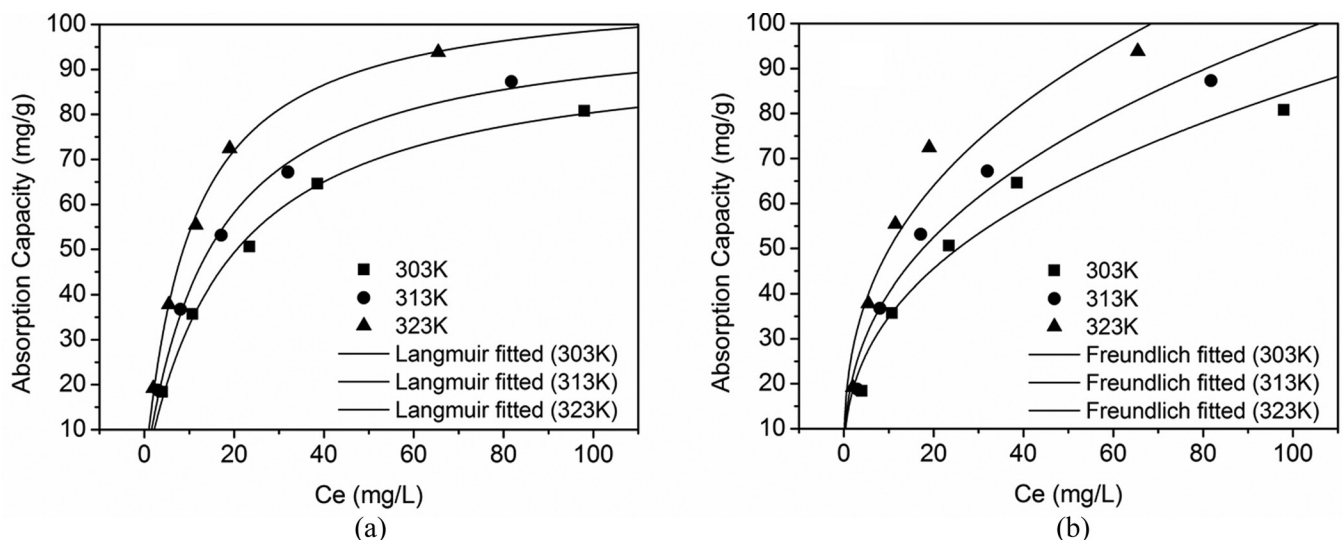


Figure 5. Adsorption isotherms for Cu(II) fitted by Langmuir model (a) and Freundlich model (b).

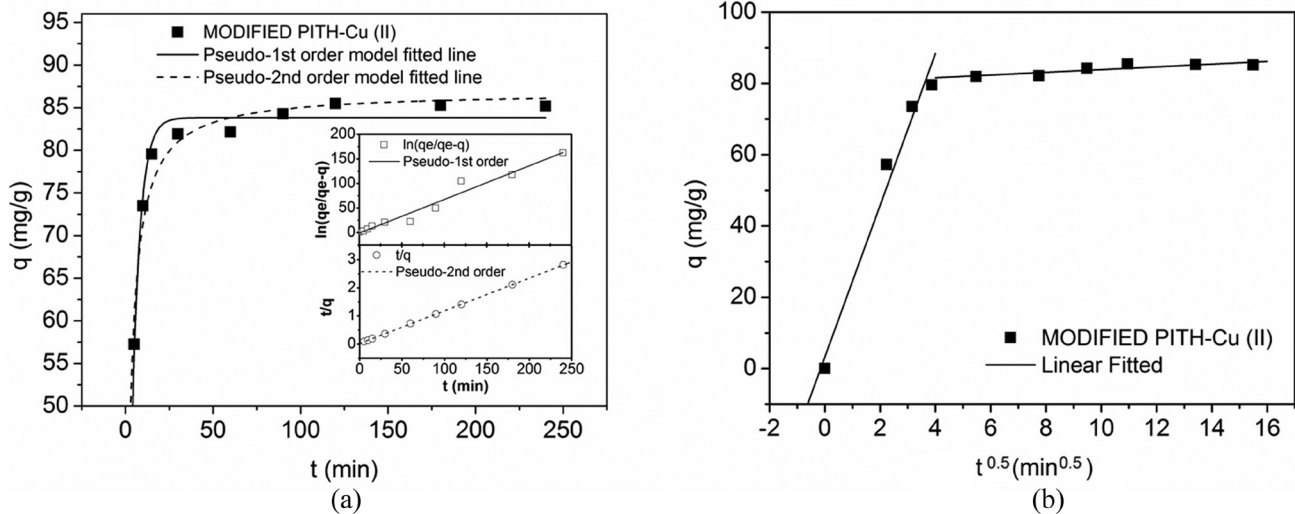


Figure 6. Adsorption of Cu ions by modified pith fitted by kinetics model (a) and diffusion model (b) at pH 6 and 25°C.

The experimental data can be fitted well by Langmuir isotherm model ($R^2 > 0.99$, as shown in Table 1). The R_L , between 0 and 1, indicated that the sorption is favourable. However, the Freundlich isotherm model could not the experimental data fitted well. The regression coefficients are only between 0.90 and 0.99 (as shown in Table 1). The n values, in the range 0.1 to 1, indicated the adsorptions were favorable [26]. Therefore, it can be concluded the bond energies increased with surface density increasing.

3.5. Thermodynamic Investigations

Thermodynamic parameters were obtained by equation of lecture [27]. The values are listed in Table 2. Positive value of Enthalpy Change (ΔH°) indicated the adsorption of Cu(II) was endothermic process. The positive value of Entropy Change (ΔS°) corresponded to freedom degree of the adsorbed species increase in adsorption. The negative values of Gibbs function change (ΔG°) confirmed the adsorption is feasible and spontaneous. ΔG° values increased with temperature rising.

3.6. Adsorption Kinetics Investigations

The pseudo-1st order and pseudo-2nd order models were applied, as Equations (5) and (6) [24]:

$$q = q_e(1 - e^{-k_1 t}) \quad (5)$$

$$q = \frac{q_e^2 k_2 t}{1 + q_e k_2 t} \quad (6)$$

where q (mg/g) is the amount of ion adsorbed at time t ; q_e is the amount of ion adsorbed at equilibrium; k_1 (1/min) is the adsorption rate constant of the pseudo-1st order model, and k_2 (g/(mg·min)) is the adsorption rate constant of the pseudo-2nd order model.

In Figure 6(a), the data is not fitted well by the pseudo-1st-order model ($R^2 < 0.98$, not listed). It indicated pseudo-1st-order kinetics could not described the adsorption of Cu(II) well, which underestimates metal uptake. However, the experimental equilibrium data implied the adsorption abided by the pseudo-2nd order kinetic ($R^2 > 0.99$, not listed). Thus, it could be concluded chemisorption is the control factor, which include valency electrons sharing or exchanging between the sorbent and sorbate [27].

Diffusion is very important in adsorption. To investigate the diffusion of metal ion, Webber's pore diffusion model, a intra-particle diffusion model, was described as Equation (7) [28],

$$q = k_{diff} t^{1/2} \quad (7)$$

where k_{diff} is the diffusion rate constant in intra-particle (mg/(g·min^{0.5})). If the plot was linear and y-intercept passed through 0, the rate limiting step will be intra-particle diffusion.

Table 2. The Values of Parameters and Correlation Coefficient for Each Isotherm Model.

T (K)	ΔH (kJ/mol)	ΔG (kJ/mol)	ΔS (kJ/mol)
303		-7.3824	0.1060
313	24.73	-7.0225	0.1015
323		-6.2319	0.0959

Based on the data in Figure 6(b), it suggested the adsorption would be in two steps. Intra-particle diffusion would not be the rate-limiting step, and more than one processes affect the sorption. The initial segment of the plots implied first step is external mass-transfer, and the latter segment of the plots implied the second step is pore or intra-particle diffusion [24].

4. CONCLUSIONS

Bagasse pith was the main by-product from sugar and paper industry. The physical structure and chemical components make it with a good sorption property.

From the studies, it was found that the functional groups have been introduced by chemical modification based on the morphologies analysis. The adsorption of heavy metal ion could be illustrated by Langmuir isotherm and the pseudo-2nd order model. If bagasse pith, a solid waste, would be modified effectively, it could be one of good renewable bio-adsorbents to removal heavy metal ions from waste water, and recovered the ions by burning it in the further.

5. ACKNOWLEDGEMENTS

This work was financially supported by National Science Foundation of China (21366005), Guangxi Natural Science Foundation (2013GXNSFFA019005 & 2014GXNSFBA118093).

6. REFERENCES

- Guo, X., Zhang, S., Shan, X.-Q. "Adsorption of metal ions on lignin", *J. Journal of Hazardous Materials*, Vol. 151, No. 1, 2008, pp. 134–42. <http://dx.doi.org/10.1016/j.jhazmat.2007.05.065>
- Lu, Q. F., Huang, Z. K., Liu, B., Cheng, X. S. "Preparation and heavy metal ions biosorption of graft copolymers from enzymatic hydrolysis lignin and amino acids", *J. Bioresource Technology*, Vol. 104, 2012, pp. 111–8. <http://dx.doi.org/10.1016/j.biortech.2011.10.055>
- Li, T., Yuan, S., Wan, J., Lu, X. "Hydroxypropyl-beta-cyclodextrin enhanced electrokinetic remediation of sediment contaminated with HCB and heavy metals", *J. Journal of Hazardous Materials*, Vol. 176, No. 1-3, 2010, pp. 306–12. <http://dx.doi.org/10.1016/j.jhazmat.2009.11.029>
- Zhang, C., Wang, Y., Zhang, Z., Wang, D., Luo, C., Xu, F. "Health Risk Assessment of Heavy Metals and As in Vegetable and Soil System in Chongqing, Southwest of China", *J. Journal Of Residuals Science & Technology*, Vol. 12, No. 4, 2015, pp. 231–40. <http://dx.doi.org/10.12783/issn.1544-8053/12/4/6>
- Wang, J., Chen, C. "Biosorbents for heavy metals removal and their future", *J. Biotechnology Advances*, Vol. 27, No. 2, 2009, pp. 195–226. <http://dx.doi.org/10.1016/j.biotechadv.2008.11.002>
- Kumar, U., Bandyopadhyay, M. "Sorption of cadmium from aqueous solution using pretreated rice husk", *J. Bioresource Technology*, Vol. 97, No. 1, 2006, pp. 104–9. <http://dx.doi.org/10.1016/j.biortech.2005.02.027>
- Sun, B., Mi, Z.-T., An, G., Liu, G., Zou, J.-J. "Preparation of biomimetic materials made from polyaspartyl polymer and chitosan for heavy-metal removal", *J. Industrial and Engineering Chemistry Research*, Vol. 48, No. 22, 2009, pp. 9823–9. <http://dx.doi.org/10.1021/ie900673h>
- Xu, L., Wang, J. N., Meng, Y., Li, A. M. "Fast removal of heavy metal ions and phytic acids from water using new modified chelating fiber", *J. Chinese Chemical Letters*, Vol. 23, No. 1, 2012, pp. 105–8. <http://dx.doi.org/10.1016/j.ccl.2011.09.029>
- Fan, X. D., Zhang, X. K. "Adsorption of Heavy Metals by Adsorbents from Food Waste Residue", *J. Journal Of Residuals Science & Technology*, Vol. 12, 2015, pp. S155–S8. <http://dx.doi.org/10.12783/issn.1544-8053/12/S1/22>
- Sanjuan, R., Anzaldo, J., Vargas, J., Turrado, J., Patt, R. "Morphological and chemical composition of pith and fibers from Mexican sugarcane bagasse", *J. Holz als Roh - und Werkstoff*, Vol. 59, No. 6, 2001, pp. 447–50. <http://dx.doi.org/10.1007/s001070100236>
- Lee, S. C., Mariatti, M. "The effect of bagasse fibers obtained (from rind and pith component) on the properties of unsaturated polyester composites", *J. Materials Letters*, Vol. 62, No. 15, 2008, pp. 2253–6. <http://dx.doi.org/10.1016/j.matlet.2007.11.097>
- Anoop Krishnan, K., Sreejalekshmi, K. G., Baiju, R. S. "Nickel(II) adsorption onto biomass based activated carbon obtained from sugarcane bagasse pith", *J. Bioresource Technology*, Vol. 102, No. 22, 2011, pp. 10239–47. <http://dx.doi.org/10.1016/j.biortech.2011.08.069>
- Kaushik, C. P., Tuteja, R., Kaushik, N., Sharma, J. K. "Minimization of organic chemical load in direct dyes effluent using low cost adsorbents", *J. Chemical Engineering Journal*, Vol. 155, No. 1–2, 2009, pp. 234–40. <http://dx.doi.org/10.1016/j.cej.2009.07.042>
- Nevine Kamal, A. "Removal of reactive dye from aqueous solutions by adsorption onto activated carbons prepared from sugarcane bagasse pith", *J. Desalination*, Vol. 223, No. 1–3, 2008, pp. 152–61.
- Liu, X., Zhu, H., Qin, C., Zhou, J., Zhao, J. R., Wang, S. "Adsorption of heavy metal ion from aqueous single metal solution by aminated epoxy-lignin", *J. BioResources*, Vol. 8, No. 2, 2013, pp. 2257–69. <http://dx.doi.org/10.15376/biores.8.2.2257-2269>
- Hu, C., Fang, G., Wang, X., Li, J. "Synthesis of Straw Alkaline Lignin-based Epoxy Resin", *J. Journal of North-East Forestry University*, Vol. 35, No. 4, 2007, pp. 53–5.
- Rasul, M. G., Rudolph, V., Carsky, M. "Physical properties of bagasse", *J. Fuel*, Vol. 78, No. 8, 1999, pp. 905–10. [http://dx.doi.org/10.1016/S0016-2361\(99\)00011-3](http://dx.doi.org/10.1016/S0016-2361(99)00011-3)
- Rainey, T., Doherty, W. S., Martinez, D. M., Brown, R., Kelson, N. "Pressure Filtration of Australian Bagasse Pulp", *J. Transp Porous Med*, Vol. 86, No. 3, 2011, pp. 737–51. <http://dx.doi.org/10.1007/s11242-010-9649-x>
- Singh, R., Singh, S., Trimukhe, K. D., Pandare, K. V., Bastawade, K. B., Gokhale, D. V., Varma, A. J. "Lignin-carbohydrate complexes from sugarcane bagasse: Preparation, purification, and characterization", *J. Carbohydrate Polymers*, Vol. 62, No. 1, 2005, pp. 57–66. <http://dx.doi.org/10.1016/j.carbpol.2005.07.011>
- Schwanninger, M., Rodrigues, J. C., Pereira, H., Hinterstoisser, B. "Effects of short-time vibratory ball milling on the shape of FT-IR spectra of wood and cellulose", *J. Vibrational Spectroscopy*, Vol. 36, No. 1, 2004, pp. 23–40. <http://dx.doi.org/10.1016/j.vibspec.2004.02.003>
- Shin, E. W., Karthikeyan, K. G., Tshabalala, M. A. "Adsorption mechanism of cadmium on juniper bark and wood", *J. Bioresource Technology*, Vol. 98, No. 3, 2007, pp. 588–94. <http://dx.doi.org/10.1016/j.biortech.2006.02.024>
- Crist, R. H., Martin, J. R., Crist, D. R. "Heavy metal uptake by lignin: Comparison of biotic ligand models with an ion-exchange process", *J. Environmental Science and Technology*, Vol. 36, No. 7, 2002, pp. 1485–90. <http://dx.doi.org/10.1021/es011136f>
- Figueira, M. M., Volesky, B., Ciminelli, V. S. T., Roddick, F. A. "Biosorption of metals in brown seaweed biomass", *J. Water Research*, Vol. 34, No. 1, 2000, pp. 196–204. [http://dx.doi.org/10.1016/S0043-1354\(99\)00120-7](http://dx.doi.org/10.1016/S0043-1354(99)00120-7)
- Albadarin, A. B., Al-Muhtaseb, A. H., Al-Laqtah, N. A., Walker, G. M., Allen, S. J., Ahmad, M. N. M. "Biosorption of toxic chromium from aqueous phase by lignin: Mechanism, effect of other metals ions and salts", *J. Chemical Engineering Journal*, 2011
- Singh, T. S., Pant, K. K. "Equilibrium, kinetics and thermodynamic

- studies for adsorption of As(III) on activated alumina”, *J. Separation and Purification Technology*, Vol. 36, No. 2, 2004, pp. 139–47. [http://dx.doi.org/10.1016/S1383-5866\(03\)00209-0](http://dx.doi.org/10.1016/S1383-5866(03)00209-0)
26. Hubbe, M. A., Hasan, S. H., Ducoste, J. J. “Cellulosic substrates for removal of pollutants from aqueous systems: A review. 1. Metals”, *J. Bioresources*, Vol. 6, No. 2, 2011, pp. 2161–914.
27. Albadarin, A. B., Al-Muhtaseb, A. a. H., Walker, G. M., Allen, S. J., Ahmad, M. N. M. “Retention of toxic chromium from aqueous phase by H₃PO₄-activated lignin: Effect of salts and desorption studies”, *J. Desalination*, Vol. 274, No. 1–3, 2011, pp. 64–73. <http://dx.doi.org/10.1016/j.desal.2011.01.079>
28. Ho, Y., McKay, G. “Kinetic models for the sorption of dye from aqueous solution by wood”, *J. Trans IChemE*, Vol. 76, 1998, pp. 183–91. <http://dx.doi.org/10.1205/095758298529326>

Modified Electro-spun Polyvinyl Alcohol Nanofibers Used as Super Adsorbing Material for Lead Ions in Aqueous Solution

NTAOTE DAVID SHOOTO^{1,*}, DONBEBE WANKASI¹, LUCKY MASHUDU SIKHWIVHILU²
and EZEKIEL DIXON DIKIO¹

¹Applied Chemistry and Nano-Science Laboratory, Department of Chemistry, Vaal University of Technology P.O. Box X021, Vanderbijlpark 1900, South Africa

²Advanced Materials Division, Mintek, Nanotechnology Innovation Centre, Private Bag X3015, Randburg 2125, South Africa

ABSTRACT: Polyvinyl alcohol nanofibers (PVA) and novel polyvinyl alcohol nanofibers incorporated with cobalt metal organic framework (PVA/Co-MOF) sorbents were produced via electrospinning. The produced nanofibers were confirmed by scanning electron microscope (SEM), thermogravimetric analysis (TGA) and Fourier transform infrared (FTIR). SEM images showed consistent and beads free nanofibers were synthesized. FTIR spectra's exhibited shifts in critical functional groups positions thus it confirmed that there was a given amount of cobalt metal organic frameworks implanted in the incorporated nanofibers. TGA plots also confirmed that PVA/MOF nanofibers exhibited higher decomposition temperatures than that of the pure polyvinyl alcohol nanofibers. Therefore, it affirmed the amalgamation between cobalt metal organic frameworks and polyvinyl alcohol nanofibers. The ability of PVA and novel PVA/Co-MOF nanofibers to remove Pb²⁺ ions from solution was investigated. The sorption Pb²⁺ ions on incorporated nanofibers (novel PVA/Co-MO) were two-fold as compared to the pure polyvinyl alcohol nanofibers. The thermodynamic parameters: Gibbs free energy (ΔG°) and apparent enthalpy (ΔH°) showed that the adsorption Pb²⁺ ions onto the electro-spun nanofibers were spontaneous and exothermic.

INTRODUCTION

HEAVERY metals are chemical elements such as lead Pb²⁺ and chromium Cr⁶⁺ that have a relatively high density and toxic at lower concentrations [1]. These metals induce severe water and environment contaminations [2]. To date prominent environmental problem is Pb²⁺ pollution which is a concerning issue all around the world. Therefore, the liberation of toxic lead ions from solution to acceptable levels before disposal is necessary. Main sources of lead pollution are companies such as mines, metal plating facilities, nuclear power plant, petroleum, battery recycling, lead glazed pottery and leaded paint plants [3].

Pb²⁺ ions in aqueous solution are non-biodegradable and are known to accumulate in human beings, causing many sickness and imparted health [4–6]. Its toxic effects are subtle with a possibility of causing permanent health problems [7]. It hinders numerous body functions majorly affecting nervous system [8–9], hemato-

poietic [10], hepatic [11], impaired renal function and fertility [12,13] causing severe disorders and mortality [14]. It also inhibits the production of haemoglobin and porphyrins, overtime accumulates in the bones replacing calcium thus negatively affect metabolism of vitamin D [15]. These inspired researchers to explore for novel sorbents that will effectively liberate Pb²⁺ ions in aqueous solution.

Adsorption is a surface phenomenon; defined as a process where one or more components (adsorbate) are attracted and bonded to the surface of a solid (adsorbent) [16]. This process is superior to most of the existing conventional techniques used for the liberation of lead ion from solution, as it is less cost effective, environmental friendly, feasible and removes targeted metals more effectively [17].

Nano scale adsorbents have attracted considerable interest in sorption applications owing to their extraordinary surface area, porous topology, physical and chemical attributes [18]. Many potential nanofibers adsorbents have been reported in recent years. Shooto *et al.* and Saeed *et al.* respectively reported modified PVA/Cu-MOF nanofibres [19] and modified PAN

*Author to whom correspondence should be addressed.
Email: davidshooto12@gmail.com; phone +2716 950 9606

nanofibers [20] shown excellent sorption capability for lead ions in aqueous solution. Nanofibers are remarkable materials that are widely used in many applications hence recently they are extensively applied as adsorbents in the liberation of lead ions in solution owing to their attributes of extraordinary properties [21]. Electrospinning technique uses polymeric solutions to fabricate nanofibers [22].

The present work reports the fabrication of PVA and novel PVA/Co-MOF nanofibers via electrospinning, then characterization and followed by the investigation of these materials as potential adsorbents of Pb^{2+} ions in aqueous solution. Characterization was carried out by SEM, TGA and FTIR. Adsorption isotherms and kinetic models were also explored. Finally PVA nanofibers embedded with Co-MOFs were found to render higher Pb^{2+} removal than did raw PVA nanofibers.

EXPERIMENTAL

Materials

Polyvinyl alcohol $[(CH_2CH(OH))_n]$, PVA, fully hydrolysed, Sigma-Aldrich], *N,N*-Dimethylformamide $[HCON(CH_3)_2]$, DMF, 99.8%; AnalaR], Cobalt(II) nitrate hexahydrate $[Co(NO_3)_2 \cdot 6H_2O]$, 99.95%, Sigma-Aldrich], 1,2,4,5-Tetrabenzenecarboxylic acid $[C_6H_2(CO_2H)_4]$, 96%, Sigma-Aldrich], Lead nitrate $[Pb(NO_3)_2]$, 99% Radchem], Methanol $[CH_3OH]$, 99.9%; Sigma-Aldrich].

All reagents were purchased from commercial sources in South Africa (Johannesburg) and were used as they were, without any modification.

Method

Preparation of Cobalt Metal Organic Framework (Co-MOF)

Solvothermal method was used to synthesize cobalt metal organic frameworks [23]. Whereby (0.012 mol) respectively of cobalt(II)nitrate and 1,2,4,5-tetrabenzenecarboxylic acid were dissolved in 80 ml dimethylformamide by mild stirring in a round bottom flask. The solution was refluxed for 2 hours at 120°C. Tint pink crystalline material was produced and insulated by centrifugation and rinsed several times to remove excess dimethylformamide. The produced crystalline material was dried out in oven for 30 min and was used as it is without any alterations for further experiments.

Preparation of Nanofibers

Nanofibers were prepared by dissolving (2.7 g) polyvinyl alcohol powder into hot distilled water (27.3 g). From the as prepared polymer solution (10 ml) was mixed with (0.01 g) cobalt-metal organic framework powder for 1 hrs on a magnetic stirrer. The polymer solution mixture was transferred into a 20 ml syringe. The experimental set-up used was composed of a power supply, syringe and a collector (aluminium foil). A positive terminal was connected to a 15 kV which was applied to a syringe needle tip to charge the polymer solution. The electro-spun nanofibers were accumulated on aluminium foil connected to electrically grounded metal plate, 15 cm apart from the syringe needle. Electrospinning process was operated at ambient environment.

Adsorption Procedure

Batch adsorption experiments were performed to better understand the influence of concentration, temperature and time effect. 0,1 g of incorporated nanofibers and initial Pb^{2+} ion concentrations of 20, 40, 60, 80, and 100 mg/L, were employed to study concentration effect at room temperature. Time dependence studies, identical mass of nanofibers sample was used with reaction time of 10, 20, 30, 40, and 60 min at room temperature. Temperature effect studies were carried out at 25, 40, 60, and 80°C.

The pH of all lead ion solutions used throughout adsorption experiments was 5.03 and 20 ml of lead ion solution was used for all experiments.

Same procedure as mentioned above for concentration, time and temperature effect was followed to evaluate Pb^{2+} ability to be adsorbed by polyvinyl alcohol nanofibers mat.

CHARACTERIZATION

The characteristics of the produced nanofibers was confirmed by scanning electron microscope (SEM), Fourier transformed infrared spectroscopy (FTIR) and thermogravimetry analysis (TGA). The morphology analysis was performed by a JOEL 7500F scanning electron microscope from Japan. Perkin Elmer TGA 4000 (USA) was used to record the thermogravimetric analyses, it was performed; 30 to 900°C at a heating rate of 10°C/min under inert atmosphere. Perkin Elmer FT-IR, spectrum 400 (USA). The measuring range extended from 4000 to 520 cm^{-1} . Atomic Absorption

Spectroscopy (AAS), from North America Shimadzu ASC 7000 was used.

DATA ANALYSIS

The sorbed amount of Pb^{2+} onto the adsorbent was determined using the following equation:

$$q_e = \frac{V}{M}(C_o - C_e) \quad (1)$$

q_e = Pb^{2+} concentration sorbed onto nano-composite at equilibria point (mg of metal ion/g of sorbent).

C_o = Initial concentration of Pb^{2+} in solution (in mg/L).

C_e = Equilibria point concentration of Pb^{2+} in solution (in mg/L).

V = Initial volume of Pb^{2+} solution used (in L).

M = Weight of nano-composite.

Langmuir graphs were plotted by applying the following equation

$$\frac{m}{x} = \frac{1}{abC_e} + \frac{1}{b} \quad (2)$$

x = Pb^{2+} sorbed per mass of nano-composite (in mg/L)

a, b = Langmuir constants received from the slope and intercepts of the plots.

Langmuir isotherm was presented in form of formula of separation factor (S_f). It determines a type of adsorption isotherm. When (S_f) is greater than one, it indicates that the isotherm is not favourable; if (S_f) is one (linear), if zero < (S_f) < one (favourable), and (S_f) = zero (irreversible).

$$S_f = \frac{1}{1 + aC_o} \quad (3)$$

The surface coverage degree of the sorbent covered by lead ions was calculated using

$$\theta = 1 - \frac{C_e}{C_o} \quad (4)$$

The potential of nanofibers to liberate Pb^{2+} in solution was assessed by total cycles of equilibrium sorp-

tion required according to the value of the partition coefficient (K_d) in Equation (5)

$$K_d = \frac{C_{ads}}{C_{aq}} \quad (5)$$

where,

C_{aq} = Pb^{2+} concentration in solution, (in mg/L)

C_{ads} = Pb^{2+} concentration in nano-composite (in mg/L)

Suzuki equation was used to determine the heat of adsorption (Q_{ads}) as expressed in the below equation

$$\ln \theta = \frac{\ln K_o C_o}{T^{0.5}} + \frac{Q_{ads}}{RT} \quad (6)$$

where,

T = Temperature of the solution (in K)

K_o = Constant

R = Constant (8.314 J/Kmol)

Linearized Arrhenius equation was used to obtained data to determine; activation energy (E_a) and sticking probability (S^*).

$$\ln(1 - \theta) = S^* + \frac{E_a}{RT} \quad (7)$$

Gibbs energy (ΔG°) equation was used to evaluate the spontaneity of the sorption process.

$$\Delta G^\circ = RT \ln K_d \quad (8)$$

Enthalpy (ΔH°) and entropy (S°) was determined by Equation (9).

$$\Delta G^\circ = \Delta H^\circ - T\Delta S^\circ \quad (9)$$

The number of hopping (n) was determined by linking it to surface coverage (θ).

$$n = \frac{1}{(1 - \theta)\theta} \quad (10)$$

Sorption potential (A) was examined by

$$A = -RT \ln \frac{C_o}{C_e} \quad (11)$$

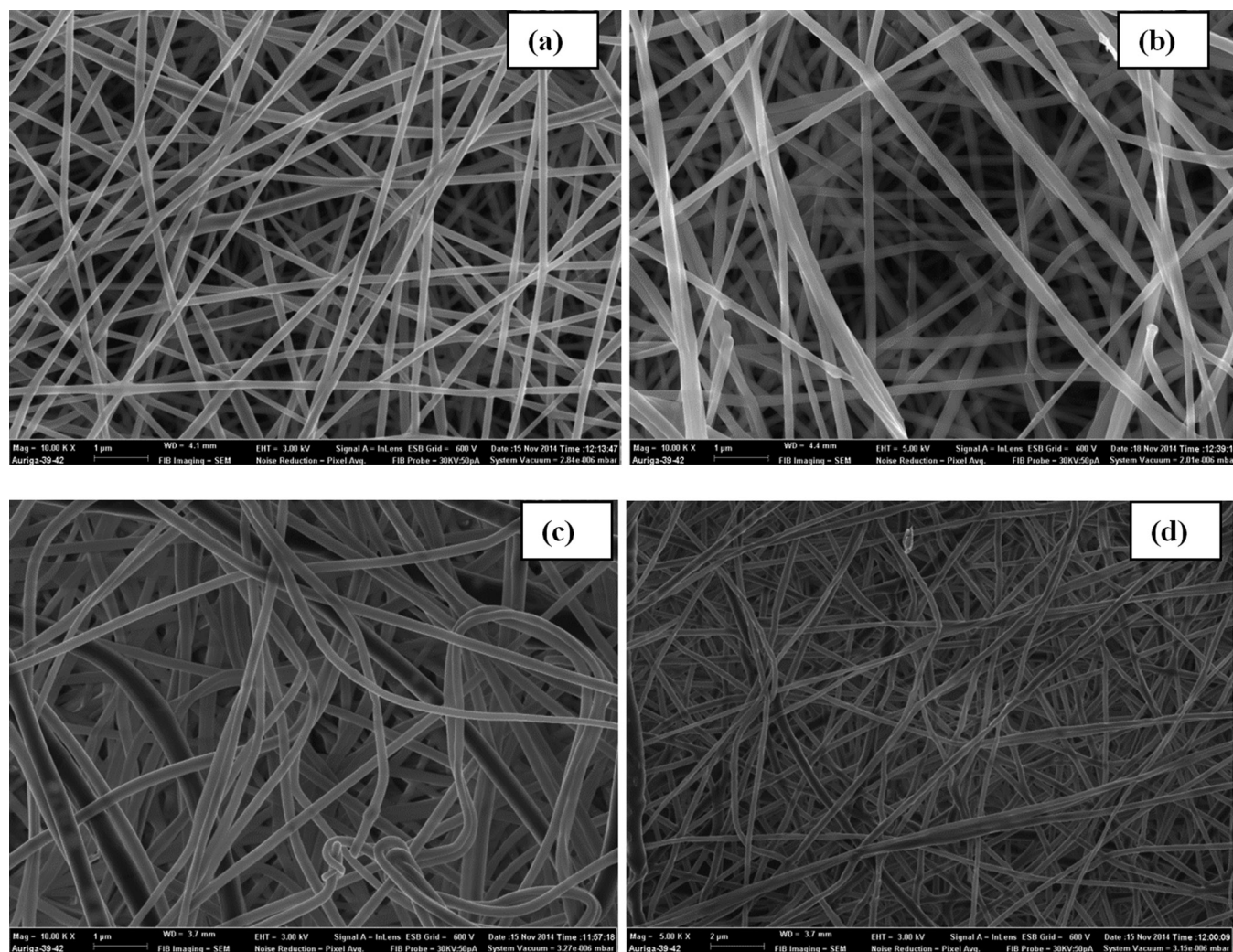


Figure 1. (a) and (b) SEM micrographs of PVA nanofibers. (c) and (d) micrographs of PVA/Co-MOF nanofibers.

RESULTS AND DISCUSSION

Figures 1(a)–1(d) show SEM micrographs of electro-spun polyvinyl alcohol and incorporated nanofibers with relatively uniform morphologies. It is seen that the nanofibers are non-beaded. PVA nanofibers in Figures 1(a) and 1(b) show that no specific alignment direction was followed by the fabricated nanofibers. Incorporated nanofibers in Figures 1(c) and 1(d) show dense entanglement and network nanofibers, it is also visible that some thick individual fibers were observed. Other than that no morphological changes was observed in the view of the SEM images.

In order to examine whether cobalt metal organic frameworks were incorporated to electro-spun polyvinyl alcohol nanofibers, FTIR spectra of both electro-spun polyvinyl alcohol nanofibers and incorporated nanofibers were measured to monitor changes in the IR spectra as shown in Figure 2. On the spectra of

electro-spun polyvinyl alcohol nanofibers mat, the major peaks observed were as follows: bands at 3293 and 1660 cm^{-1} are attributed to the stretching and bending vibrations of (O–H) respectively, two vibration bands at 2936 and 2911 cm^{-1} are attributed to (C–H), a sharp band at 1100 is attributed to the vibration of (C–C), a medium shoulder peak at 917 cm^{-1} is linked to the vibration of (C–O). The asymmetric and symmetric stretching vibrations of (COO–) from carboxylate group were observed at 1437 and 1339 cm^{-1} . By comparing the spectra of polyvinyl alcohol nanofibers and incorporated nanofibers, several shifts in peaks were observed. On the spectra of electro-spun incorporated nanofibers mat, stretching and bending vibrations of (O–H) shifted to 3275 and 1579. Also (C–H) bands shifted to 2930 and 2915 cm^{-1} . Asymmetric and symmetric stretching vibrations of (COO–) are shifted to 1434 and 1380 cm^{-1} . Another major change can be observed at 679 cm^{-1} whereby a new peak is formed

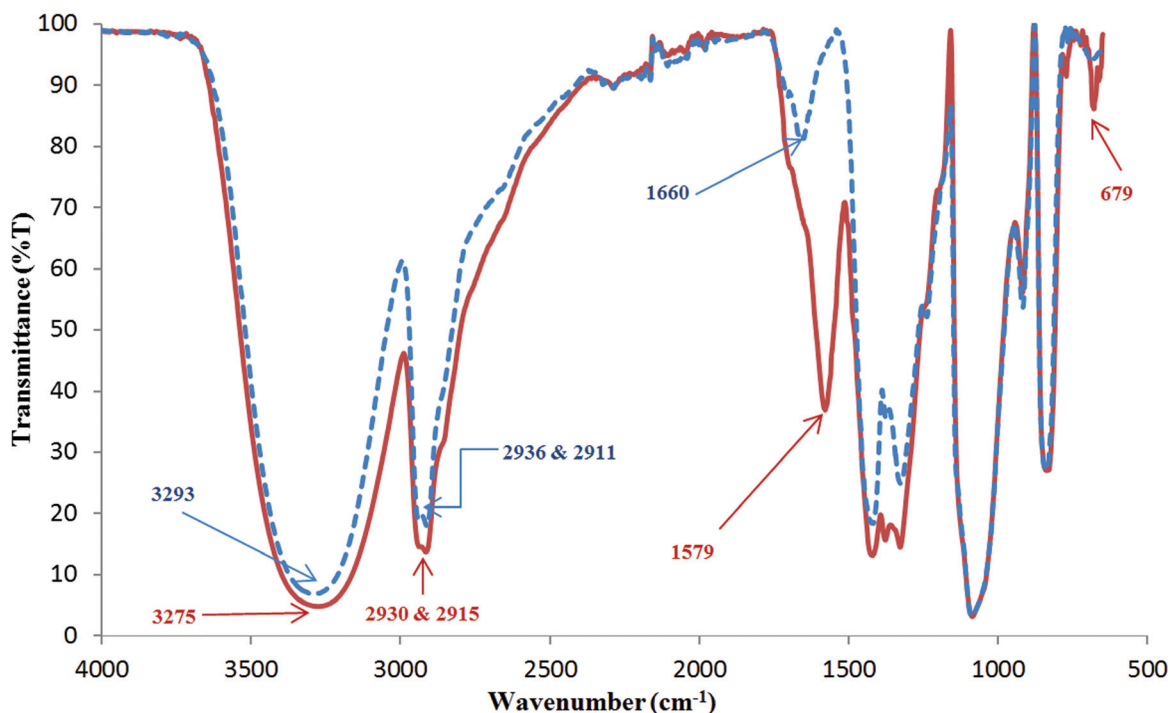


Figure 2. FTIR spectra of PVA nanofibers (dotted line) and PVA/Co-MOF nanofibers (solid line).

which is due to (Co–O). It is concluded that there were a given amount of cobalt metal organic frameworks in electro-spun fibrous mat.

TGA was used to study the thermal stability of the as-prepared electro-spun polyvinyl alcohol nanofibers and incorporated nanofibers. TGA-DTA curves in Figure 3(a) polyvinyl alcohol nanofibers and Figure 3(b) incorporated nanofibers. In Figure 3(a) it was observed that the nano-composite undergoes multiple decomposition stages: first decomposition occurred between 30–75°C which was mainly caused by the loss of water molecules that was physisorbed. Second decomposition occurred between 149–371°C of which this is the most intense weight loss it corresponds to the side chains of polyvinyl alcohol nanofibers, the loss of H-bond (hydrogen) between polyvinyl alcohol molecules and O-bond (oxygen) between C–O. Third decomposition 378–489°C corresponds to the disintegration of the main chain of polyvinyl alcohol. Incorporated nanofibers on Figure 3(b) it was observed that decomposition points slightly moved higher. First decomposition occurred between 30–91°C, second decomposition 201–343°C, and the third decomposition 360–501°C. Incorporated nanofibers exhibit higher decomposition temperature than polyvinyl alcohol nanofibers. Thus, it confirmed the interactive force between cobalt metal organic frameworks and polyvinyl alcohol nanofibers.

The effect of temperature on adsorption Pb^{2+} to

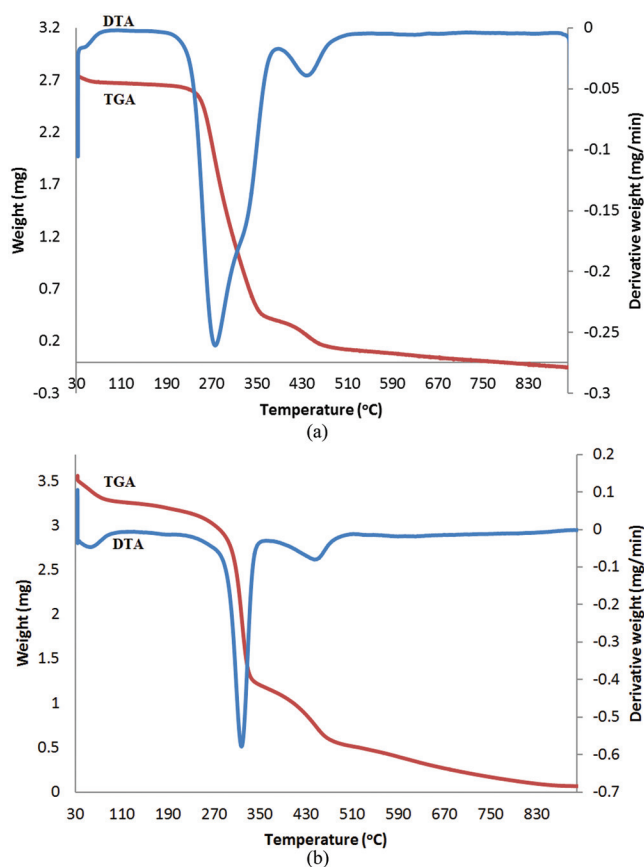


Figure 3. Thermalgravimetric analysis (TGA) and Derivative thermogravimetric analysis (DTA) of (a) PVA nanofibers, and (b) PVA/Co-MOF nanofibers.

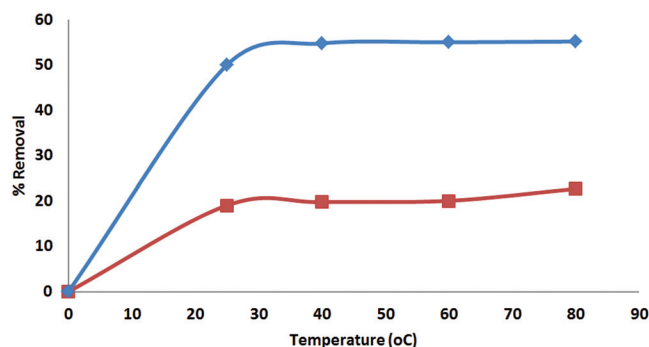


Figure 4. Plot of temperature effect on the removal of Pb^{2+} ions by (■) PVA nanofibers and (◆) PVA/Co-MOF nanofibers.

polyvinyl alcohol nanofibers and incorporated nanofibers was investigated at different temperatures of 25, 40, 60 and 80°C as shown in Figure 4. It was observed in particular at the beginning phases, rate of adsorption was high. After which no significant change in adsorption was observed as temperature increased further increased as the system reached equilibrium. This results shows that temperature has no effect on the adsorption Pb^{2+} onto nanofibers composites.

Time effect indicates the duration required for maximum sorption to occur. Figure 5 shows the effect of time at (10, 20, 30, 40 and 60 min) on the sorption Pb^{2+} ions onto electro-spun nanofibers. It was observed that sorption Pb^{2+} onto polyvinyl alcohol nanofibers and incorporated nanofibers was very rapid at the initial stages especially first 10 min of the contact period. This is because of the presence of multiple vacant sites at the beginning of the sorption process but proportionally as the sorption sites decreased in number and became saturated, the sorption rate was slowed down. Maximum sorption's were 10.25% and 44.51% occurred at 60 min for polyvinyl alcohol nanofibers and incorpo-

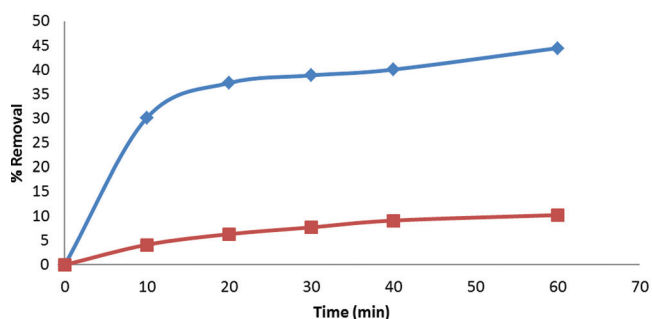


Figure 5. Plot of time dependant studies on the removal of Pb^{2+} ions by (■) PVA nanofibers and (◆) PVA/Co-MOF nanofibers.

rated nanofibers respectively. Nanofibers surface vacant sites were filled relatively fast, this suggests that Pb^{2+} uptake was rapid and subsequently the unreacted vacant sites were out of reached due to the repulsive forces between Pb^{2+} ions. Results showed that incorporated nanofibers adsorbed far much better than plain polyvinyl alcohol nanofibers.

The percentage sorption Pb^{2+} by polyvinyl alcohol nanofibers and incorporated nanofibers at different concentrations of Pb^{2+} (20, 40 and 60, 80 and 100 mg/L) is presented in Figure 6. It was observed that the increasing concentration increased also the adsorption until equilibrium was reached. This is due to readily useable active sites at low Pb^{2+} concentrations, but at high Pb^{2+} concentrations, nanofibers sorption capability was lessened due to decreased accessible active sites.

The surface covered by Pb^{2+} ions is given as 0.2206 and 0.4964 for polyvinyl alcohol nanofibers and incorporated nanofibers respectively as shown in Table 4. This suggests that over 22 and 49% of the surfaces of polyvinyl alcohol nanofibers and polyvinyl alco-

Table 1. Temperature Effect Data for Pb^{2+} Adsorption Conditions.

PVA Nanofibers					
C_o (mg/L)	C_e (mg/L)	q_e (mg/g)	Temperature (°C)	pH	Adsorption Time (min)
60	48.5562	19.073	25	5.03	30
60	48.11415	19.80975	40	5.03	30
60	47.95	20.08333	60	5.03	30
60	46.3651	22.72483	80	5.03	30
PVA/Co-MOF Nanofibers					
C_o (mg/L)	C_e (mg/L)	q_e (mg/g)	Temperature (°C)	pH	Adsorption Time (min)
60	29.985	50.025	25	5.03	30
60	27.1058	54.82367	40	5.03	30
60	26.95845	55.06925	60	5.03	30
60	26.858	55.23667	80	5.03	30

Table 2. Time Dependence Studies Data for Pb²⁺ Adsorption Conditions.

PVA Nanofibers					
C _o (mg/L)	C _e (mg/L)	q _e (mg/g)	Temperature (°C)	pH	Adsorption Time (min)
60	57.5116	4.147333	25	5.03	10
60	56.2039	6.326833	25	5.03	20
60	55.3663	7.722833	25	5.03	30
60	54.5291	9.118167	25	5.03	40
60	53.8489	10.25183	25	5.03	60
PVA/Co-MOF Nanofibers					
C _o (mg/L)	C _e (mg/L)	q _e (mg/g)	Temperature (°C)	pH	Adsorption Time (min)
60	41.8953	30.1745	25	5.03	10
60	37.594	37.34333	25	5.03	20
60	36.6552	38.908	25	5.03	30
60	35.9377	40.10383	25	5.03	40
60	33.28995	44.51675	25	5.03	60

hol nanofibers incorporated with cobalt metal organic frameworks were covered by the Pb²⁺ ions. It further indicated that higher degree adsorption occurred on incorporated nanofibers (49%) as compared to (22%) polyvinyl alcohol nanofibers.

To determine whether Pb²⁺ to electro-spun nanofibers sorption were favourable or not, separation factor (S_f) was calculated. (S_f) values were 0.7028 and 0.4964 for polyvinyl alcohol nanofibers and polyvinyl alcohol nanofibers incorporated with cobalt metal organic frameworks respectively. Both (S_f) obtained values were under one and above zero indicated that the sorption Pb²⁺ ions onto electro-spun composites was favourable as presented in Table 4.

The potential of electro-spun nanofibers composites to liberate lead ions in solution was determined by

cycles of equilibria sorption process required according to the magnitude of the partition coefficient (K_d) as presented in Table 4. The obtained values (3.5315) and (1.0143) for polyvinyl alcohol and incorporated nanofibers. This indicated that incorporated nanofibers was more effective as the required cycles of equilibria sorption were fewer to liberate the levels of Pb²⁺ ions in aqueous solution.

Percentage removals of the electro-spun composites were calculated to be 25.50 and 59.41 mg/g for polyvinyl alcohol nanofibers and incorporated nanofibers respectively using Equation (1) as shown in Table 4. This indicated that more Pb²⁺ ions up-take occurred on incorporated nanofibers.

The heat of adsorption (Q_{ads}) for the sorption Pb²⁺ ions was calculated and obtained the values of

Table 3. Concentration Effect Data for Pb²⁺ Adsorption Conditions.

PVA Nanofibers					
C _o (mg/L)	C _e (mg/L)	q _e (mg/g)	Temperature (°C)	pH	Adsorption Time (min)
20	17.435	12.825	25	5.03	30
40	32.2475	19.38125	25	5.03	30
60	47.5379	20.77017	25	5.03	30
80	61.0884	23.6395	25	5.03	30
100	77.9327	22.0673	25	5.03	30
PVA/Co-MOF Nanofibers					
C _o (mg/L)	C _e (mg/L)	q _e (mg/g)	Temperature (°C)	pH	Adsorption Time (min)
20	11.54	42.3	25	5.03	30
40	19.102	52.245	25	5.03	30
60	30.52	49.13333	25	5.03	30
80	39.954	50.0575	25	5.03	30
100	50.35698	49.64302	25	5.03	30

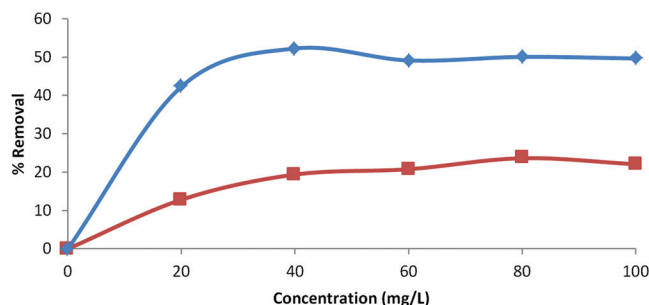


Figure 6. Plot of concentration effect on the removal of Pb^{2+} ions by (■) PVA nanofibers and (◆) PVA/Co-MOF nanofibers.

(-5.3145) and (-1.9306) respectively for polyvinyl alcohol nanofibers and incorporated nanofibers. Negative values indicated that the sorption that occurred was exothermic. Pb^{2+} to electro-spun nanofibers sorption favoured more of low temperatures. Thus increased temperatures did not improve the sorption processes.

(E_a) and (S^*) were determined by using Equation (8). The values of (E_a) and (S^*) are respectively presented in Table 5 as (-2.1584) and (0.7734) for polyvinyl alcohol nanofibers, (-7.2235) and incorporated nanofibers gave (0.450). On both instances (E_a) values indicated that very low energy was required to start the sorption and the followed processes were exothermic. (S^*) evaluated the ability of Pb^{2+} ion to stay attached onto nanofibers. If $S^* > one$ (no sorption), $S^* = one$ (variety of physisorption and chemisorption), $S^* = zero$ (bound, chemisorption), $zero < S^* < one$ (bound, physisorption). The obtained S^* values for Pb^{2+} ions sorption onto electro-spun nanofibers were less than one which indicated the sorption was favourable and physisorption mechanism was dominant.

The Gibbs free energy (ΔG_o) was determined to assess the spontaneity of the sorption process. Obtained

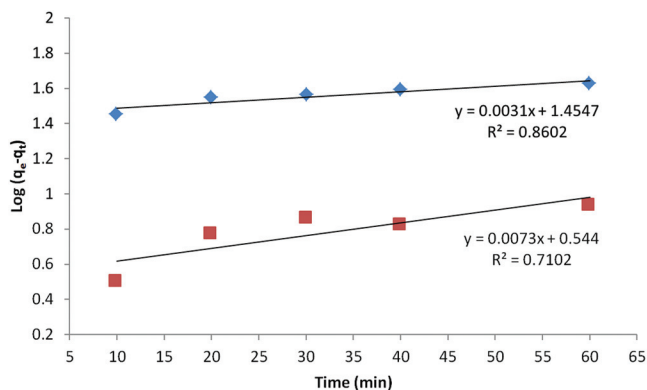


Figure 7. Plot of $\text{Log}(q_e - q_t)$ vs. t for adsorption of Pb^{2+} onto (■) PVA nanofibers and (◆) PVA/Co-MOF nanofibers.

(ΔG_o) values of (-3.592) for polyvinyl alcohol nanofibers and (-0.617) for incorporated nanofibers, were in the negative region indicated that the sorption were spontaneous, no extra energy was required to kick start the process.

The apparent enthalpy (ΔH_o) and entropy (ΔS_o) of adsorption were also calculated as shown in table 5. The values of enthalpy change (ΔH_o) were (-2.6857) and (-1.4977) for polyvinyl alcohol and incorporated nanofibers respectively. Negative values for (ΔH_o) suggested that the sorption favoured lower temperatures. The entropy change (ΔS_o) gave positive values (2.9) and (6.1) for polyvinyl alcohol nanofibers and incorporated nanofibers respectively, this indicated that Pb^{2+} ions were not restricted in the electro-spun nanofibers and physisorption mechanism was dominant.

Chance of Pb^{2+} in finding out active site on the surface of electro-spun nanofibers was determined by the number of hopping (n). Polyvinyl alcohol nanofibers and incorporated nanofibers respectively gave the (n)

Table 4. Equilibrium and Kinetic Parameters.

Composite	Surface Coverage (θ)	Separation Factor (S_f)	Sorption Coefficient (K_d)	Percentage Removal (%)
PVA Nanofibers	0.2206	0.7028	3.5315	25.50
PVA/Co-MOF Nanofibers	0.4964	0.3572	1.0143	59.41

Table 5. Thermodynamic Parameters.

Composite	Heat of Adsorption, Q_{ads} (KJ/mol·K)	Sticking Probability, S^*	Activation Energy, E_a (JK·mol)	Gibbs Free Energy of Adsorption, ΔG_o (KJ/mol)	Apparent Entropy, ΔS_o (J/mol·K)	Apparent Enthalpy, ΔH_o (J/mol)	Hopping Number, n	Adsorption Potential, A (KJ/mol)
PVA Nanofibers	-5.3145	0.7734	-2.1584	-3.592	2.9	-2.6857	1	0.7566
PVA/Co-MOF Nanofibers	-1.9306	0.450	-7.2235	-0.617	6.1	-1.4977	2	2.359

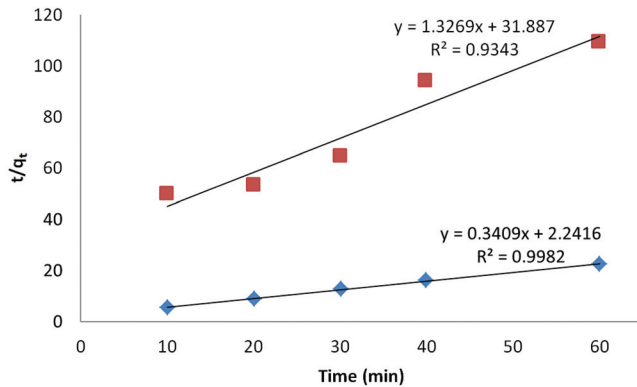


Figure 8. Plot of t/q_t vs. t for adsorption of Pb^{2+} onto (■) PVA nanofibers and (◆) PVA/Co-MOF nanofibers.

values of (1) and (2). Faster sorption is indicated by a lower hopping number. Obtained number of hopping (n) values for both polyvinyl alcohol nanofibers and incorporated nanofibers indicated that the sorbed Pb^{2+} ions were very rapid.

The apparent change in chemical potential that took place as Pb^{2+} ions was attracted from the solution to the surface of electro-spun nanofibers were determined to be (0.7566) for polyvinyl alcohol nanofibers and (2.359) for incorporated nanofibers.

Plots of pseudo first and second order are shown in Figures 7 and 8 respectively. Best fitted kinetic model is evaluated by the magnitude of coefficient of determination (R^2) given in Table 6. It is clearly seen that the magnitude of the coefficient of determination for pseudo second order model are greater than those of the pseudo first order model. It is concluded that the experimental data best fitted pseudo second order kinetic mechanism.

Table 6. Kinetics Parameters for Pb^{2+} Adsorption onto PVA and PVA/Co-MOF Nanofibers Coefficient of Determination (R^2).

	Coefficient of Determination (R^2)	
	Pseudo First Order	Pseudo Second Order
PVA Nanofibers	0.7102	0.9343
PVA/Co-MOF Nanofibers	0.8602	0.9982

Table 7. Isotherm Parameters of Langmuir and Freundlich Coefficient of Determination (R^2).

	Coefficient of Determination (R^2)	
	Langmuir	Freundlich
PVA Nanofibers	0.9734	0.9814
PVA/Co-MOF Nanofibers	0.957	0.97

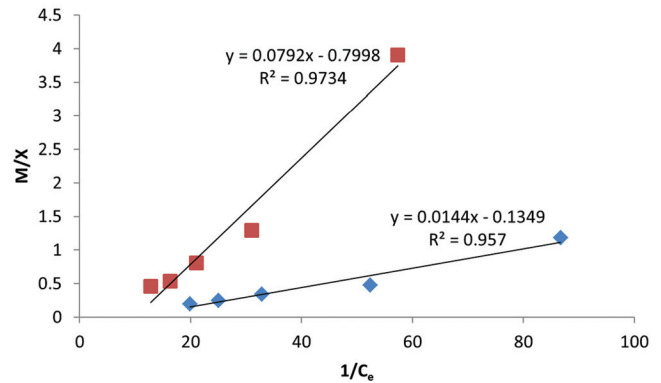


Figure 9. Plot of Langmuir isotherm plots, M/X against $1/C_e$ (■) PVA nanofibers and (◆) PVA/Co-MOF nanofibers.

Figure 9 and 10 shows Langmuir and Freundlich isotherms plots respectively and their coefficients of determination (R^2) values are given in Table 7. The experimental data of polyvinyl alcohol nanofibers and incorporated nanofibers (R^2) values shows that Langmuir isotherm fitted better than Freundlich isotherm.

Current reported work, incorporated (PVA/Co-MOFs) nanofibers is superior to previously reported nanofibers adsorbents; polyacrylonitrile nanofibers modified with 2-(20-pyridyl)imidazole [24], electro-spun chitosan nanofiber membranes [25].

CONCLUSION

In summary we successfully enhanced polyvinyl alcohol nanofibers adsorption capability. Percentage liberation of Pb^{2+} ions from aqueous solution increased after incorporating polyvinyl alcohol nanofibers with cobalt metal organic frameworks, percentage removal increased from (25.50%) polyvinyl alcohol nanofibers to (59.41%) incorporated nanofibers. Kinetics studies showed that the uptake of lead ions by the nanofibers

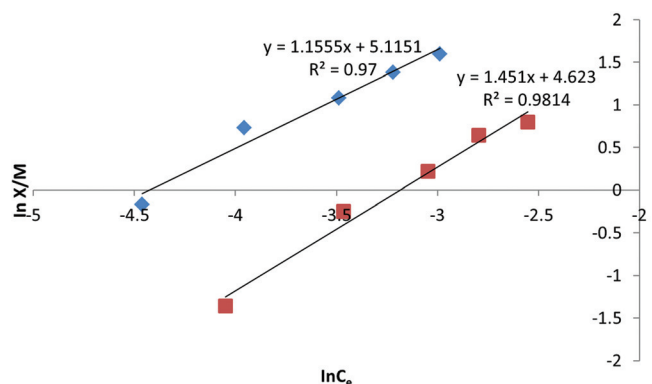


Figure 10. Plot of Freundlich isotherm plots, $\ln X/M$ against $\ln C_e$ (■) PVA nanofibers and (◆) PVA/Co-MOF nanofibers.

was very rapid, favoured at low temperatures and predominated by physisorption mechanism. Pseudo second order model kinetics was followed by adsorption Pb^{2+} ions processes. Incorporated (PVA/Co-MOFs) nanofibers demonstrated to be more effective adsorbent than plain polyvinyl alcohol nanofibers. Data from this study will add to the knowledge base on the fabrication, characterization and the use of nanofibers incorporated with metal organic frameworks for the sorption studies.

ACKNOWLEDGEMENTS

This work was supported by a research grant from the Faculty of Applied and Computer Science Research and Publications Committee of Vaal University of Technology and National research fund (NRF). Mintek is gratefully acknowledged for letting us to use their equipment.

REFERENCES

- Tchounwou, P. B., Yedjou, C. G., Patlolla, A. K. and Sutton, D. J., "Heavy Metals Toxicity and the Environment", *PubMed Central*, Vol. 101, 2012, pp. 133–164. http://dx.doi.org/10.1007/978-3-7643-8340-4_6
- Dastbaz, A. and Keshtkar, A. R., "Adsorption of Th^{4+} , U^{6+} , Cd^{2+} , and Ni^{2+} from aqueous solution by anovel modified polyacrylonitrile composite nanofiber adsorbentprepared by electrospinning", *Applied Surface Science*, Vol. 293, 2014, pp. 336–344. <http://dx.doi.org/10.1016/j.apsusc.2013.12.164>
- Javadian, H., "Application of kinetic, isotherm and thermodynamic models for the adsorption of Co(II) ions on polyaniline/polypyrrole copolymer nanofibers from aqueous solution", *Journal of Industrial and Engineering Chemistry*, Vol. 20, No. 6, 2014, pp. 4233–4241. <http://dx.doi.org/10.1016/j.jiec.2014.01.026>
- Chakravarty, P., Sarma, N. and Sarma, H. P., "Biosorption of cadmium(II) from aqueous solution using heartwood powder of *Areca catechu*", *Chemical Engineering Journal*, Vol. 162, No. 3, 2010, pp. 949–955. <http://dx.doi.org/10.1016/j.cej.2010.06.048>
- Kilic, M., Kirbiyik, C., Cepeliogullar, O. and Putun, A. E., "Adsorption of heavy metalions from aqueous solutions by bio-char, a by-product of pyrolysis", *Applied Surface Science*, Vol. 283, 2013, pp. 856–862. <http://dx.doi.org/10.1016/j.apsusc.2013.07.033>
- Stojiljković, S., Stamenković, M., Kostić, D., Miljković, M., Arsić, B., Savić, I. and Miljković, V., "The influence of organic modification on the structural and adsorptive properties of bentonite clay and its application for the removal of lead", *Science of Sintering*, Vol. 45, No. 3, 2013, 363–376. <http://dx.doi.org/10.2298/SOS1303363S>
- Erhabor, O. and T.-O. Adias. 2013. *Haematology made easy: Haemolytic anaemia*, Bloomington, PA: AuthourHouse.
- Luo, W., Ruan, D., Yan, C., Yin, S. and Chen, J., "Effects of chronic lead exposure on functions of nervous system in Chinese children and developmental rats", *Neurotoxicology*, Vol. 33, No. 4, 2012, pp. 862–871. <http://dx.doi.org/10.1016/j.neuro.2012.03.008>
- Needleman, H. L. and Bellinger, D., "Studies of lead exposure and the developing central nervous system: A reply to Kaufman", *Archives of Clinical Neuropsychology*, Vol. 16, No. 4, 2001, pp. 359–374. <http://dx.doi.org/10.1093/arclin/16.4.359>
- Kales, S. N., Christophi, C. N. and Saper, R.B., "Hematopoietic toxicity from lead containing Ayurvedic medications", *Medical Science Monitor*. Vol. 13, No. 7, 2007, pp. 295–298.
- Sokkary, G. H., Rahman, G. H. and Kamel, E. S., "Melatonin protects against lead-induced hepatic and renal toxicity in male rats", *Toxicology*, Vol. 213, No. 1-2, 2005, pp. 25–33. <http://dx.doi.org/10.1016/j.tox.2005.05.003>
- Adham, M. L., "Renal effects of environmental and occupational lead exposure", *Environmental Health Perspectives*, Vol. 105, No. 9, 1997, pp. 928–939. <http://dx.doi.org/10.1289/ehp.97105928>
- Apostoli, P. and Catalani, S., "Metal ions affecting reproduction and development", *Metal Ions in Life Sciences*, Vol. 8, 2011, pp. 263–303
- Jaworska, M. and Gorczyca, A., "The effect of metal ions on Mortality, pathogenicity and reproduction of entomopathogenic nematodes *Steinernema feltiae* filipjev (Rhabditida, Steinernematidae)", *Polish Journal of Environmental Studies*, Vol. 11, No. 5, 2002, pp. 517–519.
- Savic, I. M., Savic, I. M., Stojiljkovic, S. T. and Gajic, D. G., "Modeling and optimization of energy-efficient procedures for removing lead(II) and zinc(II) ions from aqueous solutions using the central composite design", *Energy*, Vol. 77, 2014, pp. 66–72. <http://dx.doi.org/10.1016/j.energy.2014.04.088>
- Savic, I. M., Stojiljkovic, S. T., Stojanovic, S. B. and Moder, K., "Modeling and optimization of Fe (III) adsorption from water using bentonite clay: comparison of central composite design and artificial neural network", *Chemical Engineering & Technology*, Vol. 35, No. 11, 2012, pp. 2007–2014. <http://dx.doi.org/10.1002/ceat.201200085>
- Gunatilake S. K., "Methods of Removing Heavy Metals from Industrial Wastewater", *Journal of Multidisciplinary Engineering Science Studies*, Vol. 1, No. 1, 2015, pp. 12–18.
- Chaturvedi, S., Dave, P. N. and Shah, N. K., "Applications of nanocatalyst in new era". *Journal of Saudi Chemical Society*, Vol. 16 No. 3, 2012, pp. 307–325. <http://dx.doi.org/10.1016/j.jscs.2011.01.015>
- Shooto, N. D., Wankasi, D., Sikhwivhilu, L., Dikio, E. D., Mfunzi, F. and Maubane, M. S., "Novel Super Adsorbents (PVA and PVA/Cu-MOF Nanofibres) as Effective Lead Ions Remover in Aqueous Solution", *Digest Journal of Nanomaterials and Biostructures*, Vol. 11, No. 2, 2016, pp. 425–434.
- Saeed, K., Park, S. Y. and Oh, T. J., "Preparation of hydrazine-modified polyacrylonitrile nanofibers for the extraction of metal ions from aqueous media", *Journal of Applied Polymer Science*, Vol. 121, No. 2, 2011, pp. 869–873. <http://dx.doi.org/10.1002/app.33614>
- Lee, Y. I., Lee, J. S., Park, E. S., Jang, D. H., Lee, J. E., Kim, K., Myung, N. V. and Choa, Y.H., "Effect of calcination temperature on the photocatalytic properties of electrospun TiO_2 nanofibers", *Journal Nanoscience and Nanotechnology*, Vol. 14, No. 10, 2014, pp. 8005–8009. <http://dx.doi.org/10.1166/jnn.2014.9445>
- Bhardwaj, N. and Kundu, S. C., "Electrospinning a fascinating fiber fabrication technique", *Biotechnology Advances*, Vol. 28, No. 3, 2010, pp. 325–347. <http://dx.doi.org/10.1016/j.biotechadv.2010.01.004>
- Pachfule, P., Das, R., Poddar, P. and Banerjee, R., "Solvothermal Synthesis, Structure, and Properties of Metal Organic Framework Isomers Derived from a Partially Fluorinated Link", *Crystal Growth and Design*, Vol. 11, No. 4, 2011, pp. 1215–1222. <http://dx.doi.org/10.1021/cg101414x>
- Ndayambaje, G., Laatikainen, K., Laatikainen, M., Beukes, E., Fatoba, O., Walt, N., Petrik, L. and Sainio, T., "Adsorption of nickel(II) on polyacrylonitrile nanofiber modified with 2-(20-pyridyl)imidazole", *Chemical Engineering Journal*, Vol. 284, 2016, pp. 1106–1116. <http://dx.doi.org/10.1016/j.cej.2015.09.065>
- Li, L., Li, Y. and Yang, C., "Chemical filtration of Cr (VI) with electrospun chitosan nanofiber membranes", *Carbohydrate Polymers*, Vol. 140, 2016, pp. 299–307. <http://dx.doi.org/10.1016/j.carbpol.2015.12.067>

GUIDE TO AUTHORS

1. Manuscripts shall be sent electronically to the Editor-in-Chief, Dr. P. Brent Duncan at pduncan@unt.edu using Microsoft Word in an IBM/PC format. If electronic submission is not possible, three paper copies of double-spaced manuscripts may be sent to Dr. P. Brent Duncan, (Editor of the *Journal of Residuals Science & Technology*, University of North Texas, Biology Building, Rm 210, 1510 Chestnut St., Denton, TX 76203-5017) (Tel: 940-565-4350). Manuscripts should normally be limited to the space equivalent of 6,000 words. The editor may waive this requirement in special occasions. As a guideline, each page of a double-spaced manuscript contains about 300 words. Include on the title page the names, affiliations, and addresses of all the authors, and identify one author as the corresponding author. Because communication between the editor and the authors will be electronic, the email address of the corresponding author is required. Papers under review, accepted for publication, or published elsewhere in journals are normally not accepted for publication in the *Journal of Residuals Science & Technology*. Papers published as proceedings of conferences are welcomed.
2. Article titles should be brief, followed by the author's name(s), affiliation, address, country, and postal code (zip) of author(s). Indicate to whom correspondence and proofs should be sent, including telephone and fax numbers and e-mail address.
3. Include a 100-word or less abstract and at least six keywords.
4. If electronic art files are not supplied, submit three copies of camera-ready drawings and glossy photographs. Drawings should be uniformly sized, if possible, planned for 50% reduction. Art that is sent electronically should be saved in either a .tif or .JPEG files for superior reproduction. All illustrations of any kind must be numbered and mentioned in the text. Captions for illustrations should all be typed on a separate sheet(s) and should be understandable without reference to the text.
5. DEStech uses a numbered reference system consisting of two elements: a numbered list of all references and (in the text itself) numbers in brackets that correspond to the list. At the end of your article, please supply a numbered list of all references (books, journals, web sites etc.). References on the list should be in the form given below. In the text write the number in brackets corresponding to the reference on the list. Place the number in brackets inside the final period of the sentence cited by the reference. Here is an example [2].
Journal: 1. Halpin, J. C., "article title", *J. Cellular Plastics*, Vol. 3, No. 2, 1997, pp. 432–435.
Book: 2. Kececioglu, D. B. and F.-B. Sun. 2002. *Burn-In Testing: Its Quantification and Optimization*, Lancaster, PA: DEStech Publications, Inc.
6. Tables. Number consecutively and insert closest to where first mentioned in text or type on a numbered, separate page. Please use Arabic numerals and supply a heading. Column headings should be explanatory and carry units. (See example at right.)
7. Units & Abbreviations. Metric units are preferred. English units or other equivalents should appear in parentheses if necessary.
8. Symbols. A list of symbols used and their meanings should be included.
9. Page proofs. Authors will receive page proofs by E-mail. Proof pages will be in a .PDF file, which can be read by Acrobat Reader. Corrections on proof pages should be limited to the correction of errors. Authors should print out pages that require corrections and mark the corrections on the printed pages. Pages with corrections should be returned by FAX (717-509-6100) or mail to the publisher (DEStech Publications, Inc., 439 North Duke Street, Lancaster, PA 17602, USA). If authors cannot handle proofs in a .PDF file format, please notify the Editor, Dr. P. Brent Duncan at pduncan@unt.edu.
10. Index terms. With proof pages authors will receive a form for listing key words that will appear in the index. Please fill out this form with index terms and return it.
11. Copyright Information. All original journal articles are copyrighted in the name of DEStech Publications, Inc. All original articles accepted for publication must be accompanied by a signed copyright transfer agreement available from the journal editor. Previously copyrighted material used in an article can be published with the *written* permission of the copyright holder (see #14 below).
12. Headings. Your article should be structured with unnumbered headings. Normally two headings are used as follows:
Main Subhead: DESIGN OF A MICROWAVE INSTALLATION Secondary Subhead: Principle of the Design Method
If further subordination is required, please limit to no more than one (*Third Subhead*).
13. Equations. Number equations with Arabic numbers enclosed in parentheses at the right-hand margin. Type superscripts and subscripts clearly above or below the baseline, or mark them with a caret. Be sure that all symbols, letters, and numbers are distinguishable (e.g., "oh" or zero, one or lowercase "el," "vee" or Greek nu).
14. Permissions. The author of a paper is responsible for obtaining releases for the use of copyrighted figures, tables, or excerpts longer than 200 words used in his/her paper. Copyright releases are permissions to reprint previously copyrighted material. Releases must be obtained from the copyright holder, which is usually a publisher. Forms for copyright release will be sent by the editor to authors on request.

Table 5. Comparison of state-of-the-art matrix resins with VPSP/BMI copolymers.

Resin System	Core Temp. (DSC peak)	T _E	Char Yield, %
Epoxy (MY720)	235	250	30
Bismaleimide (H795)	282	>400	48
VPSP/Bismaleimide copolymer			
C379: H795 = 1.9	245	>400	50
C379: H795 = 1.4	285	>400	53

General: The *Journal of Residuals Science & Technology* and DEStech Publications, Inc. are not responsible for the views expressed by individual contributors in articles published in the journal.